UNIVERSITY OF OSLO
Department of Physics

A DMSP satellite study of magnetospheric plasma convection and particle precipitation states during passage at Earth of interplanetary magnetic clouds monitored by the Wind spacecraft

Master Thesis

Arvind Sharma

June 2007

Abstract

In this study we take advantage of the slow, smooth rotation of the strong magnetic fields in interplanetary magnetic clouds to identify transitions between particle precipitation/plasma convection states of the magnetosphere and relate them unambiguously to the interplanetary conditions. Focus is placed on magnetospheric states driven by the passage at Earth of the following three magnetic clouds: August 12-13, 2000; May 20-21, 2005; and June 12-13, 2005. Interplanetary field and plasma data were acquired by the Wind spacecraft. Plasma convection and particle precipitation states are identified from passages of spacecraft DMSP F13 across the northern hemisphere polar regions in approximate dusk–to–dawn orbits.

Emphasis is placed on the discriminating between different categories of plasma convection cells and the corresponding particle precipitation and field Aligned current characteristics. Supplementary information on the magnetospheric states is obtained both from magnetic field deflections detected by the same satellite as it traverses systems of field-aligned currents as well as from FUV (Far-UltraViolet) images and convection pattern obtained from spacecraft IMAGE and SuperDARN radar network, respectively .

By this technique we are able to establish the correspondence between polar cap convection/-precipitation states and parameters such as the (i) the orientation of the magnetic field in the cloud as parametrized by the clock angle of the magnetic field in the magnetic cloud, (ii) the IMF B_y and B_x polarities, and (iii) solar wind density/dynamic pressure. The conclusions extend recent work in the area.

Acknowledgments

This master thesis is dedicated to my beloved sister Reeta. The way you spread your love is something we will never forget.

I would like to thank my supervisors Per Even Sandholt, University of Oslo, Department of Physics and Charles J. Farrugia, University of New Hampshire, Experimental Space Plasma Group, for their guidance in the field of plasma & space physics. Your ideas and comments were priceless while I was working on my thesis project. Thank you for your great enthusiasm not only in science but also in everyday life. I thank Per Even Sandholt for sending me to Charles J. Farrugia in Durham, New Hampshire, USA. I will never forget the hospitality you showed me, Charlie

To my mother, father and brother, who has supported me from day one, I would never have come so far without your guidance and encouragement. I love you with all my heart.

I also wish to thank all my friends who does not know anything about space physics, but all about being friends. To my mates Bingo, Tore and Balvar I would like to say that I have never ”wasted” so many hours on lunch and tea drinking, but it has been worth it. Thanks to all my friends for motivating me to accomplish my goals and dreams.
Further I would like to express my gratitude to the whole Plasma & Space Physics Group at the University of Oslo. Thank you for the unique atmosphere which you all create.

There are people and institutions we would like to thank for their contribution in providing us with data to this thesis; We thank Charlie Farrugia for providing the Wind data used in this study. The IMAGE data was provided by Nikolai Østgaard and Kalle Laundal at the University of Bergen, Department of Physics and Technology. A special thanks to Kalle Laundal who was always willing to provide more data for this study. We also want to take the opportunity to thank Bill Denig for giving us access to the DMSP data base at the Space Weather Data Survey website. Thanks to Dr. Marc Hairston, Dr. Robin Coley, and the University of Texas at Dallas Center for Space Science for supplying the DMSP cross-track plasma drift data through their website.

The graphics in this thesis has been processed and edited by Nitin Dhamelia.

Finally, I thank my beloved Sunshine. Thank you for supporting me and making me smile every single second of the day.

Table of Contents

Chapter 1

Introduction

The Sun is continuously emitting a stream of high-speed plasma, called the solar wind. Sometimes huge eruptions from the Sun into interplanetary space, called coronal mass ejections (CMEs), occur. These eruptions can be of a few billion tons of plasma and embedded within this plasma are magnetic fields from the Sun's corona. It is believed that magnetic clouds (MCs) are a subset of coronal mass ejections, with a specific magnetic field configuration and unique plasma properties. The magnetic cloud has a strong magnetic field that slowly rotates over a period of 30-40 hours. We want to take advantage of these properties when we study the interaction of magnetic cloud with the Earth's magnetosphere in order to determine the association between the interplanetary magnetic field (IMF) and solar wind plasma parameters and the different states of the magnetosphere as monitored by polar cap precipitation, and plasma convection.

With the help of satellites that traverse the central polar cap combined with ground-based radars and ultraviolet images from satellites orbiting the Earth we want to discriminate between the different plasma convection and particle precipitation states that occur during the magnetic cloud passage. The different quasi-stable IMF conditions, produced by the smooth and slow rotation of the cloud field, will make it easier to determine the IMF orientations corresponding to the different plasma convection/precipitation states. Our focus in this thesis is placed on magnetospheric states driven by the passage at Earth of the following three magnetic clouds: August 12-13, 2000; May 20-21, 2005; and June 12-13, 2005. This thesis will hopefully contribute to get a more comprehensive understanding about the solar wind - magnetosphere interaction.

This thesis is organized as follows: In Chapter 2 we present the conceptual basis needed for this thesis and Chapter 3 describes the theoretical analysis and the instrumentation used. Chapter 4, 5 and 6 are case studies of how the plasma convection and particle precipitation changes during passage of three interplanetary magnetic clouds. The summary and discussion of our findings are presented in Chapter 7.

Chapter 2

Sun-Earth Environment

The sun is continuously emitting a stream of high-speed plasma, called the solar wind. The origin of the solar wind are the huge pressure difference between Sun's hot corona and interstellar space (Kivelson and Russell, 1995, chap. 4.1). Embedded in the outflowing solar wind plasma is a weak magnetic field ($\sim 1 - 50$ nT, about 10 nT near Earth) known as the interplanetary magnetic field (IMF). The IMF is "frozen into" the solar wind. The frozen magnetic field theorem states that plasma particles located on a certain field line at time t_1 are constrained in their motion to stay on the same field line at all later times (Paschmann, 1991). In table 2.1 the average parameters of the solar wind at the Earth's location is given. The density of the solar wind near Earth, i.e. at one astronomical unit (1 AU = 1.5 $\times 10^8$ km), is quite low ($\sim 5\ cm^{-3}$) and the solar wind is then considered to be a collisionless plasma. This collisionless plasma is reasonably well described as an ideal MHD fluid (Parker, 1958). The implication is then that the plasma of the solar wind can not simply jump from a interplanetary magnetic field line to another one belonging to a planetary magnetic field. The Earth's magnetic field deflects the solar wind around the Earth, like a rock in a water slow down and forces the water to flow around it. This leads to a draping of interplanetary field lines around the magnetosphere.

The Earth's magnetic field is generated by the electrical currents in the fluid outer core. The solar wind interacts and deforms the Earth's basically dipolar magnetic field, compressing the field lines on the dayside and stretching them out to form a long comet-like tail (the magnetotail) on the nightside. The cavity formed in solar wind, which is connected to and controlled by the Earth's magnetic field is referred to as the magnetosphere. A shock wave is formed in front of the nose of the magnetopause as the supersonic (and super-Alfv́enic) solar wind slows down and

Proton Density	6.6 cm^{-3}
Electron Density	7.1 cm^{-3}
He^{2+} Density	0.25 cm^{-3}
Flow Speed	450 km/s
Proton Temperature	$1.2 \times 10^5 K$
Electron Temperature	$1.4 \times 10^5 K$
Magnetic Field	$7 \times 10^{-9} T$

Table 2.1: *Observed properties of the solar wind plasma near the orbit of the Earth (Kivelson and Russell, 1995)*

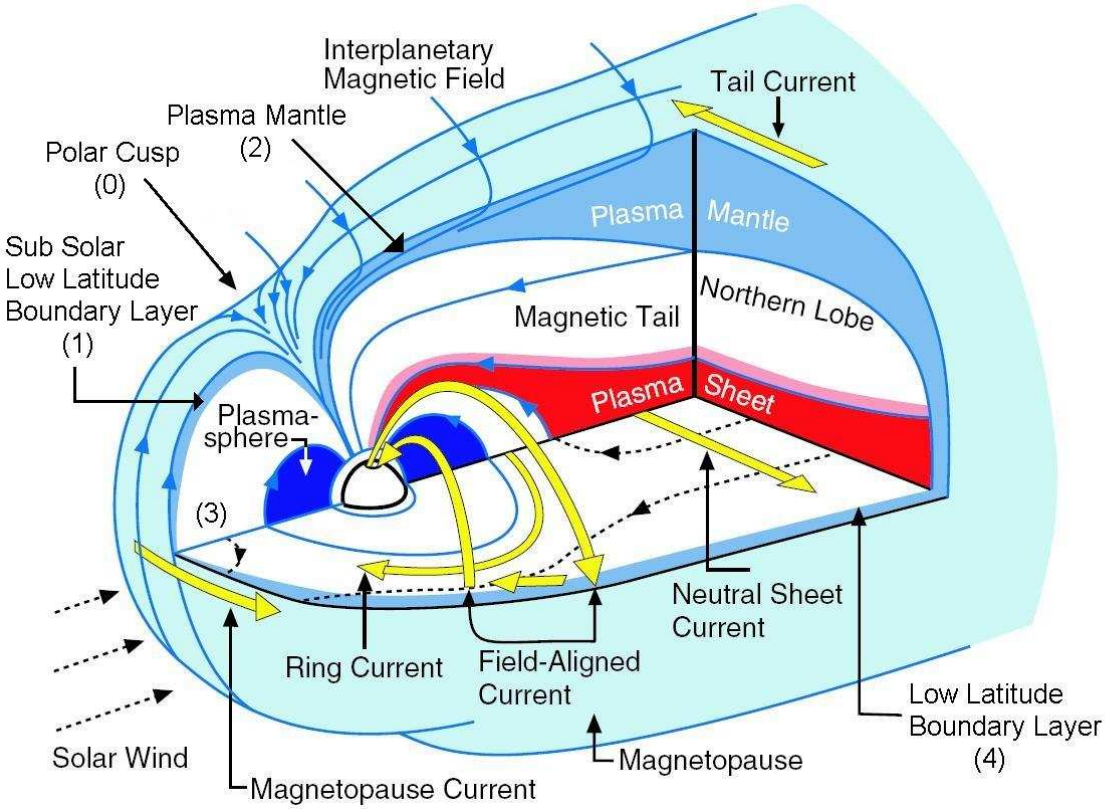

Figure 2.1: *Three-dimensional view of the magnetosphere. The light blue outer surface is the magnetopause, its boundary layers are shown in darker blue. Magnetic field lines are shown in blue, electric currents in yellow. The polar region where the magnetic field lines converge is the polar cusp. The bow shock has been omitted for clarity. Adapted from Kivelson and Russell (1995).*

becomes subsonic when it approaches the magnetosphere as an "obstacle" in the flow. When the plasma travels through the shock, which ranges in thickness from roughly 100 km to 2 Earth radii ($1R_E = 6378\ km$), the solar wind is slowed, compressed, and heated. The region behind the bow shock is occupied by the shocked solar wind plasma known as the magnetosheath (e.g. (Paschmann, 1991; Sonnerup, 1985; Russell, 1972). The interface between the magnetosheath and the magnetosphere is called the magnetopause.

2.1 Magnetosperic Framework

The shape and position of the magnetopause (see the light blue outer surface in figure 2.1) is a direct result of pressure balance between the solar wind and the magnetosphere. The day-side magnetopause is found to be at around 10 R_E (Fairfield, 1971), corresponding to a solar wind dynamic pressure of ~2.5 nPa. In the idealized picture of the interaction between the solar wind and the Earth's magnetic field, the outer boundary of the magnetosphere, referred to as the magnetopause, is acting as a current sheet and carrying the so-called Chapman-Ferraro current (given by Ampére's law, $\nabla \times \vec{B} = \mu_0 \vec{j}$, where B is the magnetic field, μ_0 the permeability of vacuum and j the current) that completely separates the magnetic fields and the plasmas on

the two sides. No mass flow is permitted across this sheet (Kivelson and Russell, 1995, chap. 9.2). A current sheet can be defined as a thin surface across which the magnetic field strength and/or direction change substantially. The magnetopause can be represented as a tangential discontinuity, in which the magnetic field component normal to the boundary is zero. Plasma flow across the current layer, from the magnetosheath side to the magnetosphere side, could be present only as a result of diffusion so long as the magnetopause is a tangential discontinuity.

During magnetic reconnection/merging, however, the normal magnetic field component is non-zero (i.e. the magnetopause becomes a rotational discontinuity), and at the magnetopause plasma flows across the discontinuity from the magnetosheath into the magnetosphere and in the opposite direction (Paschmann, 1984). A boundary layer on open field lines adjacent to the magnetopause is found (Paschmann, 1991; de Keyser et al., 2005). There are two different kinds of plasma processes at the magnetopause. Both where proposed in same year as the magnetopause was first observed (1961) The plasma processes at the magnetopause are: (1) Viscous interaction, i.e. plasma diffusion across a tangential discontinuity (Axford and Hines, 1961), and (2) magnetic reconnection (Dungey, 1961). Plasma enters the magnetosphere along open field-lines created by reconnection on the dayside magnetopause (Phan et al., 1996; Sonnerup et al., 1981; Paschmann et al., 1979). Alternatively, magnetosheath plasma may perhaps directly enter onto closed magnetic field lines on the dayside by other processes like viscous interaction (de Keyser et al., 2005 and references therein). The main focus in this thesis will be on dayside reconnection as shown by in situ observations from the DSMP satellites.

2.1.1 Viscous Interaction

Viscous interaction implies a drag exerted by the streaming solar wind along the magnetopause. It usually includes diffusive mass transfer with associated momentum and energy transfer (viscous shear stress). As a result the magnetospheric magnetic flux tubes are pulled antisunward past the dusk and dawn flanks and into the magnetictail. This sets up a convection system and associated electric field. A way to generate viscous sheer stress/momentum transfer across the magnetopause is by the Kelvin-Helmholtz instability and kinematic viscosity. Viscous type convection is for the most part an antisunward flow on closed geomagnetic field lines on the dawn and dusk flanks of the magnetopause (Cowley, 1984).

2.1.2 Magnetic Reconnection

Magnetic reconnection is a process occurring in a magnetized plasma , where it changes the topology of magnetic fields by breaking the frozen-in field condition of ideal MHD. The magnetic lines of force from the magnetosheath and magnetosphere interconnect. In doing so, magnetic energy may be converted into other forms such as kinetic energy, heat and light. A simple two-dimensional reconnection configuration involving a single X-line/Sweet-Parker magnetic reconnection, where suggested by Sweet (1958) and Parker (1957). The low reconnection rate in the Sweet-Parker model where a problem compared to observations. Petschek (1964) introduced a model where the reconnection rate can be strongly enhanced by the use of slow shocks and small diffusion regions. Thus, this result represented a great breakthrough in reconnection research.

A problem with the present reconnection models applied to the magnetopause is the shortcoming of describing where and when the process will occur, i.e. the spatial and temporal variability. There are three different factors that affect the probability of reconnection onset and the rate of reconnection occurrence. The three factors are:

1. The local magnetic shear;
2. The local Alfv́enic-Mach number; $M_A = \frac{v}{v_A}$
3. The plasma β; where $\beta = \frac{p}{B^2/2\mu_0}$

When it comes to the high local magnetic shear, i.e. cases where the magnetic fields on the two sides of the magnetosphere form a large angle relative to each other, it is still discussed if the field lines have to be completely antiparallel or not (e.g. Phan et al., 1994; Luhmann et al., 1984; Crooker et al., 1979; Sonnerup et al., 1981; Sonnerup, 1974; Cowley, 1973). A longer time of interaction because of the low flow velocity (sub-Alfv́enic flow) means that the probability for reconnection increases. A lower β in the magnetosheath next to the magnetopause is considered favourable for reconnection onset (e.g. Paschmann et al., 1986).

2.1.3 Magnetopause Reconnection Geometries For Different IMF Orientations

Both theoretical studies and observations have shown that different IMF orientation will give rise to different reconnection geometries at the magnetopause. One configuration takes place for southward IMF with a non-zero east - west component, B_y. Reconnection should then extend along an X-line from prenoon to postnoon through the subsolar point of the magnetopause (the front of the magnetosphere near equator) where the external and internal fields are antiparallel. This is one variety of the reconnection configuration that opens the dayside magnetopause. The interplanetary magnetic field becomes connected to the magnetic field of the Earth. The open magnetic field lines, with one foot in the ionosphere and one in interplanetary space, are then dragged along by the solar wind giving rise to a global convective motion, as first introduced by Dungey (1961) and is often referred to as the Dungey convection cycle (as shown in figure 2.2). This convective motion, as we will show in section 2.2, maps down to the ionosphere. For northward IMF the reconnection line is occurring over the poles beyond the cusp (Russell, 2003). Northward IMF reconnection is often referred to as lobe reconnection because it involves reconnection on the – already open – lobe field lines tailward of the cusps. The resulting lobe cell convection will be discussed more extensively in section 2.3. A variety of reconnection geometries for northward IMF conditions are considered in the article by Cowley (1981). The plasma convection pattern for reconnection under due northward IMF is a pair of reverse convection cells at high latitudes, i.e. with sunward convection over the polar cap. Reconnection can also occur for other IMF orientations. A strong east-west component (IMF B_y) will introduce dusk/dawn asymmetries in magnetospheric convection, (see section 2.2). The IMF B_z is an important parameter for reconnection but more and more focus has been shifted into the two other IMF components, B_x and B_y in the recent years (e.g. Eriksson et al., 2003; Gosling et al., 1996; Crooker and Rich, 1993). The lesson is that all 3 IMF components are important for the magnetopause reconnection topology. Also the Earth's dipole tilt needs to be considered. In this thesis we look at different magnetosphere states and compare them to IMF

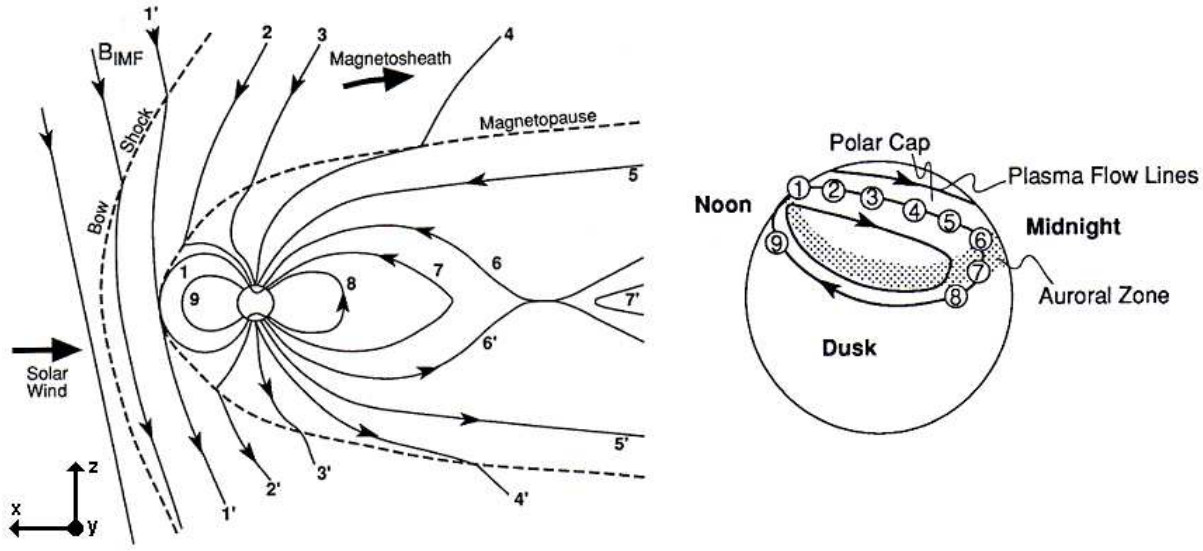

Figure 2.2: *Dungey-type convection pattern and its mapping into the auroral ionosphere. From Kivelson and Russell (1995).*

orientation and clock angle. With respect to this we note that the three cases we study are all in the summer period (May 2005, June 2005 and August 2000) when we are discussing dayside magnetopause reconnection.

2.1.4 Antiparallel vs Component Reconnection

In the picture of the antiparallel reconnection model, reconnection is restricted to places where the magnetic shear between magnetospheric and magnetosheath field lines is close to 180° (antiparallel) (Luhmann et al., 1984; Crooker et al., 1979). In this model the line of reconnection is determined by the location of the antiparallel fields, i.e. the reconnection site moves away from the subsolar region as the IMF rotates away from due south. One example is that for southward (negative) B_z and for dusk-dawn ($B_y \neq 0$) pointed fields the reconnection line splits up into segments in the north/dusk and south/dawn (see figure 8 in Russell, 2003).

In the 1970's Sonnerup introduced the component reconnection model (e.g., Sonnerup, 1974). In this model reconnection occurs along an X-line where the magnetic fields on either side of this line need not be oppositely directed. In this scenario, the reconnection rate approaches zero only when/where the magnetic field shear fall below a minimum angle (Gonzalez and Mozer, 1974; Hill, 1975). Gosling et al. (1990) and Onsager and Fuselier (1994) among others have showed evidence supporting the component reconnection model by in situ observations.

A recent theoretical study by Moore et al. (2002) concluded that merging rates should be appreciable near the subsolar magnetopause for most IMF clock angles and that subsolar reconnection should stop completely only for northward directed IMF. Moore et al. (2002) furthermore showed that reconnection during B_y dominated periods occurs in form of a tilted X-line running through the subsolar point which extends to the north/dusk and south/dawn sectors. A figure adapted from Sandholt (Private communication, 31. Jan 2007) gives a general view of the con-

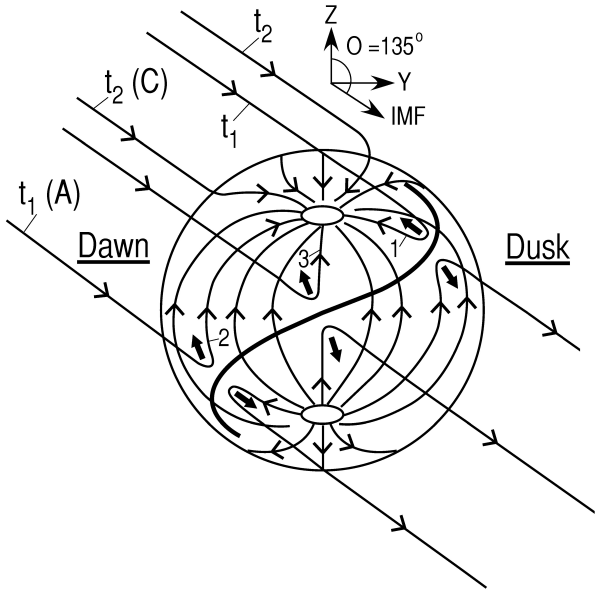

Figure 2.3: *Reconnection topology for a southeast directed IMF. The Earth's field (just inside the magnetopause) is indicated. The perspective is from the Sun towards the Earth. IMF field lines merges with the Earth's field liens, where t_1 is newly-opened field lines and t_2 is old-open field lines. A tilted reconnection line (the S-shaped X-line), representing component reconnection at the subsolar (marked 3), and antiparallel merging at higher latitudes in the northern (postnoon, marked 1) and southern (prenoon, marked 2) hemisphere.*

cept of S-shaped X-line reconnection (See figure 2.3). This figure is consistent with work done by Park et al. (2006), Moore et al. (2002), and Rijnbeek et al. (1984). In this figure we see a schematic view from the Sun towards the Earth of magnetic field lines at the dayside magnetopause for an IMF clock angle of 135°. The single S-shaped X-line shows both antiparallel and component reconnection in different sectors. The antiparallel reconnection are located at the north/dusk and south/dawn flanks on high- and low-latitudes. Newly reconnected field lines in these sectors are marked 1 and 2 in figure 2.3. The figure also shows reconnection also occurring at the subsolar point marked as 3. The letter case represent component reconnection. Park et al. (2006) showed with help of MHD simulation that both antiparallel and component reconnection are important factors at the dayside magnetopause when the IMF B_y component and the dipole tilt is non-zero, i.e. during the winter and summer seasons.

2.2 The Coupling Of The Solar Wind Momentum to The Magnetosphere and Ionosphere

A really important consequence of the coupling processes which is occurring at the magnetopause boundary of the Earth's magnetosphere and in the geomagnetic tail is the large-scale convective flow that pervades the magnetosphere-ionosphere system. In an open model magnetosphere (Dungey, 1961) the solar wind electric field in the high latitude boundary layer (HLBL) is mapped down into the ionosphere by newly reconnected magnetic field lines, where it creates a horizontal $E \times B$ plasma drift, called convection. The dependence of the flow pattern

on IMF has been illustrated by Reiff and Burch (1985); Heppner and Maynard (1987), and recently reviewed by Cowley (1998). Cowley (1998) summarized a sequence of steady-state flow patterns parametrised by the direction and strength of the IMF (see figure 2.4). Merging cells are marked with notation M–CELL, and their convection is on open field lines over the polar cap. The lobe cells are marked with L–CELL and are entirely on open field lines. "Viscously-driven" convection (marked V–CELL) is indicated by the flow vortices and are located wholly on closed field lines (Cowley, 1998). This newly opened flux is transferred antisunward from noon (dayside) to midnight (nightside) over the polar cap for southward ($B_z < 0$) IMF (antiparallel reconnection at the subsolar point). In the magnetotail the low-latitude open field lines from each hemisphere reconnects and create a sunward return flow at low latitudes and give rise to a two-cell ionospheric convection pattern. As mentioned in section 2.1.3 figure 2.2 shows the convecting magnetic field lines and their footprint motion in the ionosphere for southward IMF. For due northward ($B_z > 0$) IMF, reconnection occurs in form of open lobe field lines tailward of one or both of the cusps, see section 2.3. In an article by Sandholt et al. (2000) the variety of lobe cell reconnection occurring in only one or both hemispheres where discussed. In the first case, i.e. lobe reconnection occurring in one hemisphere, Sandholt et al. showed (see figure 2.5a) that a two cell lobe convection pattern is confined to the region of open field lines (lower panel, middle figure, in figure 2.4). A two cell lobe convection pattern will also be present in the latter case, i.e. when lobe reconnection in both hemisphere is occurring but not necessary simultaneously. Sandholt et al. pointed out that the difference in this case is that the convection will involve both open and closed field lines (see figure 2.5b). This case is not shown in figure 2.4. In both cases the convection pattern is a reversed two-cell pattern (i.e., the circulation is opposite to the standard two-cell ionospheric convection pattern for southward ($B_z < 0$) IMF (Dungey, 1963).

The upper panel in figure 2.4 shows the flow for negative IMF B_z. The lower panel show idealized convection pattern for positive IMF B_z with the requirement of only steady reconnection in one lobe. The figure also represent a dawn-dusk shifts associated with IMF B_y (negative on the left, positive on the right). Lower panel middle figure shows a two lobe cell convection located wholly on open field lines, as mention before, for due north IMF. When the IMF B_z is positive and with a non-zero B_y component a single lobe cell located wholly on open field lines will be present (lower panel, right and left figure). The cells in the lower panel of figure 2.4 is mainly driven by the IMF B_z component. Reiff and Burch (1985) and Crooker (1992) were the first to predict that a composite circulation pattern of merging and lobe cells occur for B_z negative conditions, clock angle between $90 - 135^\circ$ (upper panel of figure 2.4). The lobe cell that circulates inside the merging cell is mainly driven by IMF B_y component.

Sudden changes in the IMF components results in changes in the ionosphere convection pattern. The response time for ionospheric flow is found to be of order ∼10-15 min ± 5 min at noon.(Todd et al., 1988; Khan and Cowley, 1999; Pryse et al., 2000; Lockwood et al., 2006). As we move further back in the ionosphere from 12 MLT (noon) to 18 MLT (dusk) and 6 MLT (dawn) the response time for ionospheric flow will increase till somewhere around 20-25 min. In a transient state, i.e. when the IMF condition change on time scale shorter then the response time for the ionospheric flow pattern, it is hard to determine which IMF state the convection pattern maps back to. If the IMF oscillations is much shorter then the response time, the global ionospheric convection will not show any changes. In our case we want to take a closer look

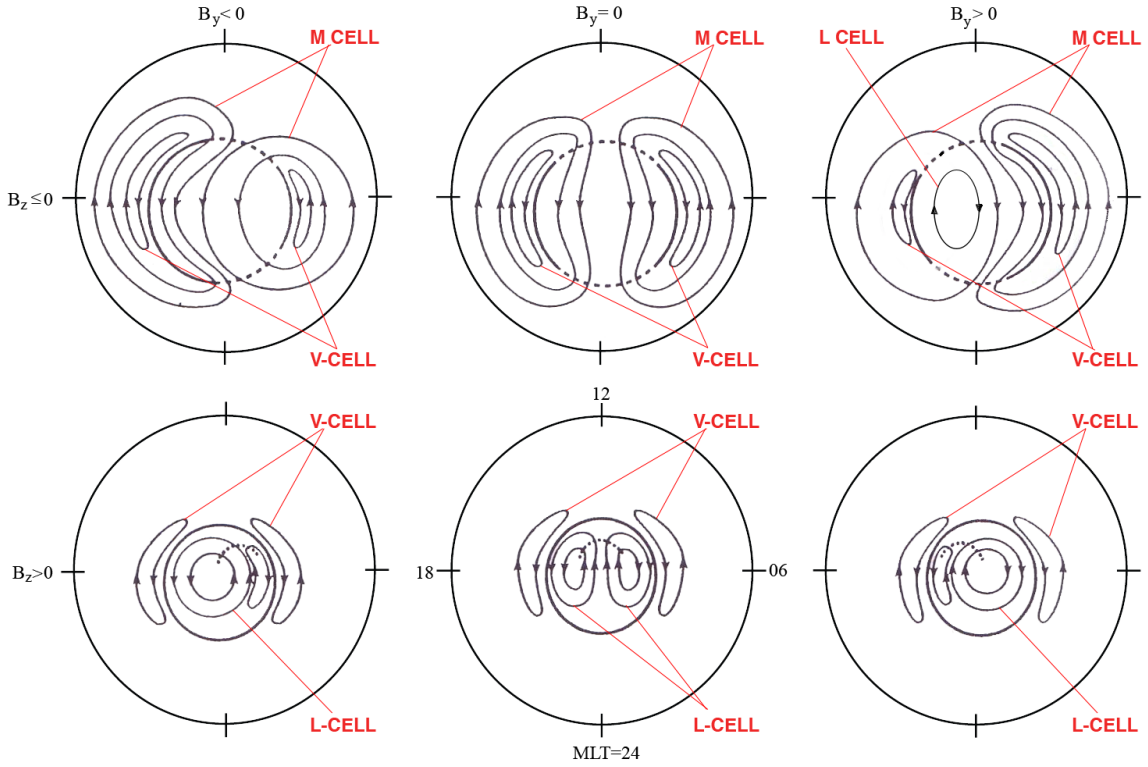

Figure 2.4: *Sketches of the northern hemisphere ionospheric flow ordered according to the direction of the IMF. The arrowed solid lines show the plasma streamlines, while the centre circle represents the boundary between open and closed magnetic flux, the dashed portions of which the upper row (negative IMF B_z) are the "merging gap" segments which map to the magnetopause reconnection sites. In the lower row (positive IMF B_z) the dashed lines map to the lobe magnetopause reconnection site, but do not lie on the open-closed field line boundary if reconnection for a given IMF field line takes place in one hemisphere only. Merging cells are marked with a M–CELL, lobe cells are marked with a L–CELL and "viscously-driven" convection is marked with V–CELL is indicated by the flow vortices located wholly on closed field lines (Cowley, 1998).*

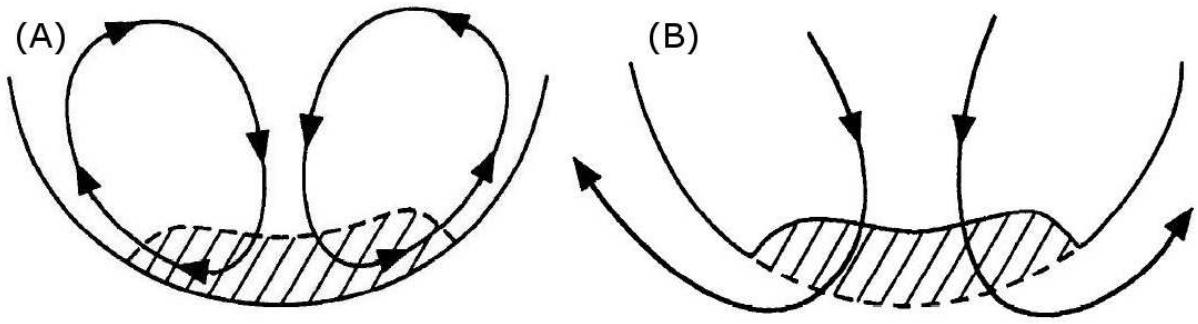

Figure 2.5: *(a) A reversed two cell convection pattern associated with one-lobe reconnection for purely northward IMF. (b) A reversed two cell convection pattern associated with two-lobe reconnection for purely northward IMF. In both figures the open-closed field lines boundary is marked with a solid line and the hatched area is the cusp aurora.*

at for which IMF condition and/or clock angle regimes the excitation and eventual decay of the composite ionospheric flow pattern maps back to. A way to circumvent the problem of response time is to look at ionospheric flow patterns during a magnetic cloud passage. In this thesis we will take a closer look at this problem by studying three different examples. We will discuss this moreover in section 3.1.

2.3 Lobe Cell Convection

We apply the term ”lobe cell” as described by Burch et al. (1985) and Reiff and Burch (1985), to any convection cell located wholly on open field lines (Cowley and Lockwood, 1992). This open-open transfer stirs up already-opened flux in the tail lobes. Lobe cell reconnection and convection is possible for all IMF orientation when the tail lobe is partially draped over the day-side magnetosphere (Crooker, 1992). The concept of lobe reconnection and the associated lobe convection was first introduced by Russell (1972) as merging of a purely northward IMF with the southward directed magnetic field of the open tail lobe poleward of the cusps. Figure 2.6 shows the lobe cell generation by merging of open geomagnetic field lines with the northward directed IMF.

Dungey (1963) had the original idea that lobe reconnection is possible when the northward directed IMF is antiparallel to the geomagnetic field of a completely closed magnetosphere. The requirement of northward IMF was the only condition that was recognized in the past for lobe cell convection. In 1981 Cowley discussed and schematically sketched several (five) possibilities of magnetic merging between a northward-directed IMF and either open or closed tail lobe field. This sketches involves reconnection at one or both lobes (simultaneous or sequential merging). Crooker (1992) showed that the presence of an overdraped tail lobe can be created by the earth’s dipole tilt and/or the tilt toward or away from the sun, IMF B_x. The IMF B_x and B_y components seem to be important additional factors for lobe reconnection and convection (Eriksson et al., 2003; Crooker et al., 1998; Cowley, 1981). Other factors that seem to influence the lobe reconnection process are the Alfv́en Mach number and plasma β values in the adjacent magetosheath (e.g. Eriksson et al., 2003; Crooker et al., 1998; Gosling et al., 1996). The lobe

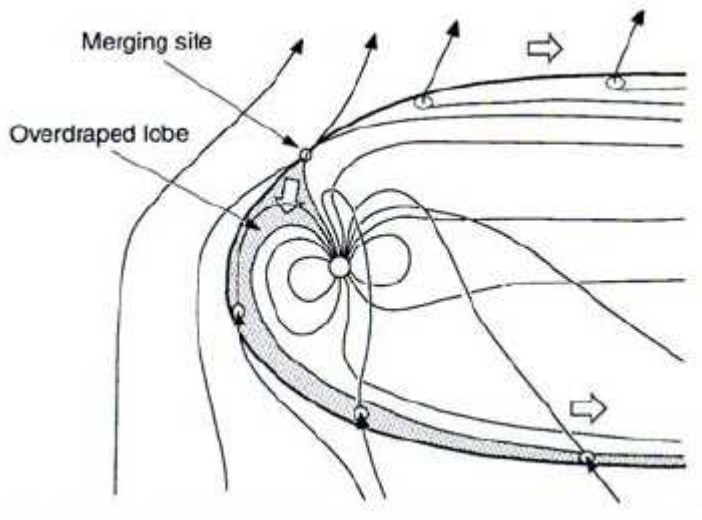

Figure 2.6: *Lobe cell generation by merging of open geomagnetic lines with the IMF. The region of draped lobe field lines is indicated by shaded area over the dayside (Crooker and Rich, 1993)*

cell strength seems to be weaker for larger Alfv́en Mach number at the merging site. Eriksson has suggested in two articles (2002; 2003) that there is a close IMF B_y dependent connection between lobe cell convection and polar rain precipitation. We will discuss this in more detail later in the thesis.

In an article by Crooker and Rich (1993) the relationship between lobe cell convection and season was pointed out. They showed a preference for reconnection in the summer hemisphere, since the sunward dipole tilt produces an antiparallel configuration tailward of the cusp. Similarly the northern hemisphere is favoured over the southern as a site of reconnection for negative IMF B_x. The summer lobe cell was observed circulating inside the duskside merging convection cell for B_y positive (dawnside merging convection cell for negative B_y). Weimer (1995)) has confirmed that summer is a favoured season for lobe cell excitation. They all point out that this phenomenon is caused by the Earth's dipole tilt and that the dipole tilt may be more important for lobe cell convection than the IMF B_x. At summer the dipole tilt and a negative (antisunward) IMF B_x component are both factors favourable with different magnitude for lobe cell generation in the northern hemisphere. The first direct in situ spacecraft observations of reconnection poleward of cusp during northward IMF was presented in an article by Kessel et al. (1996). It supported the general view of sunward flow over the polar cusp expected for reconnection at high-latitude when the IMF is positive (northward) (e.g. Cowley, 1981; Crooker, 1992). A few year later Sandholt et al. (1999) gave an example of the entry of magnetosheath plasma when the reconnection poleward of both cusps occurred simultaneously during strongly northward IMF conditions. They used multi-instrument observations to show how the magnetosheath plasma was captured sequentially in the magnetosphere by the Song and Russell (1992) mechanism. The same year Sandholt et al. (1999) also confirmed the occurrence of a large reconfiguration of plasma convection, consistent with the presence of a lobe cell, when the IMF conditions changes from southward to northward.

2.4 Particle Precipitation Characteristics

When we are looking at the DMSP data we will try to identify the different magnetospheric boundary layers and therefore a brief introduction is given here. Earthward of the magnetopause current layer, spacecraft have observed different boundary layers. The properties of the boundaries are closely associated with the structure of plasma domains in the magnetosphere. Figure 2.1 in section 2 gives a three-dimensional view of the dynamical location of the different layers. The central plasma sheet (CPS), marked 3 in figure 2.1, is the dayside extension of the nightside plasma sheet (shown in red). In this region the solar wind plasma has normally no direct access and the plasma is of magnetospheric origin. The low-latitude boundary layer in the sub solar region (LLBL), marked 1 in figure 2.1, forms a boundary layer between the CPS and magnetosheath (Eastman et al., 1976; Sckopke et al., 1981; Newell and Onsager, 2003). A Cusp configuration, marked 0 in figure 2.1, is found where the magnetic field lines converge, and is a site of direct plasma entry from the solar wind, mainly by diffusive processes (Sandholt et al., 2002, chap. 2.2). The high-latitude boundary layer, also called the plasma mantle (marked 2), is found near that part of the magnetopause that separates the tail lobe from the magnetosheath. The low-latitude boundary layer on the post noon flanks is marked as 4. The plasma sheet boundary layer or boundary plasma sheet (BPS) forms the boundaries between the tail lobe and the CPS (Vasyliunas, 1979). CPS and BPS was defined by Winningham et al. (1975).

At ionospheric altitudes the precipitating electrons and ions of different energies and physical characteristics can be traced back to different boundary layers. Maps of the ionospheric precipitation regions with superposed convection maps for different IMF conditions was presented by Newell et al. (2004); Newell and Meng (1992). Their statistical survey was based on 11 years of DMSP particle data. Figure 2.7 shows the particle precipitation characteristics for different IMF conditions. As we can see in figure 2.7 the particle precipitation region changes for the different IMF orientations. We need to keep this in mind when studying the three cases. A brief description of the major particle precipitation region and their characteristics is given below.

Central Plasma Sheet (CPS): 1-10 keV ions and electrons. A region of unstructured trapped electrons with a temperature of several keV giving rise to diffuse aurora. Shown as dark green in figure 2.7.

Boundary Plasma Sheet (BPS): Mixture of low- and high- energy particles. A region of structured electrons which have been subject to some acceleration. Electron energy $\sim 0.5 - 10$ keV give rise to discrete auroral forms. Shown as dark blue in figure 2.7.

Low-Latitude Boundary Layer LLBL: Similar to cusp but reduced particle fluxes. Average ion energy $\sim 0.6 - 3$ keV and average electron energy $0.6 - 2.5$ keV. Marked as yellow from prenoon to postnoon in figure 2.7.

Mantle: High-latitude component of cusp-type precipitation. Average ion energy below 1 keV and average electron energies around a few hundred eV. From prenoon till postnoon and

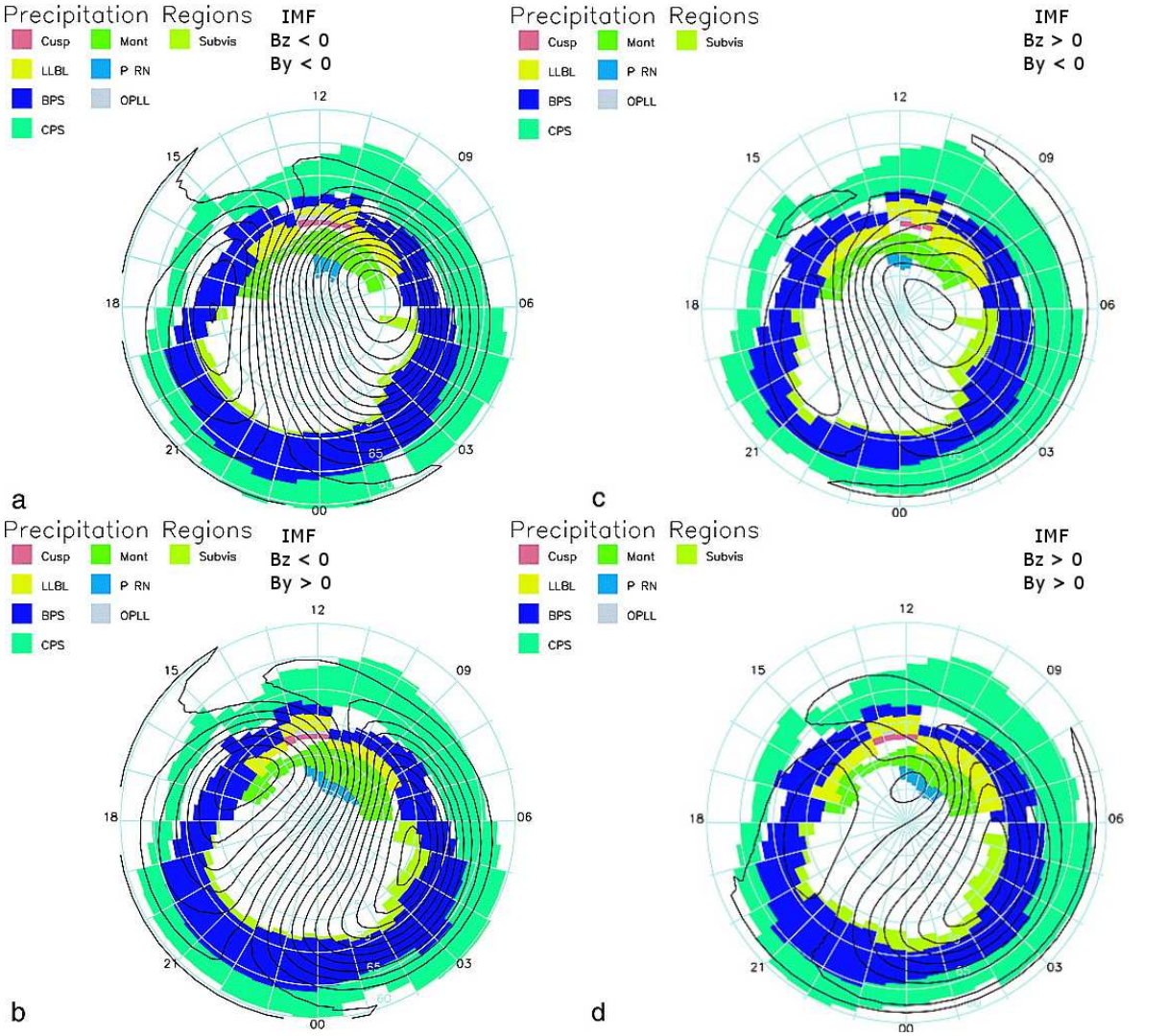

Figure 2.7: *Maps of ionospheric precipitation according to the source region, with superposed inertial convection streamlines: (a) for $B_z < 0$ and $B_y < 0$; (b) $B_z < 0$, $B_y > 0$; (c) $B_z > 0$, $B_y < 0$; (d) $B_z > 0$, $B_y > 0$. (Newell et al., 2004)*

marked as light green in figure 2.7 .

Cusp: High-intensity fluxes of electron and ion of magnetosheath origin. Average electron energy < 300 eV and average ion energy < 3 keV (Newell et al., 2004). Shown in figure 2.7 at noon and marked as light red.

Polar Rain: Low-energy electrons (few hundred eV) of magnetosheath origin. Precipitate relatively uniformly over the entire polar cap (Fairfield and Scudder, 1985). A B_y related dawn-dusk asymmetry is documented in this thesis. Marked as light blue in figure 2.7

2.5 Polar Arcs

High-latitude polar arcs (auroral arcs occurring poleward of the auroral oval) are a common phenomenon during northward IMF (Valladares et al., 1994 and references therein). The presence of polar arcs is associated with ion flow shear (irregular convection) (Reiff et al., 1978). There are many types of polar arcs and they differs in size, shape, magnetospheric and solar origin. In 2002 Kullen et al. showed by help of a statistical study the dependence of large-scale polar arcs on the IMF direction. They distinguish between five types of polar arcs which are shown each to be related to a characteristic combination of solar wind parameters. They found that the majority of polar arcs occurs under northward IMF, strong IMF magnitude and/or high solar wind speed. The results show that those polar arcs occurring after $1-2$ hour of nearly constant IMF with a positive IMF B_z and a nonzero IMF B_y component are always static polar arcs near one oval side (oval-aligned arcs). The location of polar arcs is strongly dependent on the sign of IMF B_y (Elphinstone et al., 1990; Valladares et al., 1994; Kullen and Janhunen, 2004). Oval aligned arcs usually appears near the duskside (dawnside) oval for IMF B_y positive (negative) for a broad range of time spans (average of 2 hours) and for IMF clock angle regions of $40-70^\circ$ and $70-110^\circ$ (e.g. Kullen et al., 2002). Eriksson et al. (2003) presented a study suggesting a close correlation between the lobe cell sunward convection region and particle precipitation on the flow channel boundary. These are oval-aligned arcs appearing predominately for $B_z > 0$ but they are also present for $B_z < 0$ when the ratio $|B_y/B_x| > 1$, i.e for B_y dominated IMF conditions. Field-aligned current (FAC) inside the polar cap during northward IMF, referred to as northward IMF B_z (NBZ) currents, may be related to high-latitude polar arcs (Zhu et al., 1997; Eriksson et al., 2003 and reference therein). Eriksson et al. (2005) suggested that the dayside part of the transpolar arc (TPA),e.g. oval-aligned arcs, corresponds to the enhanced sunward flow (1000 m/s) of the duskward side of a lobe convection cell for northward IMF B_z and positive IMF B_y.

Chapter 3

The Methodology

3.1 Magnetic Cloud

Coronal mass ejections (CME) are eruptions into interplanetary space of as much as a few billion tons of plasma and embedded magnetic fields from the Sun's corona. The term interplanetary CME (ICME) used as interpretation of in situ observations of CME in the solar wind near 1 AU. It is believed that magnetic clouds (MC) are a subset of coronal mass ejections, with a specific magnetic field configuration and unique plasma properties (Burlaga, 1995; Lepping and Berdichevsky, 2000). MC is not the only interplanetary ejecta that's exist, thus it is important to take care when determining if an interplanetary ejecta is a MC. Magnetic clouds may be modelled as magnetic flux ropes and are associated with disappearing filaments and solar flares (Goldstein, 1983; Burlaga, 1988). Figure 3.1 depicts the widely accepted geometry of MCs (taken from Marubashi, 1997). Burlaga et al. (1981); Klein and Burlaga (1982); Burlaga (1995) used three essential features for identification of a magnetic cloud. (1) A strong magnetic field with (2) a smooth and slow rotation of the magnetic field direction (1-2 days) through a large angle, close to 180°, as the magnetic cloud moves past the spacecraft and the earth, and (3) a low proton temperature and low proton β (< 0.1). Near 1 AU the average parameters of the cloud is 0.25 AU, with duration of 27 h, an peak magnetic strength of ~15 nT and the average solar wind speed is 400 km/s (Klein and Burlaga, 1982; Lepping and Berdichevsky, 2000). Inside the magnetic cloud the density is highly variable, often changing by nearly an order of magnitude in a few hours. Generally, the density inside the magnetic cloud is significantly lower then average, but there are occasional fluctuations which reach the ambient value (Burlaga et al., 1981). A shock appears upstream of the cloud when the speed of the cloud front is faster than the solar wind. Not all clouds move fast enough to drive a shock (Lepping and Berdichevsky, 2000). The region between the shock and the cloud proper is called the "sheath". The sheath region is turbulent with strong magnetic field fluctuations (Burlaga, 1995).

As mention earlier we want to study the interaction of a magnetic cloud with the Earth's magnetosphere in order to determine the association between the IMF and solar wind plasma orientations and the different states of the magnetosphere as monitored by polar cap precipitation. The different quasi-stable IMF conditions, produced by the smooth and slow rotation of the cloud field, makes it easier to determine the IMF orientations corresponding to the different the ionospheric flow precipitations.

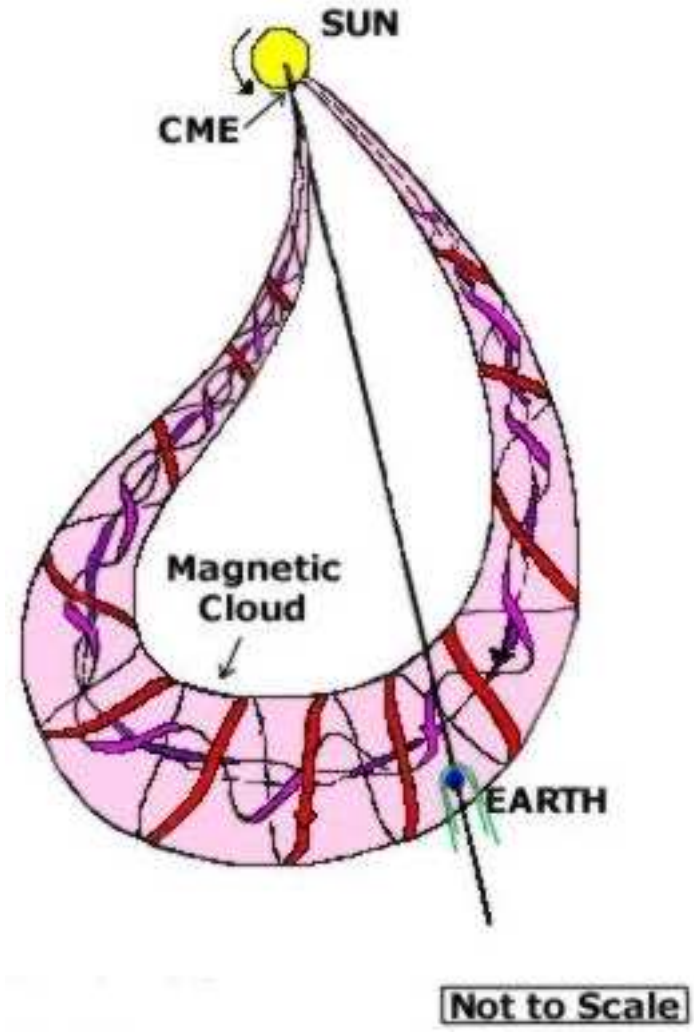

Figure 3.1: *Sketch illustrating the geometry of interplanetary MCs (from Marubashi, 1997). The central parts, i.e., the leading fronts, of the MCs are indicated by shading*

3.2 Satellite Instrumentation

3.2.1 Defence Meteorological Satellite Program F13 and F15/F16

The Defence Meteorological Satellite Program (DMSP) are a series of polar-orbiting spacecraft with orbital height of 835 km. The spacecraft are placed into orbits that are fixed in local time with equatorial crossing times near either 0600 local time and 1800 local time (DMSP F13) or near 0900 local time and 2100 local time (DMSP F15 and F16). Because of the dipole tilt of the Earth's magnetic field, the satellite's ground track "walks" back and forth over the course of a day. Thus how close the observed satellite's ground track is to theoretical orbit varies on every DMSP crossing over the polar cap. The orbit period for the DMSP satellites is roughly ~90 minutes, and they orbit the Earth around 13-14 times in 24 hours. One of missions of DMSP is to monitor the near-Earth space environment.

The instruments F13 and F15 uses to obtain data about the space weather are the SSIES package

(thermal plasma instruments including a Retarding Potential Analyser (RPA), Ion Drift Meter (IDM), Langmuir probe, and a scintillation meter) built at the Center for Space Sciences at the University of Texas at Dallas. Other sensors include the auroral particle spectrometer SSJ4 (precipitating ions and electrons monitor (30 eV - 30 keV), built by USAF Research Lab, Space Vehicles Directorate), SSM (vector fluxgate magnetometer, built by USAF Research Lab, Space Vehicles Directorate and Goddard Spaceflight Center).

The SSJ4 detector flown on F13 measure the flux of precipitating electrons and ions in the range of 30 eV to 30 keV. The measurements are made by 4 detectors, one high energy detector and one low energy detector for the each of the particle types.
The Special Sensor-Ions, Electrons, and Scintillation (SSIES) measures the thermal plasma at the location of the spacecraft. The SSIES sensors are tailored to the anticipated environment at 840 km altitude and at all latitudes, all local times, all seasons and all phases of the sunspot cycle. Typically this environment is composed of three ion species; hydrogen (H+), helium (He+) and oxygen (O+).
The SSM is a triaxial fluxgate magnetometer system used to measure the magnetic field. This field has three sources: (1) the magnetic field from the solid Earth, (2) the magnetic field from electrical currents flowing in the ionosphere and magnetosphere, and (3) the magnetic field from the spacecraft. Measurement of source 2 is the principal objective of the SSM, measurement of source 1 is a secondary objective, and measurement of source 3 is a nuisance which is eliminated from the data as much as possible during data processing. These are the essential instrument that we are using in this study. Data has been obtained from (Rich, 1994; DMSP/AFRL Space Weather Data Survey Website, 2007; DMSP SSIES Data Distribution at UT-Dallas Website, 2007).

Figure 3.2 is a example of how we are going to present the DMSP data. Each plot shows 30 minutes of data and it starts some where near 45° MLAT at dusk/dawn and covers the entire high latitude portion of the orbit and end near 45◦ MLT on the other side of the polar cap at dawn/dusk. The example we are going to present is from data obtained by spacecraft DMSP F13 during the time 1325 - 1355 UT on 13 June 2005. The DMSP F13 passes over the northern (southern hemisphere) in a dusk to dawn (dawn to dusk) orbit (1730-0530 MLT). The panels in the left figure from top to bottom show (a) electron and (b) ion precipitation (particle flux versus energy), (c) ion densities, (d) ion drift velocities transverse (violet) and along (green) to the satellite trajectory, and (e) magnetic deflection components B_x, B_y, and B_z. Under the panels the universal time (UT), the magnetic latitude (MLAT) and the magnetic local time (MLT) for the spacecraft is given. Since the number flux of electrons is much higher than the number flux of ions, there are separate flux-to-colour conversion tables for the electrons and ions (shown to the right of panel 1 and 2). The panel on the right side of figure 3.2 is the cross-track plasma drift from the same data and is derived from the SSIES thermal instrument (see below). The DMSP cross-track plasma drift data is mark with different quality flags where black being good, yellow being questionable, red being poor and blue being undetermined. In this thesis we will only use DMSP cross-track plasma drift data which we have rated as good and more proper explanation of the different flag values is given in section A.

We used vertical guidelines to divide different region in figure 3.2. By use of the data shown in the electron precipitation (panel 1), ion drift velocities transverse (violet) the satellite trajectory

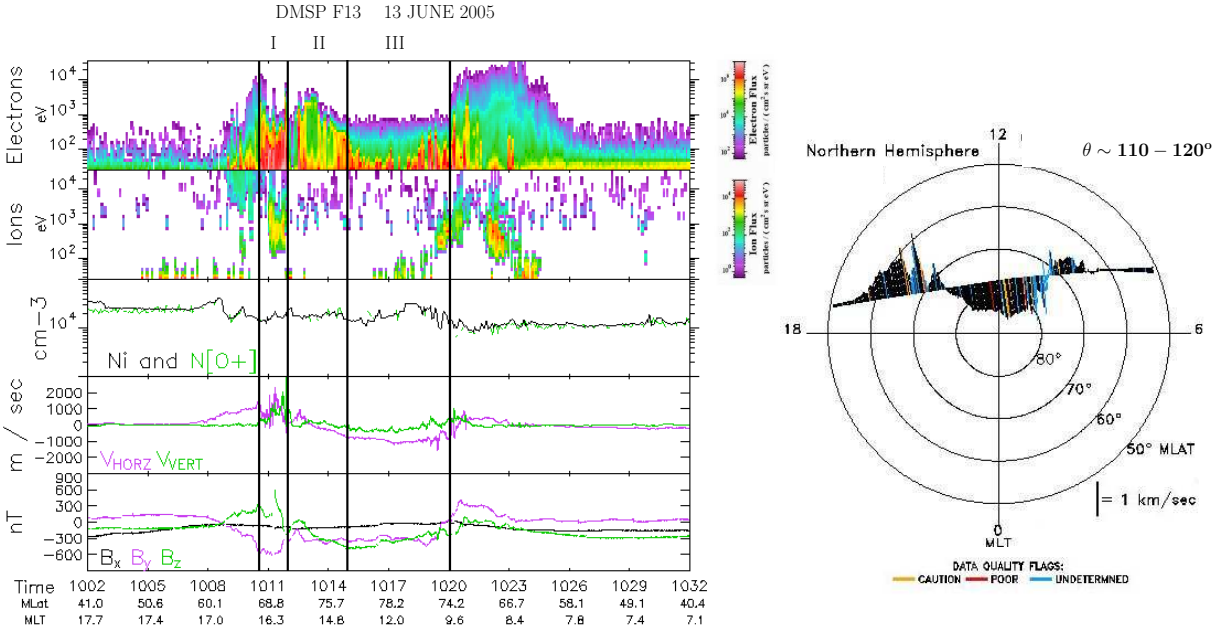

Figure 3.2: *Data obtained by DMSP F13 during the interval 1002 - 1032 UT on 13 June 2005. The panels in the left figure from top to bottom show (a) Precipitation flux of electron and (b) ions (particle flux versus energy), (c) ion densities, (d) ion drift velocities transverse (violet) and along (green) the satellite trajectory, and (e) magnetic deflection components B_x, B_y, and B_z. Different convection and precipitation regions are indicated by vertical guidelines and marked with (I,II & III). Panel to the right show the the cross-track plasma drift from the same data shown in the panels to the left. The DMSP Cross-track plasma drift data is marked with different quality flags where black being good, yellow being questionable, red being poor and blue being undetermined.*

(panel 4) and magnetic deflection components B_z (green) (panel 5) three distinct regions have been marked I, II and III.

At low latitude at dusk, equatorward of region I, homogeneous electron precipitation of $\sim$ 10 keV (panel 1) coincides with a positive gradient in the sunward flow (panel 4) and B_z (panel 5) towards dawn. A positive (negative) trend in B_z represent a downward (upward) FAC sheet along the satellite trajectory (Eriksson et al., 2005). This is CPS precipitation coupled to the a downward region 2 (R2) field-aligned current (FAC) at sunward convection.

Distinct high-latitude arcs with BPS precipitation is co-located with flow shear and small scale upward NBZ-like FAC in region II.

In region I structured electrons with with energy $\sim$ 0.5 – 10 keV (panel 1) coincides with an enhanced sunward flow channel (panel 4) and negative B_z gradient (panel 5). This is BPS precipitation with an upward R2 FAC in the enhanced sunward flow channel.

Region III shows unaccelerated homogeneous polar rain of a few hundred eV with stable anti-sunward convection.

In general when we mark the DMSP data with the notation I,II and III the data will be similar to the regions described over. This mean that prior to region I we encounter CPS precipitation. In region I BPS precipitation is seen. In region II and III high-latitude arcs and polar rain is seen, respectably.

3.2.2 Wind

The Wind spacecraft was launched by NASA in 1994. The main scientific goal of the mission is to measure the mass, momentum and energy of the solar wind. Onboard are a lot of different scientific instruments for measuring the charged particles and electric and magnetic fields that characterize the interplanetary medium. We will use Solar Wind Experiment (SWE) and the Magnetic Field Investigation (MFI) (Lepping et al., 1995) on the Wind spacecraft.

SWE The Wind SWE provide measurements of the solar wind protons and alpha particles at energy/charge up to 8 keV (Ogilvie et al., 1995). The SWE instrument also carries an array of detectors built at NASA-GSFC (Goddard Space Flight Center) for characterizing the solar wind electrons. The SWE on-board data system was provided by the University of New Hampshire. The time resolution for the SWE proton key parameters is approximately 90 seconds. The SWE instrument package is more comprehensively described in the article by Ogilvie et al. (1995) and at (WIND-Solar Wind Experiment (SWE) - MIT Space Plasma Group Website, 2007).

MFI The magnetic field experiment on Wind provides data for studies of a broad range of scales of structures and fluctuation characteristics of the interplanetary magnetic field. The basic instrument of the Magnetic Field Investigation is a boom-mounted dual triaxial fluxgate magnetometer and associated electronics (Lepping et al., 1995). The time resolution changes from 46 seconds (when the spacecraft is within $60R_E$) to 92 sec (when the radial distance is bigger then $60R_E$). The MFI instrument package is more comprehensively described in the article by Lepping et al. (1995) and at (Magnetic Field Investigation (MFI) on the WIND Spacecraft Website, 2007).

3.2.3 The Imager for Magnetopause to Aurora Global Exploration (IMAGE)

The IMAGE spacecraft was launched on March 25, 2000 and the goal of the mission is to imaging the Earth's magnetosphere. The Imager for Magnetopause to Aurora Global Exploration (IMAGE) investigates the response of the magnetosphere to the time variable solar wind (The Imager for Magnetopause-to-Aurora Global Exploration (IMAGE) Website, 2007). IMAGE employes a variety of techniques to imaging the Earth's magnetosphere and to produce the first global images of the plasma populations in the inner magnetosphere. There are many different instrumentation onboard IMAGE and one of them are the Far-UltraViolet (FUV) Imaging System instrument which employs 3 detectors: The Wideband Imaging Camera (WIC), The Spectrographic Imager (SI) and Geocorona photometers (GEO) (IMAGE Far-Ultraviolet (FUV) imager Website, 2007). The Wideband Imaging Camera (WIC) can be used to image the total intensity of the aurora in broad band for maximum spatial resolution at day and night with sensitivity in the spectral region from 140 to 190 nm (Mende et al., 2000).

Figure 3.3: *SuperDARN radar location for the northern hemisphere (Super Dual Auroral Radar Network (SuperDARN) Website, 2007).*

3.3 Ground Instrumentation

3.3.1 Ground Magnetometer

Imaging the Earth's magnetosphere by using ground-based magnetometer arrays is still one of the major techniques for investigating the dynamical features of solar wind-magnetosphere interactions. The one minute-averaged magnetogram data and pulsation data from the 210 MM network (Yumoto and the 210 degree MM magnetic observation group, 1996) can detect the shock upstream of the magnetic cloud. In general, the shock onset time coincides with the beginning of a sharp increase of the H (or X) component detected at individual ground stations in the 210 MM array. This feature is known as a sudden impulse (SI), or a sudden commencement (SC) (Nishida, 1978). SC are a global magnetospheric phenomenon caused by interplanetary shocks and other discontinuities. When the IMF of magnetic cloud in our cases shows a tendency of turbulent behaviour or the IMF is southward behind the interplanetary shock, geomagnetic storms can develop following so-called storm sudden commencements (SSC). When the IMF remains to the north behind the shocks, SC are not followed by geomagnetic storms.

3.3.2 SuperDARN (Super Dual Auroral Radar Network)

The Super Dual Auroral Radar Network (SuperDARN) is an international radar network comprised of nine radars in the northern hemisphere and six in the southern hemisphere for measuring the ionospheric plasma drift (or equivalently, the ionospheric electric field) (Greenwald et al., 1995). Figure 3.3 shows the location of the SuperDARN radars in the northern hemisphere. The radar sends out multipulse transmission sequence in the High Frequency (HF) band which are refracted toward the horizontal as they enter ionospheric regions with higher electron densities. The backscattered signals provides information about large-scale convection

and related processes (power, velocity and spectral width of the plasma) in the radar field of view. The large line-of-sight velocity measurements for each radar pair is then combined to produce maps of large scale ionospheric convection of the polar cap. By combining the Super-DARN global convection maps with other data, such as IMF data, a more accurate picture of convection pattern in polar cap is obtained.

Chapter 4

Case study 1: August 12-13, 2000

In this case study we investigate the ionospheric flows during the interval when the magnetic cloud (MC) observed on August 12-13, 2000 interacts with Earth. This MC caused a strong magnetic storm on the Earth. The cloud drives a shock that is sensed at the Earth's surface as a sudden increase in the geomagnetic field intensity, called a storm sudden commencement (SSC) (Kivelson and Russell, 1995, chap. 9.2). The magnetic cloud is oriented such that an 12.5-hour period of B_z <0 is followed by B_z >0 for the rest of the cloud interval. A strong positive B_y component (∼20nT) is present except during a 3 hour time period in the beginning of the cloud passage. From the statistical survey of Huttunen et al. (2005) this cloud was observed at ACE in the interval 0520-0200 UT August 12-13, 2000 and was classified as a South-East-North (SEN) cloud (Lepping et al., 2005). The storm index D_{st} is a measure of geomagnetic activity used to assess the severity of magnetic storms. The D_{st} index in our case had a minimum of −235 nT at 10 UT and an average of -150 nT for the rest of the day. The hourly Dst index, for the studied period, was obtained from the World Data Center for Geomagnetism, Kyoto. As a reference frame we know that a D_{st} between −100 to −200 nT is referred to as a strong storm and below −200 nT as a severe storm (Loewe and Prölss, 1997). Our focus is on four DMSP F13 passes over the northern hemisphere in the time period 1300 UT-2200 UT on August 12, 2000. All of these passes occurred in the clock angle regime between 70-115°.

4.1 Interplanetary Data Set

Figure 4.1 shows interplanetary plasma and field parameters from the solar wind experiment (SWE) (Ogilvie et al., 1995) and the magnetic field investigation (MFI) (Lepping et al., 1995) on the Wind spacecraft. The data resolutions are 3 sec (MFI) and 90 sec (SWE). From top to bottom, the panels show the proton density (cm^{-3}), temperature (K), the bulk speed (km/s), dynamic pressure (nPa), the total magnitude (nT) and GSM X, Y, and Z components of the magnetic field (nT), plasma β, and the IMF clock angle (polar angle in the GSM YZ plane) for the period 0500-2400 UT (ground time, see section 4.1.1) on 12 August, 2000. The horizontal axis shows the universal time in hours. The red trace in the temperature panel gives the expected temperature for normal solar wind expansion from the statistical studies of Lopez and Freeman (1986). In two articles Farrugia et al. (2005) and Farrugia et al. (2005) documented the correlation/coherence coefficients and length scales for ambient IMF and magnetic cloud parameters. They showed that there is a good correlation up to 400-450 R_E in the X-direction

and that also a Y displacements of ∼248 R_E is acceptable inside the MC. This means that the field inside the magnetic cloud remains coherent for large distances and therefore data obtained from satellites within these separations along and perpendicular to the Sun-Earth line gives the conditions affecting the Earth's magnetosphere.
In our case the Wind satellite was located at (-16.00, -59.4, -5.6) R_E in GSE coordinates and this means that the spacecraft is on the dawnside of the Earth. The distance between Wind and the subsolar magnetopause is ∼62 R_E and this is well inside the criteria found by Farrugia et al. (2005) and Farrugia et al. (2005). The start of the magnetic cloud can be seen in the Wind data as decrease in the the proton temperature to values lower than the expected temperatures at ∼0620 UT (see panel 2 figure 4.1 and vertical guideline). The interval prior to cloud proper is called the sheath of the MC and is characterized by strong magnetic field fluctuations. The difference between the behaviour of total magnetic field (panel 5 in figure 4.1) before and after the cloud start can be seen by the smoothness of the curve. The B–field curve is much smoother inside the cloud. This is in agreement with the three essential features of a magnetic cloud (see section 3.1). A prominent feature of these data is the strong B_y component of 20 nT from 10 UT onwards. While B_y retains its positive polarity (except for a brief transition in the beginning), the north-south component (B_z) undergoes a rotation from -25 to 15 nT (clock angle from 170° to 45°). The solar wind is a high speed stream (∼ 600-550 km/s) with high density and dynamic pressure ∼10 cm^{-3} and ∼6 nPa, respectively. From the Wind data we see that in the time period from 1230 UT till 1730 UT the density and dynamic pressure is higher than in the rest of the cloud. The first vertical guidelines mark the arrival of the cloud proper. Different time intervals have been named I and II (panel 1) and marked with vertical guidelines in figure 4.1. The intervals are mainly chosen after the behaviour of the clock angle.

4.1.1 Time Delay

A simple estimate of the Wind satellite-to-magnetopause delay, based on the normal direction of the satellite from the Earth and the solar wind speed, gives 10-11 min. Another way of visualizing this is to consider the shock. There is namely a weak shock driven by the magnetic cloud. As the shock interacts with the magnetosphere it produces a sharp rise in the H-component of the terrestrial field at low latitudes. We examined data from ground station Biak (BIK) from the 210 MM network (Yumoto and the 210 degree MM magnetic observation group, 1996) and found a weak SCC at 1848 UT. Ground station Biak is located at latitude −1.08° and longitude 136.05° in geographic coordinates (−9.74° MLAT and 207.64° MLONG). Figure 4.2 shows the shock front with the parameters density N, total velocity V and the total magnetic field B for the spacecraft's ACE, Geotail and Wind and figure 4.3 shows the SCC at the ground station Biak. The following time of arrival of the shock front and the SCC is given in the table 4.1. From table 4.1 we see that the shock arrives at ground station Biak and Wind at 1847 and 1850 UT respectively. The small delay between Wind and ground is considered unimportant because of the steady conditions of the magnetic cloud (see section 3.1).

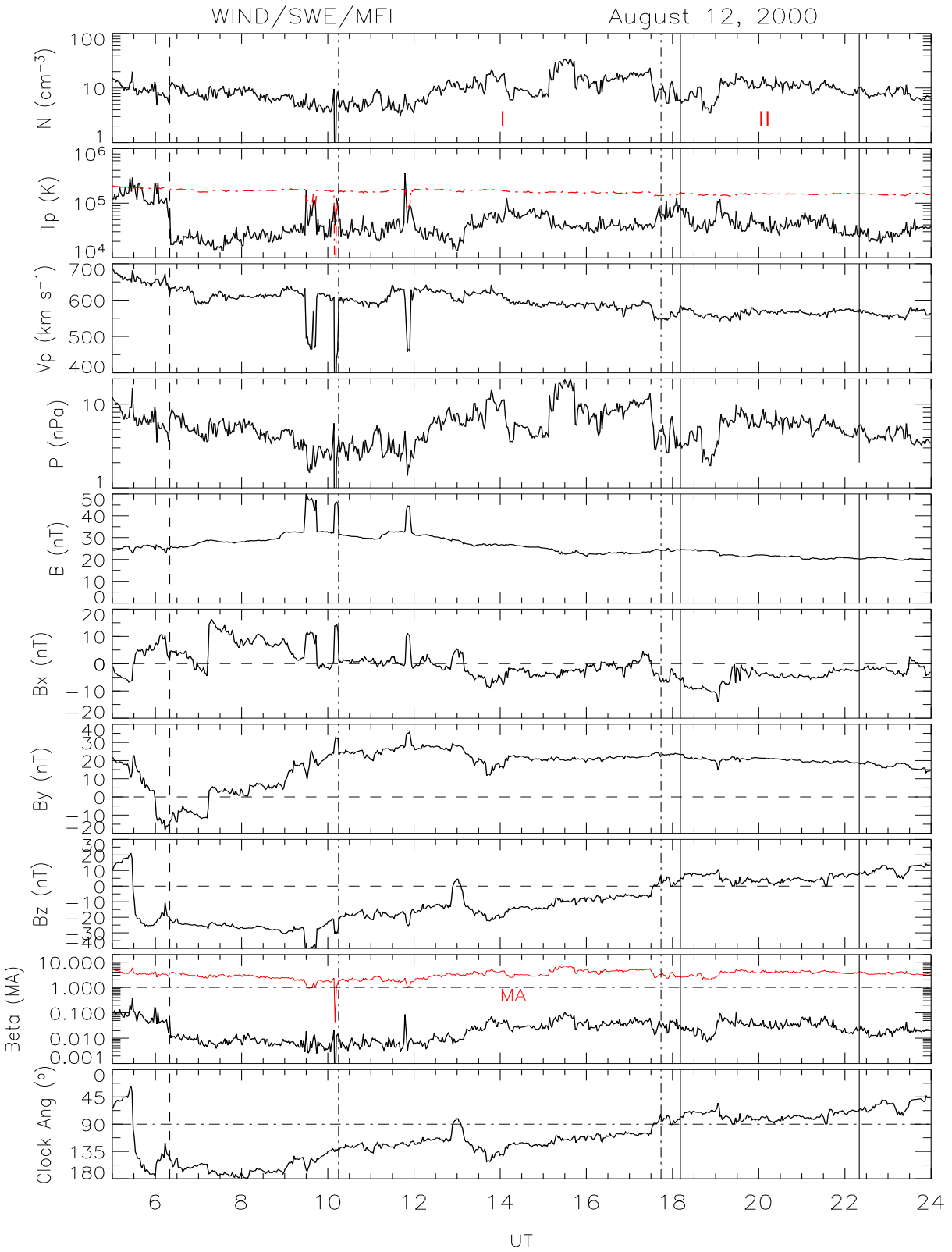

Figure 4.1: *Solar wind plasma and interplanetary magnetic field (IMF) data obtained from spacecraft Wind during the interval 0500-2400 UT (ground time) on 12 August 2000. Panels from top to bottom show proton density, temperature, bulk speed, dynamic pressure, the total field, the GSM components of the magnetic field, plasma β and Alfv́en-Mach number (the latter in red) and the IMF clock angle. The red trace in the temperature panel gives the expected temperature for normal solar wind expansion from the statistical studies of Lopez and Freeman (1986). The horizontal axis shows the universal time (UT) in hours.*

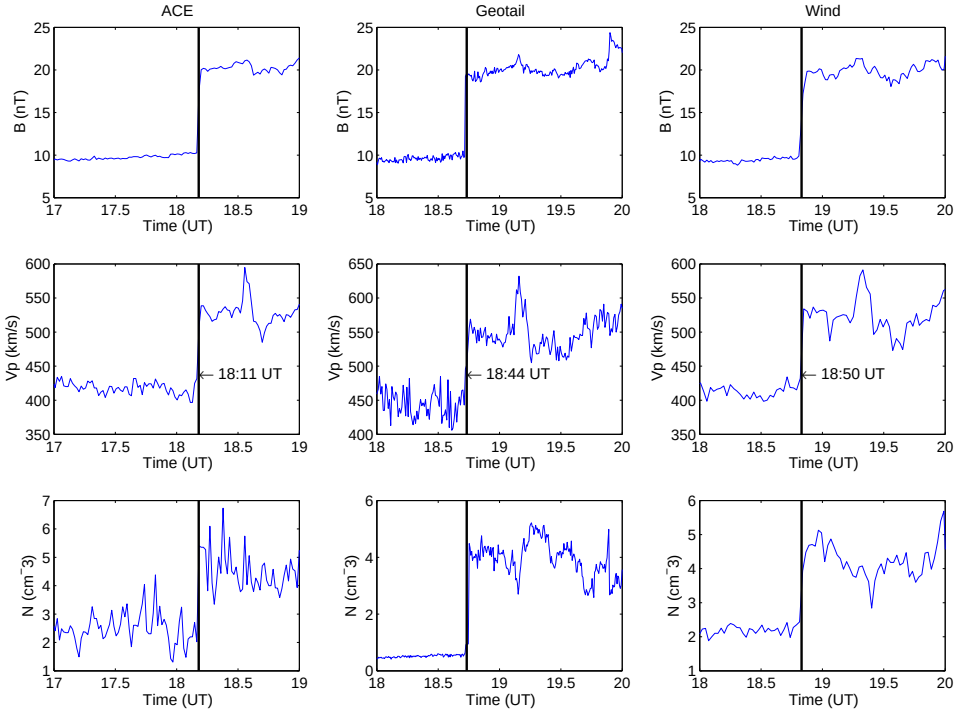

Figure 4.2: *Time of arrival of the shock front at ACE, Geotail and Wind. With the parameters (top to bottom): Density N, Total Velocity V and Total Magnetic Field B*

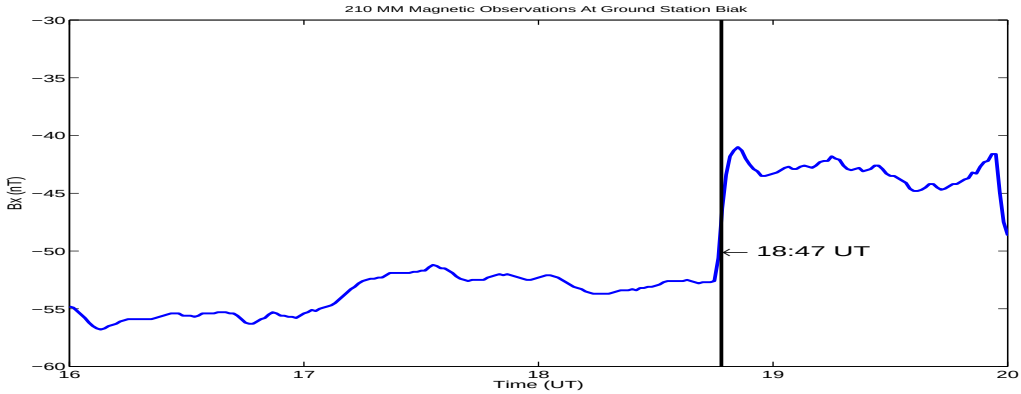

Figure 4.3: *Time of arrival of the SSC at the ground station Biak (BIK)*

Station	*Time*	*Interval*
ACE	18:11 UT	
Geotail	1844 UT	+ 33 min
BIK	1847 UT	+ 36 min
Wind	1850 UT	+ 39 min

Table 4.1: *Time of arrival for the shock*

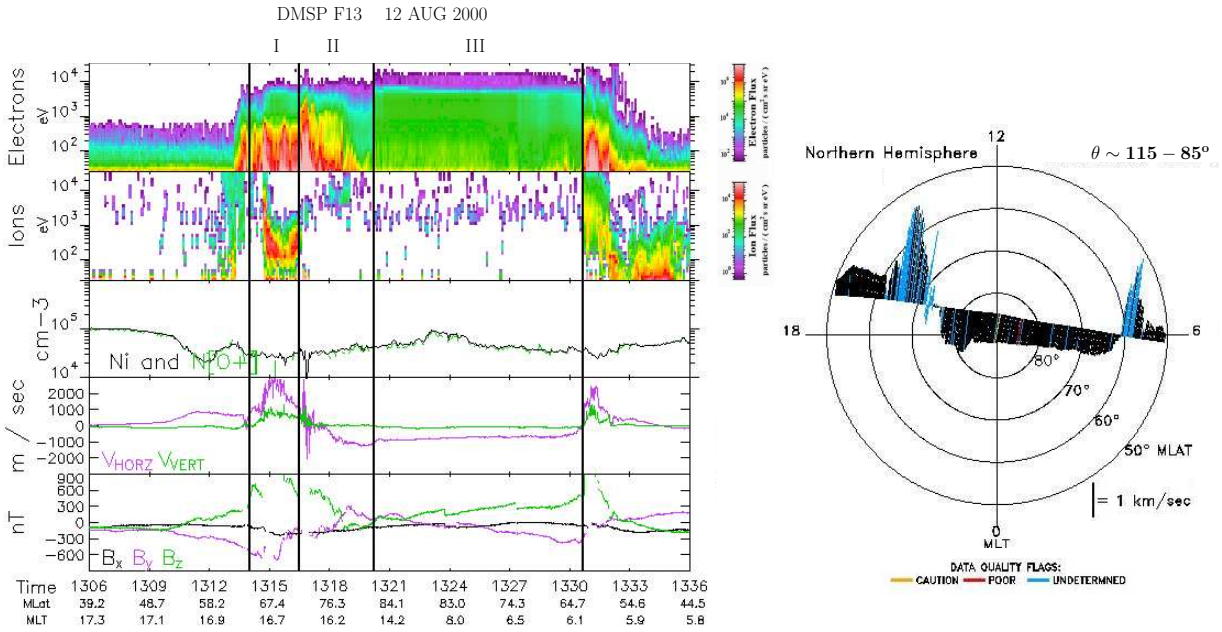

Figure 4.4: *Data obtained by DMSP F13 during the interval 1306 - 1336 UT on 12 Aug 2000. Same format as figure 3.2 in section 3.2.1)*

4.2 DMSP results

We shall now interpret the DSMP observations with the attempt to establish a one-to-one mapping of the ionospheric convection to the interplanetary conditions observed at Wind. It takes around 20-30 min for DMSP to cross the polar cap from dusk to dawn, during this time period the IMF parameters might have changed. However by using a magnetic cloud passage we get slowly varying magnetic cloud conditions and therefore it will not be a problem for us for the most of the time. The large-scale ionospheric convection pattern will be insensitive to small spikes in the IMF data which are occurring at time scales <10-15 min.

4.2.1 Interval I, 1015 - 1745 UT, Clock Angle [100-135°]

During this interval we choose to look at two DMSP F13 passes over the northern hemisphere polar cap. They occurred between 1306-1336 UT and 1630-1700 UT. Wind measured fairly stable solar wind speeds of 600-575 km/s and density fluctuating from 4-20 cm^{-3}. In this interval the cloud had a total magnetic field strength of 20-30 nT with the components as following: $B_z < 0$, $B_y > 0$ and $B_x \approx 0$. The clock angle slowly decreased from 135° to 90° with an exception in the interval ~1245 to 1430 UT. The field orientation is changing from southeast to east.

DMSP F13 1306-1336 UT, Clock Angle [115-85°]

The first DSMP pass in this interval is presented in figure 4.4. From figure 4.1 we see that the clock angle shifts from 115° to 85° and back to 115° again in a period of 18 minutes at ~1300 UT. The response time for the convection pattern in the ionosphere at dusk and dawn is around 20 min (see section 2.1.4) and because the time scale of this irregularity (18 min) is comparable to the response time, we can not be sure if the ionospheric convection pattern will respond to

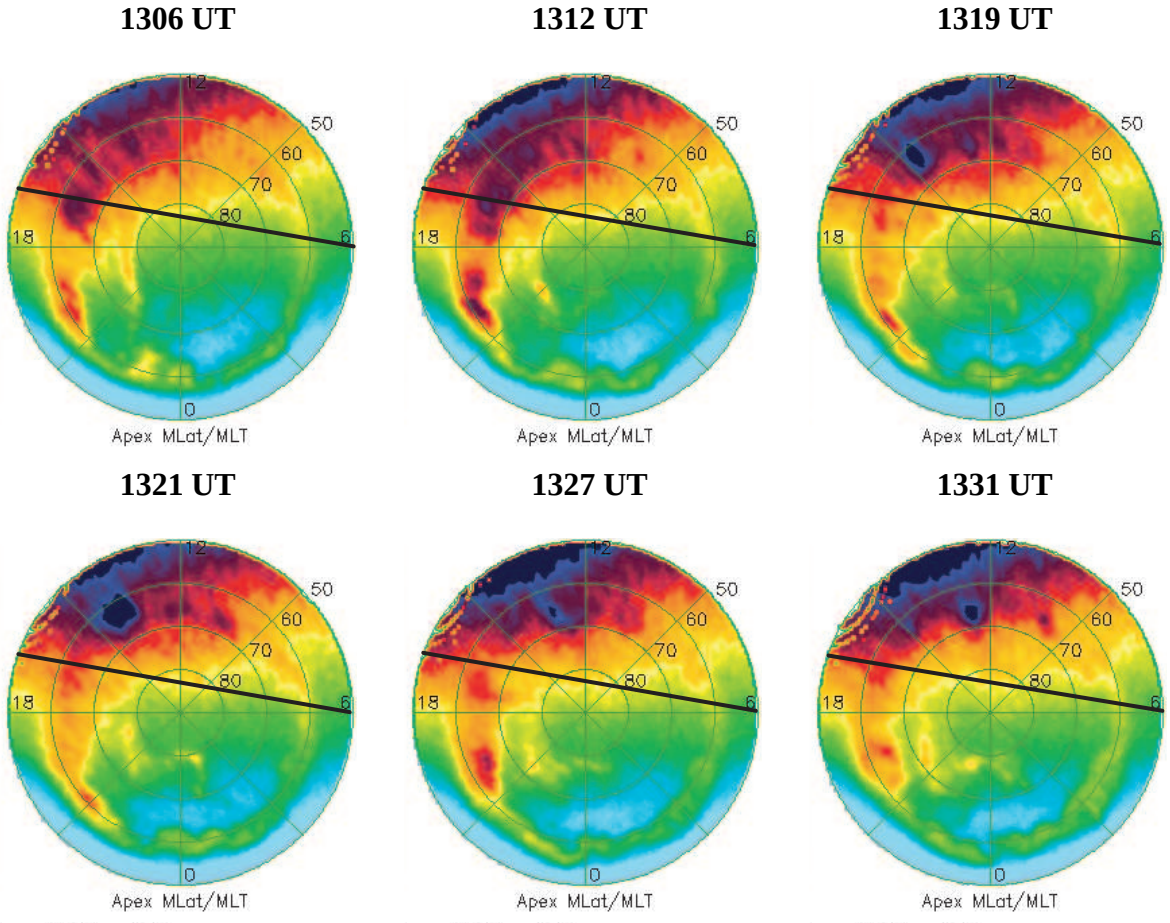

Figure 4.5: *Picture sequence from the Wide-band Imaging Camera (WIC) on the spacecraft IMAGE during the interval 1325-1335 UT. The DMSP F13 track has been overlaid as a thick black line.*

this sudden change in clock angle. It is in this interval our first DMSP pass is occurring and just to be on the safe side we set the clock angle to be in the regime between 115-85°. The format of figure 4.4 and all subsequent figures showing DSMP data in this thesis is in the same format as the figure 3.2 in section 3.2.1. We concentrate on the observations made for different convection and precipitation regions which we have marked with vertical guidelines (I,II & III) (see section 3.2.1 for further information). At low latitude at dusk homogeneous CPS precipitation with energy ~9-10 keV is seen. From 1314 to 1317 UT (marked I) the satellite traverses into region where we encountered typical BPS-like precipitation with mixture of low- and high-electrons energy (~800-900 eV). An ion dispersion is visible at 1315 UT in which the energy decreases with increasing latitude. After 1317 UT and to 1320 UT (marked as region II) the BPS-like electron precipitation from the previous region increases to distinct energies of ~2-3 keV while the intense fluxes of ions is absent. Thus in region II the spacecraft encounters a region of discrete, but relatively weak high-latitude arcs. Very intense homogeneous polar rain going up to almost 1 keV is observed in region III from 1320-1331 UT.
In the cross-track plasma drift (right panel) we see a channel of enhanced sunward convection with flows >3 km/s in region I. A strong flow shear from sunward to antisunward convection is seen in region II. A antisunward flow (~500 m/s) is encountered in the central polar cap with the

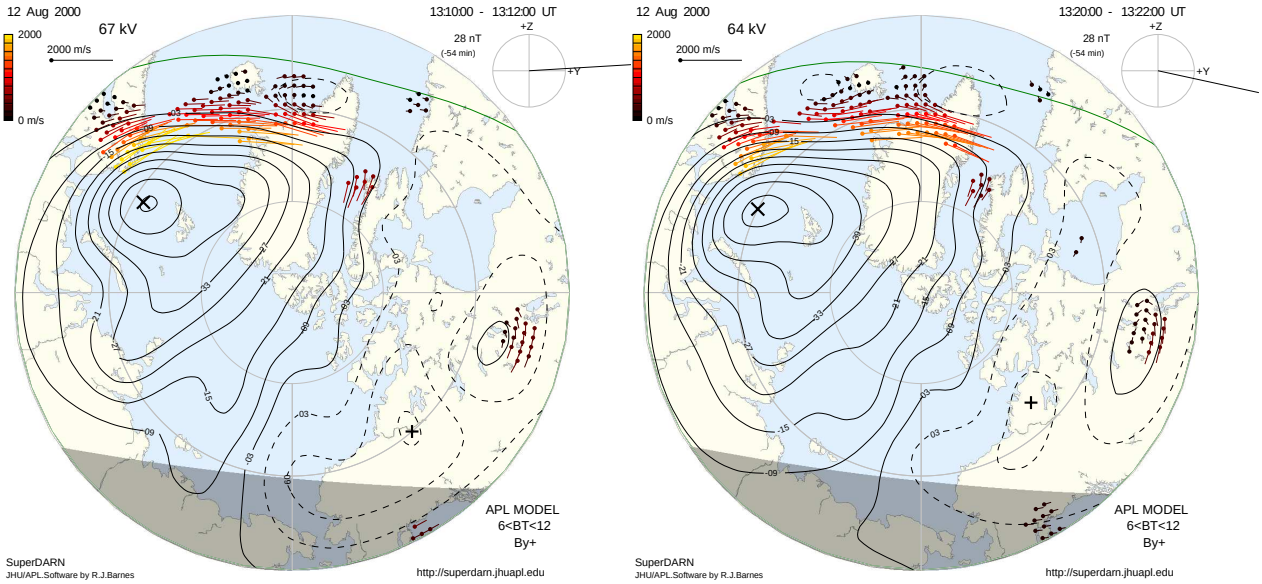

Figure 4.6: *Large scale convection maps from the SuperDARN radars at 1310 UT (left figure) and 1320 UT (right figure). The coordinate system is magnetic latitude versus magnetic local time. Noon is at the top and dusk is to the left. Equipotential contours are shown by the black traces. The coloured vectors show fitted velocities. The IMF direction is shown on the top right, and the cross-cap potential is shown on the bottom right.*

highest flows (−1.5 km/s) displaced towards dusk. This minimum occurs in the end of region II at 80° MLAT. We see that the latitudinal width of the antisunward flow pattern is big.
In the bottom panel a strong positive B_z (green) gradient which correspond to downward FAC system, (see 3.2.1) is observed until ∼1314 UT (equatorward of region I). This is a downward region 2 (R2) field-aligned current (FAC) coupled to the CPS precipitation and sunward convection. In the beginning and end of region I we observe two negative B_z gradients, i.e upward currents. This is an upward R1 FACs co-located with the strong sunward convection and BPS precipitation in region I. As the satellite enters region II (1317-1320 UT) it detects a distinct upward NBZ-like FAC. The upward NBZ-like FAC coincides with distinct high-latitude arcs with electron energy of ∼1-2 keV and flow shear.

The IMAGE WIC figures (see section 3.2.3) obtained during the DMSP F13 orbit gives an overview of the auroral oval and the development of polar arcs in the northern hemisphere between 1306–1331 UT. We have overlaid the DMSP F13 track as a thick black line in figure 4.5. For the whole sequence oval-aligned polar arcs are present poleward of the duskside aurora oval in the region between 72° and 79° MLAT. The presence of bright ”spot” localized in the premidnight sector is seen around 80 MLAT.

SuperDARN Convection maps for 1310 UT and 1320 UT

Figure 4.6 shows the plasma convection pattern obtained from the radars of the Super Dual Auroral Radar Network (SuperDARN) at 1310 UT (left figure) and 1320 UT (right figure) (Super Dual Auroral Radar Network (SuperDARN) Website, 2007). Equipotential contours, shown by

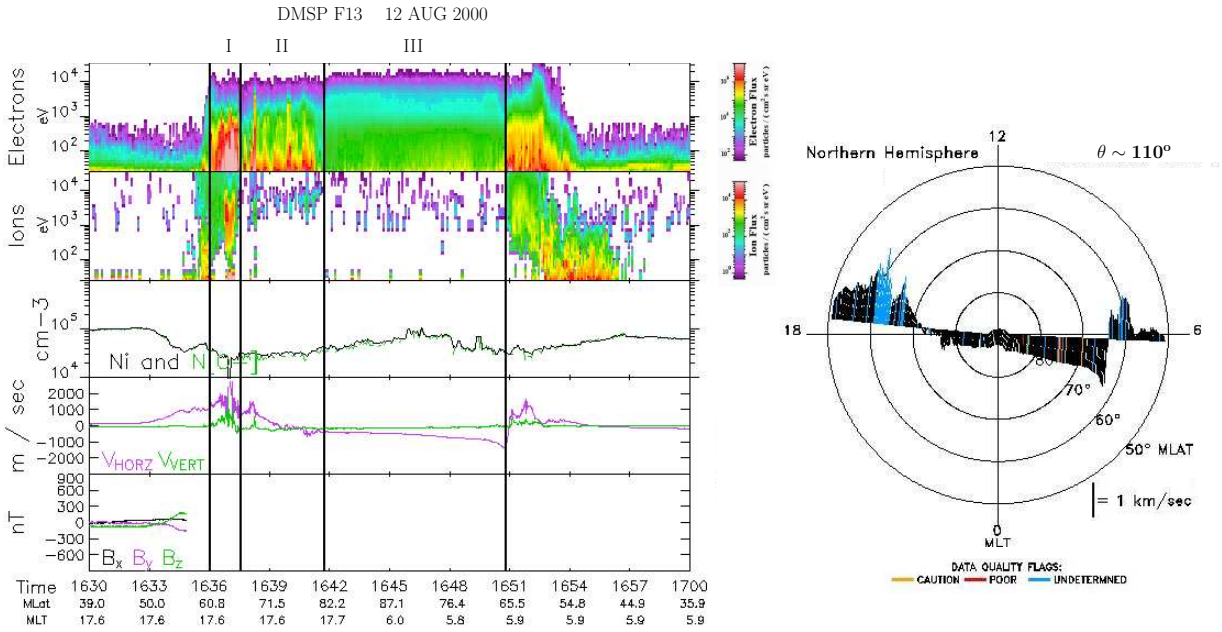

Figure 4.7: *Data obtained by DMSP F13 during the time 1630 - 1700 UT on 12 Aug 2000. Same format as figure 3.2 in section 3.2.1.*

the black lines, is combined with SuperDARN measurements using a fitting technique to produce maps of large-scale ionospheric convection (Greenwald et al., 1995). The SuperDARN convection maps are presented in a magnetic latitude (MLAT) vs magnetic local time (MLT) coordinate system, where 1200 MLT (noon) is at top and 0600 MLT (dawn) to the right. Vectors shown in color and scaled according to the bar on the left of each map, indicates the strength and direction of the ionospheric convection. The total magnetic field, $|B|$ and an IMF clock angle vector gives us a reference of the IMF parameters in the top right corner. At the bottom right the polarity of the IMF components B_z and B_y is given. In figure 4.6 strong dawnward flow in the postnoon and noon sector indicates a distorted/asymmetric convection pattern. This asymmetry in the convection pattern consists of a bigger and more rounded dusk cell compared to the crescent-shaped dawn cell. The lack of data points in the convection map shown in figure 4.6 makes it difficult to get a general view of the flows in the polar cap throughout the interval.

DMSP F13 1630-1700 UT, Clock Angle [~110°]

The second DMSP pass in this interval is presented in figure 4.7. From the Wind data in figure 4.1 we see that the clock angle (bottom panel) is steady around 100°. IMF B_y is 20 nT while the B_z and the B_x is ~ -6 nT and zero, respectively. The format of this figure is the same as the earlier and we have indicated different convection and precipitation regions by vertical guidelines marked with numbers I,II & III.

At lower latitudes at dusk homogeneous electron and ion population reminiscent of CPS precipitation is observed. From 1634 to 1638 UT (region I) BPS-like particle precipitation is observed with structured electron fluxes around 1 keV. At higher latitudes (~65-80° MLAT) signs of discrete polar arcs (high-latitude arcs) at 1638-1642 UT (region II) are seen. The polar arcs precipitation is similar to the previous region with BPS-like electrons of a few hundred eV. From 1642 UT to 1651 UT (marked III) the satellite encounters a region of steady polar rain

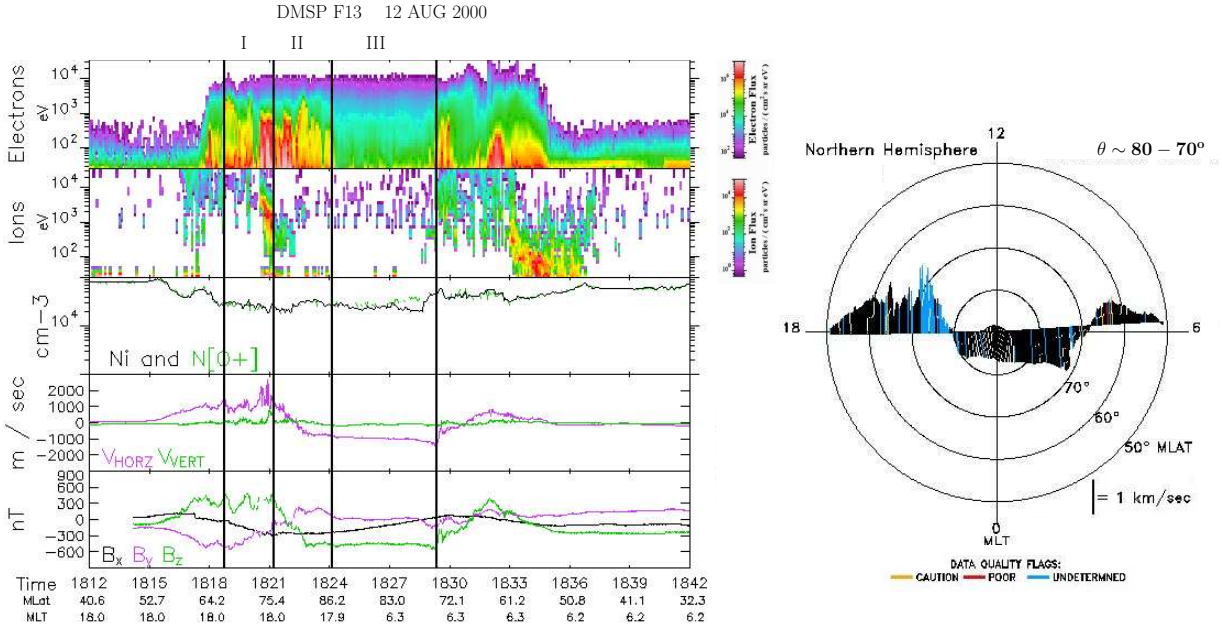

Figure 4.8: *Data obtained by DMSP F13 during the time 1812 - 1842 UT on 12 Aug 2000. Same format as figure 3.2 in section 3.2.1.*

precipitation.
The DMSP plasma drift meter instrument (panel 4) or the cross-track plasma drift (right panel) observes two latitudinally separated channel of enhanced sunward flow centred at about 1637 UT and 1638 UT . The first enhanced flow (∼2 km/s) coincides with the region of BPS precipitation (region I) while the second (∼1.2 km/s) occurs in beginning of region II. As the satellite moves further poleward and dawnward into region II we see a decrease and reversal in the convection flow at 72° MLAT. In region III (1642 UT till 1651 UT) the satellite observes a weak antisunward convection with a gradient towards dawn. We conclude that the polar arcs in region II is observed in a region of relatively strong flow shears.

4.2.2 interval II, 1811 - 2220 UT, Clock Angle [90-70°]

From 1811 UT until 2220 UT the magnetic field is predominantly eastward (positive B_y) with a total magnetic field above 20 nT. This is primarily caused by the strong dominant B_y component (> 20 nT). The B_z component fluctuates around 5 nT while the B_x parameter is weakly negative for the whole period. Because of the small B_z and the strong and dominant B_y component throughout the whole period, the clock angle only shows small signs of changes and is stable around 80°± 10°. Throughout the first 1.5 hours of this interval the density, N, drops from 20 cm^{-3} to around 5 cm^{-3} before it from 1845 UT onwards increases and fluctuates around 10 cm^{-3}. We take note of the fact that the IMF B_x acts in the same way as the density, which means that the IMF B_x goes to lower values (− 10-15 nT) in the beginning of the interval before it increases and fluctuates around − 5 nT). Figure 4.8 and 4.10 we show data from two DMSP F13 passes over the northern hemisphere. The first pass is between 1812 and 1842 UT and the the second between 2133 and 2203 UT.

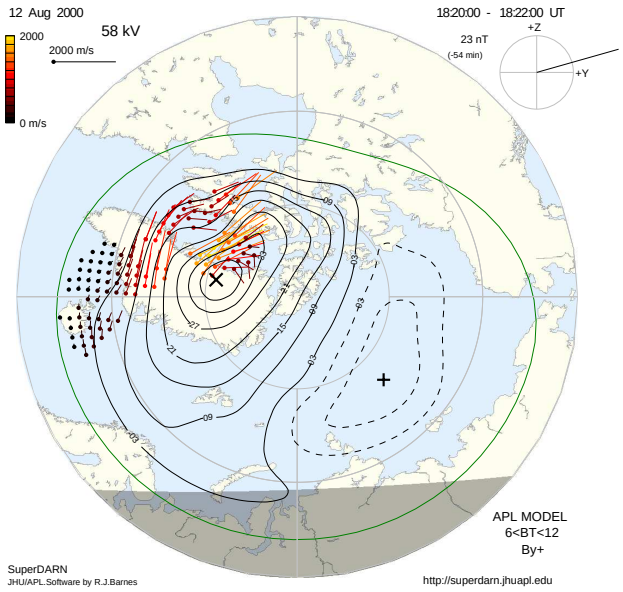

Figure 4.9: *Large scale convection maps from the SuperDARN radars at 1820 UT. The coordinate system is magnetic latitude versus magnetic local time. Noon is at the top and dusk is to the left. Equipotential contours are shown by the black traces. The coloured vectors show fitted velocities. The IMF direction is shown at top right, and the cross-cap potential is shown at bottom right.*

DMSP F13 1812 UT, Clock Angle [90-70°]

The gradual increase in the IMF B_z form 0 nT to 7-8 nT results in a decreases in the clock angle from 90° to 70° throughout this interval.
At low latitude electron fluxes of 1–10 keV indicates a CPS-like source. In region I (~1819-1821 UT) high fluxes of electron ~2 keV coincide with a ion dispersion with energy decreasing from ~6 keV at 72° MLAT to ~2 keV at 76° MLAT. The precipitation have BPS-like origin. Electron precipitation with energy varying from 0.3-3 keV at 76-87° MLAT (region II) and a total drop out in the ion fluxes indicates the presence of polar arcs with BPS precipitation. DMSP F13 encounters polar rain on open field lines after 1824 UT (marked as region III).
The cross-track plasma drift data show sunward flows at low latitude at dawn and dusk with enhanced sunward convection that reach up to 80° MLAT on the dusk side (region I). The enhanced sunward convection from 1819 UT till 1821 with flows ~2-2.5 km/s at 73-75° MLAT coincides with high fluxes of electron and ions in the end of region I. At 1822 UT a strong flow shear from sunward flow (~1000 m/s) to antisunward flow (~500 m/s) is followed by a gradually stronger antisunward convection in the region of polar rain precipitation. Furthermore, the data show an dawn-dusk convection asymmetry in the antisunward flows with stronger velocities towards dawn. As the satellite moves over the polar cap toward dawn (region III) the antisunward flow reaches a minimum at 73° MLAT and this minimum is in the close vicinity of where polar rain precipitation end.
A downward R2 FAC is observed at low latitudes in the bottom panel on the basis of an increasing gradient in B_z (green) at 1815-1818 UT. This is co-located with the CPS particle fluxes and sunward flow (equatorward to region I). Further polewards, i.e in the region of BPS-like precipitation and enhanced sunward convection the B_z–curve is structured with two distinct negative

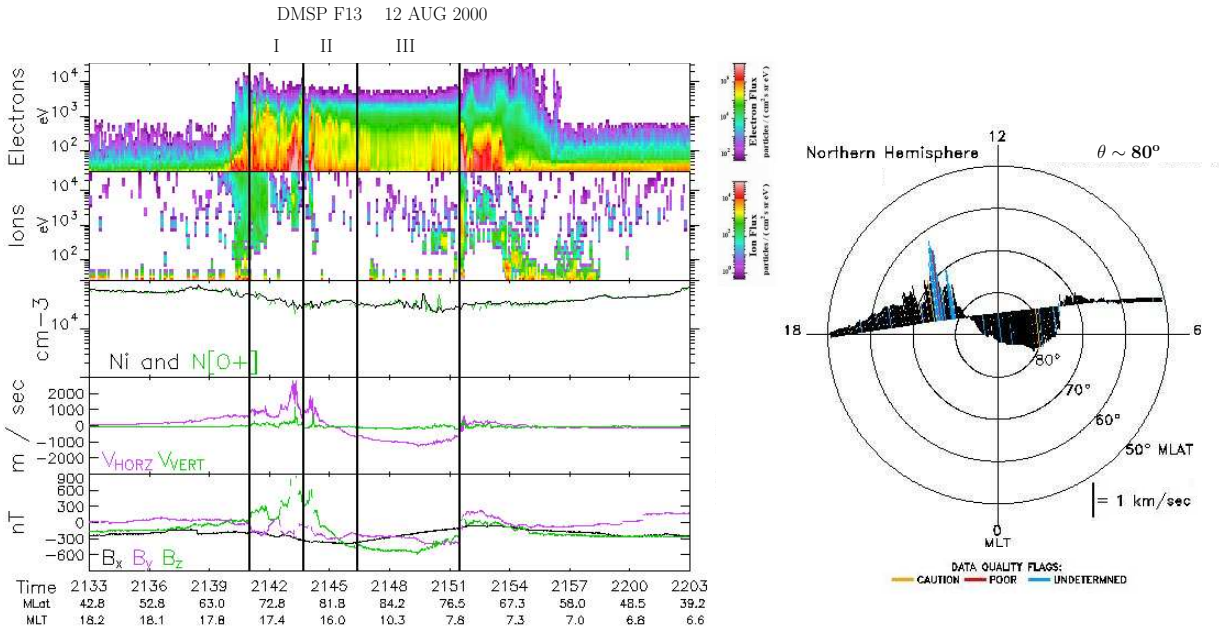

Figure 4.10: *Data obtained by DMSP F13 during the time 2133 - 2203 UT on 12 Aug 2000. Same format as figure 3.2 in section 3.2.1.*

trends at 1819 and 1820 UT (region I) and may be coupled to the two distinct upward R1 currents. Poleward of the R1 current (region II) we have a distinct upward NBZ-like FAC at 80° MLAT. Region II is again characterized by strong flow shear (convection reversal) and arc-like electron fluxes.

SuperDARN Convection map 1820 UT

Due to the low number of data points for the northern polar cap during the whole magnetic cloud passage it is hard to see the total global convection pattern with SuperDARN. Figure 4.9 obtained at 1820 UT shows data from SuperDARN during the latter DMSP F13 and we can see a convection pattern at dusk which is consistent with the DMSP data in figure 4.8. Sunward flow of ~1.5 km/s is observed at 1400-1800 MLT/65-75° MLAT. Poleward of this convection a channel of enhanced sunward flow is observed around 80° MLAT within the 1400-1700 MLT sector. At higher latitudes a flow shear from sunward convection (~2000 m/s) to antisunward convection (~500 m/s) is seen. The flow pattern appears as a large cell with a smaller cell well inside the polar cap.

DMSP F13 2133 UT, Clock Angle [80°]

During this time period the interplanetary conditions are stable and dominated by the IMF B_y component (~20 nT). The IMF clock angle is 80°; $B_y >> 0$, the major component; B_x slightly negative (~ −4 nT); B_z slightly positive (~4 nT). These extreme but stable conditions are almost identical to those prevailing during the previous three DMSP passes. So for the strongly eastward and slightly northward pointing IMF we are expecting a convection pattern similar to the previous pass at 18 UT.
Equatorward of region I at 65-67° MLAT homogeneous electron energy of ~10 keV is of CPS

origin. In region I at 68-75° MLAT increasing electron fluxes toward dawn has BPS-like particle precipitation with energy around 1 keV. Discrete fluxes of electrons (1 keV) are encountered in region II. They are identified as polar arcs with BPS-like precipitation. Region III dense polar rain with higher intensity towards dawn is seen.
At lower latitude at dusk a channel of enhanced sunward flow (~2.5 km/s) at 74° MLAT were observed (region I). A second channel of enhanced sunward flow (~1.5 km/s) at 79° MLAT followed by a decrease and reversal to antisunward flow in the convection is encountered in region II. We note that the sunward flow at dusk has now encroached over the antisunward flow cell, and the latter is now confined to an even smaller MLAT range, both at dusk as well as at dawn. A small downward R2 FAC is seen in the region of CPS precipitation. Two distinct upward R1 FAC currents at ~72-73° MLAT coincide with the increasing electron fluxes and enhanced sunward flow in region I. In conjunction with the second channel of enhanced sunward flow (region II) and the following flow shear at 80° MLAT a localized upward NBZ-like FAC is interpreted from the B_z trace in bottom panel. Once again we see polar arcs and flow shear coincide with upward NBZ-like FAC in region II.

Figure 4.11 displays the auroral oval and the development of oval–aligned polar arc in the northern hemisphere from the IMAGE WIC instrument (see section 3.2.3) between 2140–2150 UT. IMAGE observations encompass the time of the DMSP F13 and we have overlaid the track as a thick black line. For the whole sequence bright ”spots” are localized in the 12–15 MLT sector. Arcs are elongated in the antisunward direction from these bright ”spots” in the ~15-19 MLT sector.

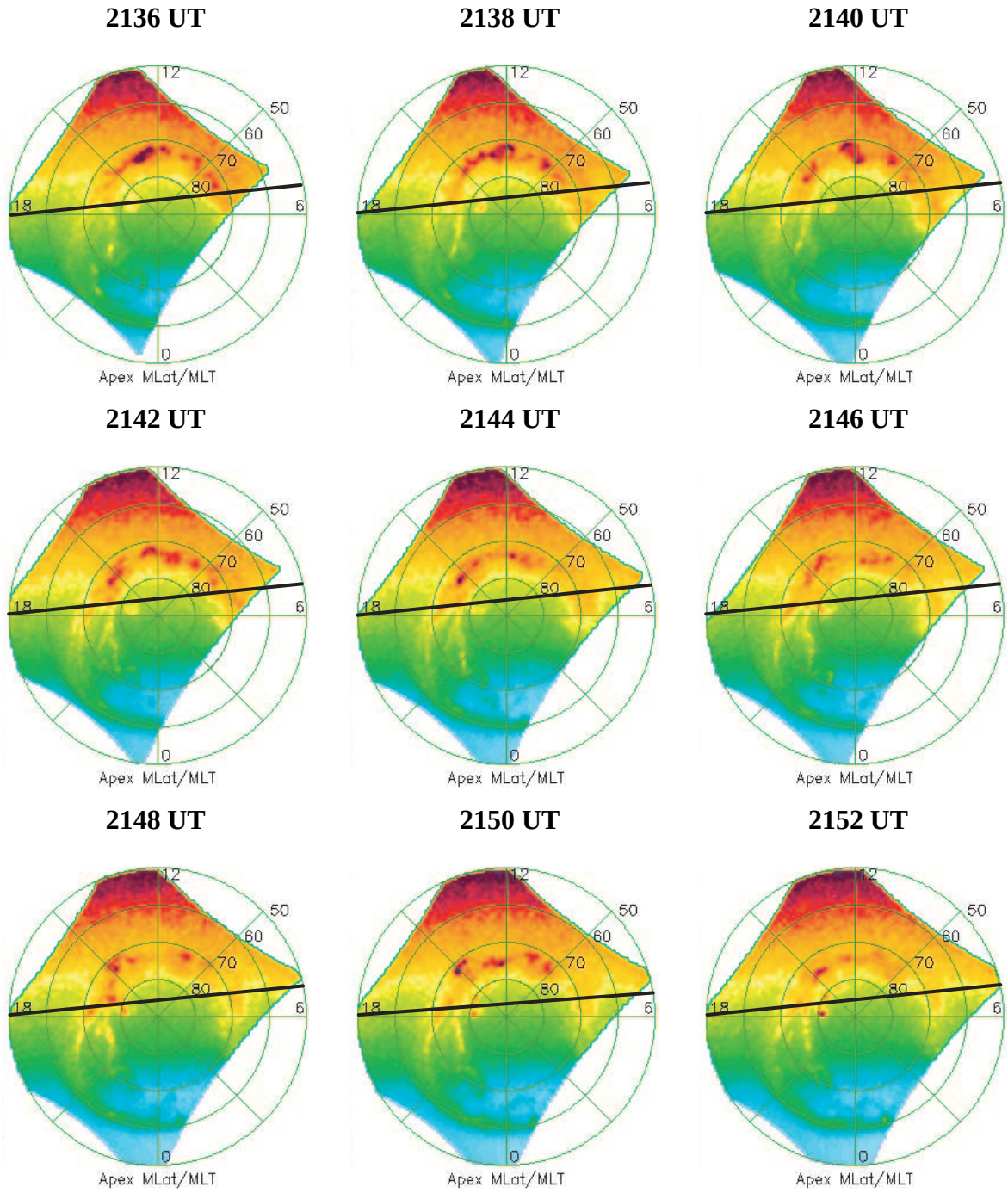

Figure 4.11: *Picture sequence from the Wide-band Imaging Camera (WIC) on the spacecraft IMAGE during the interval 2136-2152 UT. The DMSP F13 track has been overlaid as a thick black line.*

4.3 Summary and Discussion

We will try to summarize and discuss the results on the basis of the observations on August 12, 2000. The dominating IMF component in the time period we study, i.e from ~10 to 22 UT, is B_y. We note that in this time period the B_x component has a small negative value (~-5 nT). This configuration and the Earth's dipole tilt are favourable for reconnection in the magnetospheric lobes, of the northern hemisphere (Crooker and Rich, 1993) (see section 2.3). With a large IMF $B_y > 20$ nT we expect a strong dawn-dusk asymmetry. This asymmetry towards dawn is visualised at right in the upper panel in figure 2.4. For all four DMSP passes we see a clear tendency of a large rounded merging cell at dusk and a smaller ("crescent-shaped") dawn cell. All of these passes occurred in the clock angle regime between 80-115°.

In figure 4.7 at ~1640 UT and 4.10 at ~2140 UT a two latitudinally separated channel of enhanced sunward convection are seen at dusk. In both figures the first enhanced sunward channel can be related to an upward FAC R1 system. The second channel of enhanced sunward convection is followed by a strong flow shear in the region of polar arcs and upward NBZ-like FAC (region II).
In the two other figures, i.e at ~1300 and ~1800 UT there are only one clear channel of enhanced sunward convection located in the region of a distinct negative gradients (upward FAC) in B_z. This entire region is probably related to the R1 current system. Poleward of this region, where the second channel of enhanced sunward convection where in the two other passes (region II), a distinct upward FAC is accompanied by a strong flow reversal (flow shear) from sunward to antisunward flow and polar arc precipitation. We believe that the flow shears in region II with upward NBZ-like FAC which coincide with polar arcs (upper panel) are indicative of a lobe cell circulation embedded in the merging cell. We observe polar arcs in the region of upward NBZ-like FAC in all DMSP passes but the polar arcs are more distinct and stronger in the cases where we observe a second channel of enhanced sunward convection, i.e figure 4.7 and 4.10.

In figure 2.4 we see that for cases with large B_y and $B_z \lesssim 0$ antisunward flows should increase towards dawn, i.e in the region of where the flows in the merging cells are concentrated. An interesting feature about the antisunward convection is that figure 4.4 has a maximum towards dusk, while the three other passes has a gradient gradient towards dawn. A gradient towards dawn is consistent with figure 2.4 and previous work (see section 2.2). An explanation of this variety could be that a stronger lobe cell inside the merging cell is present at ~1300 UT compare to the rest of the day. We expect that the IMF B_y which is a factor of 1.5 times stronger with values around 30 nT at ~1300 UT and 20 nT in the three other DMSP passes, plays a role in the variety of the antisunward flows. With a stronger B_y a composite pattern with a "big" lobe cell at dusk will be present.

The lack of data points in the SuperDARN data for the whole day makes it impossible to get a global picture of the convection pattern but in figure 4.9 we see evidence of lobe cell around 80-84° MLAT at dusk. This correspond to the same area as the predicted lobe cell (region II) in the corresponding DMSP pass. Eriksson et al. (2002, 2003, 2005) relates a channel of enhanced sunward flow and upward NBZ-like FAC to B_y component. Further Eriksson et al. indicated a correlation between polar arcs and lobe convection signatures. IMAGE data in figure 4.5 at ~1300 UT and 4.11 at ~2130 UT shows oval-aligned polar arcs poleward of the duskside au-

rora oval in the region between 70-80° MLAT. This is where we observed a velocity shear and a upward NBZ-like FAC with distinct high-latitude arcs in the DMSP data. Figure 4.11 also displays a sequence of bright ”spot” localized around 15 MLT. This may be a signature of the lobe reconnection site (Eriksson et al., 2003). The arcs on the dusk side of the polar cap, seen both from DMSP F13 and IMAGE are taken as a signature of the presence of a lobe cell. These bright ”spots” has been related to polar arcs in previous studies (Murphree et al., 1994; Liou et al., 1999; Sandholt et al., 2006). Eriksson et al. (2003) suggest the presence of auroral bright ”spots” in the 15 MLT sector may be linked to IMF B_y dependent polar arcs. In figure 4.10 at ∼2140 UT there seems to be an intensity gradient towards dawn in the polar rain precipitation. We note how much more intense this polar cap precipitation is compared to the previous passes.

In summary we have polar arcs in conjunction with flow shears across the localized upward NBZ-like FACs inside region II. These feasters are indicative of a lobe cell circulation embedded in the merging cell. We then have a composite pattern of merging and lobe cells for this IMF clock angle regime between 80-115°.

Chapter 5

Case study 2: MAY 20-21, 2005

Throughout May 20, 2005 to May 21, 2005 a magnetic cloud interact with the Earth's magnetosphere. On average the total magnetic field is larger then 10 nT. An important feature of this cloud is the rotation of the magnetic field. The rotation of the magnetic field is South-East-North (SEN) followed by a North-West-South(South-West) (NES). We would have a double rotation and by taking advantage of this rotation we are able to study the ionospheric convection and precipitation for a wide variety of IMF conditions. To identify the changes in the convection patterns we have chosen to look at DMSP F13 passes for the wide range of IMF clock angles provided by the cloud. As in the previous case study, our focus will primarily be on DMSP F13 data correlated with IMF data from the Wind satellite. In total we will present 9 DMSP F13 passes where some of them will be investigated in more detail with help of SuperDARN convection data and IMAGE data on auroral morphology.

5.1 Interplanetary Data Set

Interplanetary plasma and field parameters from the 3D Plasma and Energetic Particle Investigation (3DP) (Lin et al., 1995) and the magnetic field investigation (MFI) (Lepping et al., 1995) from the satellite Wind in the time period from 0300 UT May 20 to 0700 UT May 21 (we will from now on refer to ground time, see section 5.1.1) are shown in figure 5.1. The format of figure 5.1 is form top to bottom, the proton density (cm^{-3}), temperature (K), the bulk speed (km/s), dynamic pressure (nPa),the total magnitude (nT) and GSM X, Y, and Z components of the magnetic field (nT), plasma β and Alfv́en-Mach number (the latter in red), and the IMF clock angle (polar angle in the GSM YZ plane. The red trace in the temperature panel gives the expected temperature for normal solar wind expansion from the statistical studies of Lopez and Freeman (1986). Judging from the (1) the high field strength, (2) the field rotation and (3) the low proton beta, the cloud seems to have started at ~0730 UT, May 20. There appears to be a weak shock front arriving at Wind around 0400 UT, May 20 (see section 5.1.1). The cloud interval seems to continue until 0600 UT, May 21. In fact, there is the distinct possibility that the period contains more than one magnetic cloud, forming a complex ejecta (Burlaga et al., 2001). This may account for the relatively high proton temperatures with respect to those expected for normal solar wind expansion (compare the red trace in panel 2). The evident breaks at 11 UT and 16 UT, where the proton plasma β increases, might delineate boundary of other ejecta forming a coalesced ejection when observed by Wind. But these matters need not concern us

here.The two first vertical guidelines mark the arrival of the shock and the cloud proper in figure 5.1. Different time intervals have been named I-V (panel 1) and marked with vertical guidelines in figure 5.1. The intervals are mainly chosen after the behaviour of the clock angle.

In Interval I from ~0730-1045 UT the clock angle rotates from 80° to 0°. All three IMF cloud parameters change sign during this interval. During the interval II ~1200-1900 UT the clock angle is < 45°. Since the cloud has a long interval of almost zero clock angle, we expect to see reverse convection in interval II. We have set interval III (1900-2200 UT) to cover the gradual increase in clock angle from ~45° to 90° caused by a change in B_z from positive (15 nT) to negative (- 5 nT) while B_y was negative (~ −15 nT). From 2200 UT to ~0200 UT (21 May), marked as interval IV, the field is pointing westward and the clock angle is stable around 90° with B_y negative (-12 nT). In interval V from ~0215 UT to 0600 UT the clock angle is fluctuating around 135°.
The solar wind is a moderately high speed stream (panel 3) with greater speeds in the beginning (~500 km/s) than in the end (~430 km/s). Both the Alfv́en Mach number (red graph) and plasma β values (panel 11) are low throughout the whole cloud.

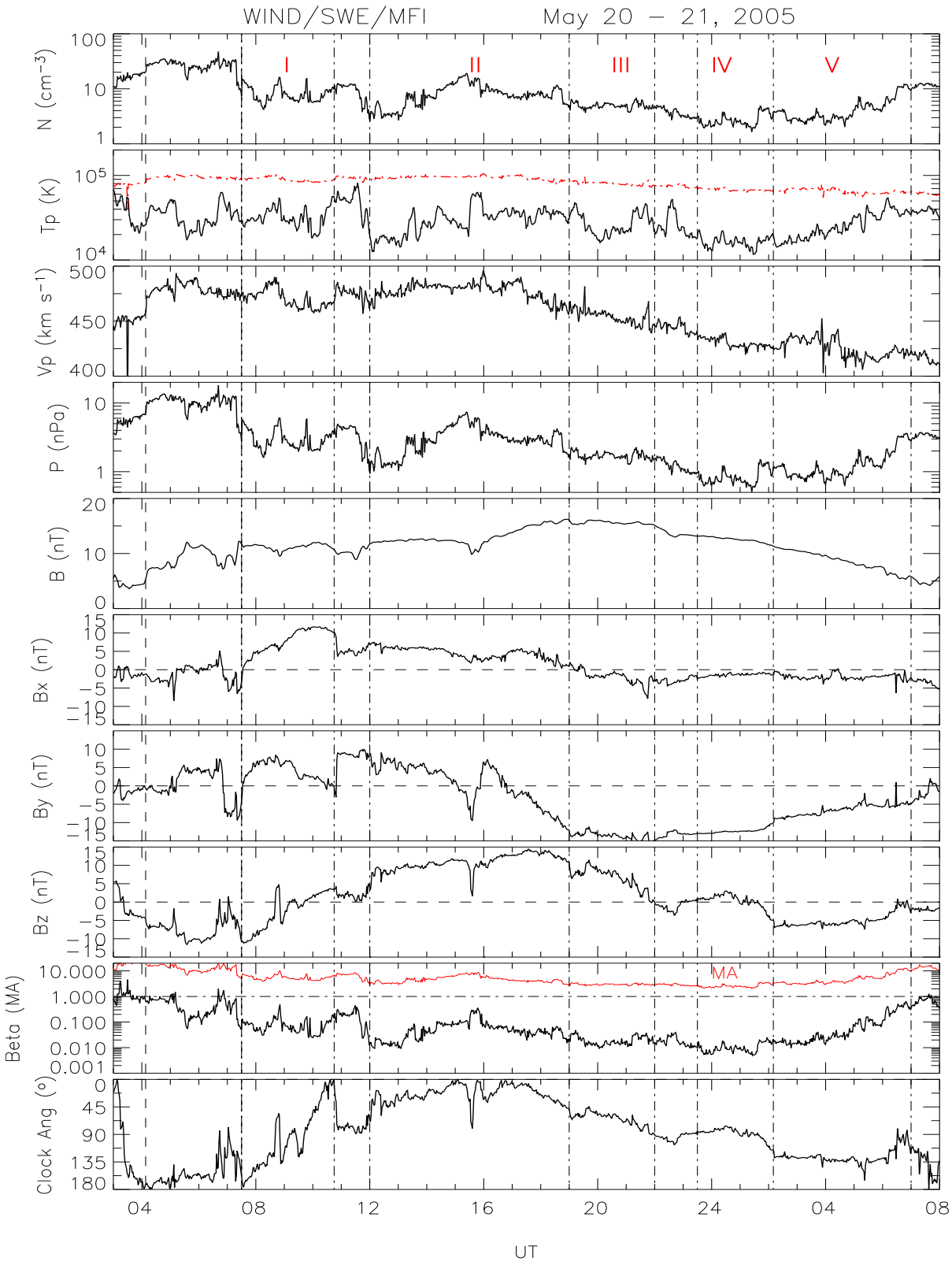

Figure 5.1: *Solar wind plasma and interplanetary magnetic field (IMF) data obtained from spacecraft wind during the interval from 0300 on 20 May 2005 to 0800 UT on 21 May 2005. Panels from top to bottom show proton density, temperature, bulk speed, dynamic pressure, the total field, the GSM components of the magnetic field, plasma β and Alfv́en-Mach number (the latter in red) and the IMF clock angle. The red trace in the temperature panel gives the expected temperature for normal solar wind expansion from the statistical studies of Lopez and Freeman (1986). The horizontal axis shows the universal time (UT) in hours when the delay time is added.*

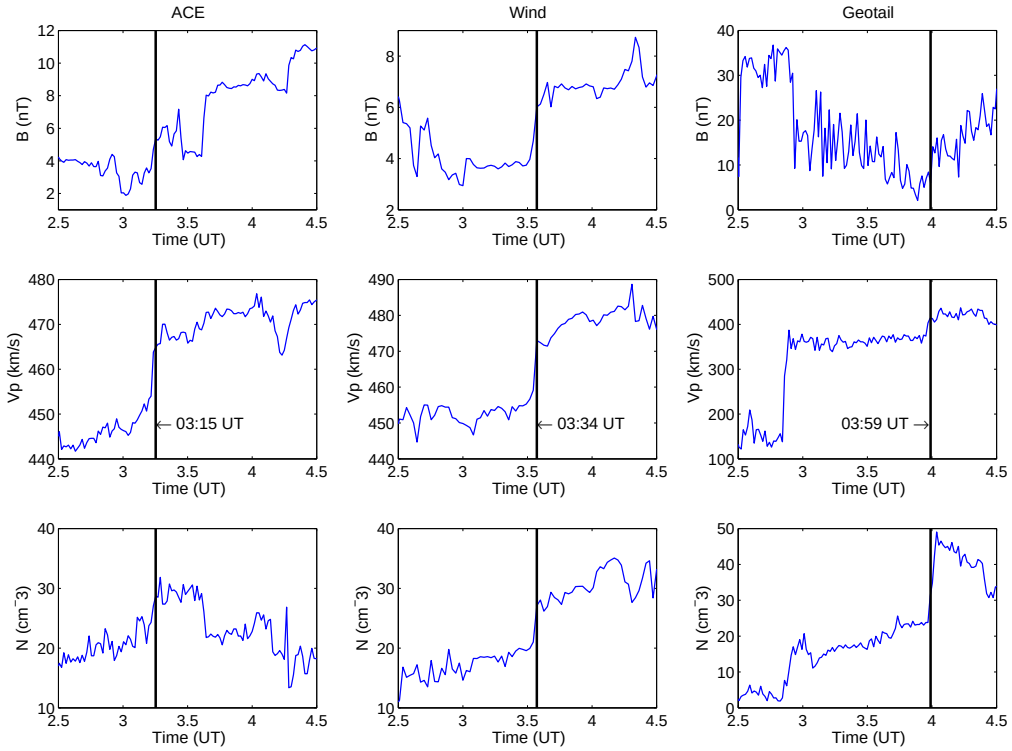

Figure 5.2: *Time of the shock for ACE, Wind & Geotail*

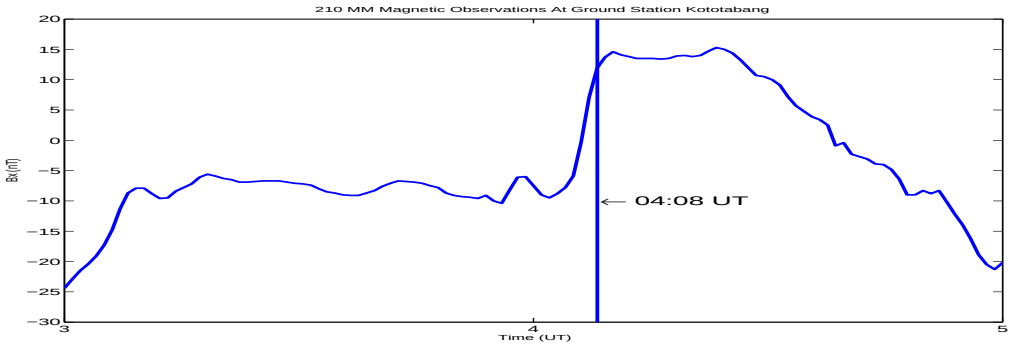

Figure 5.3: *Time of arrival of the SSC at the ground station Kototabang (KTB)*

Station	*Time*	*Interval*
ACE	03:15 UT	
Wind	03:34 UT	+ 19 min
Geotail	03:59 UT	+ 44 min
KTB	04.08 UT	+ 53 min

Table 5.1: *Arrival of Shock*

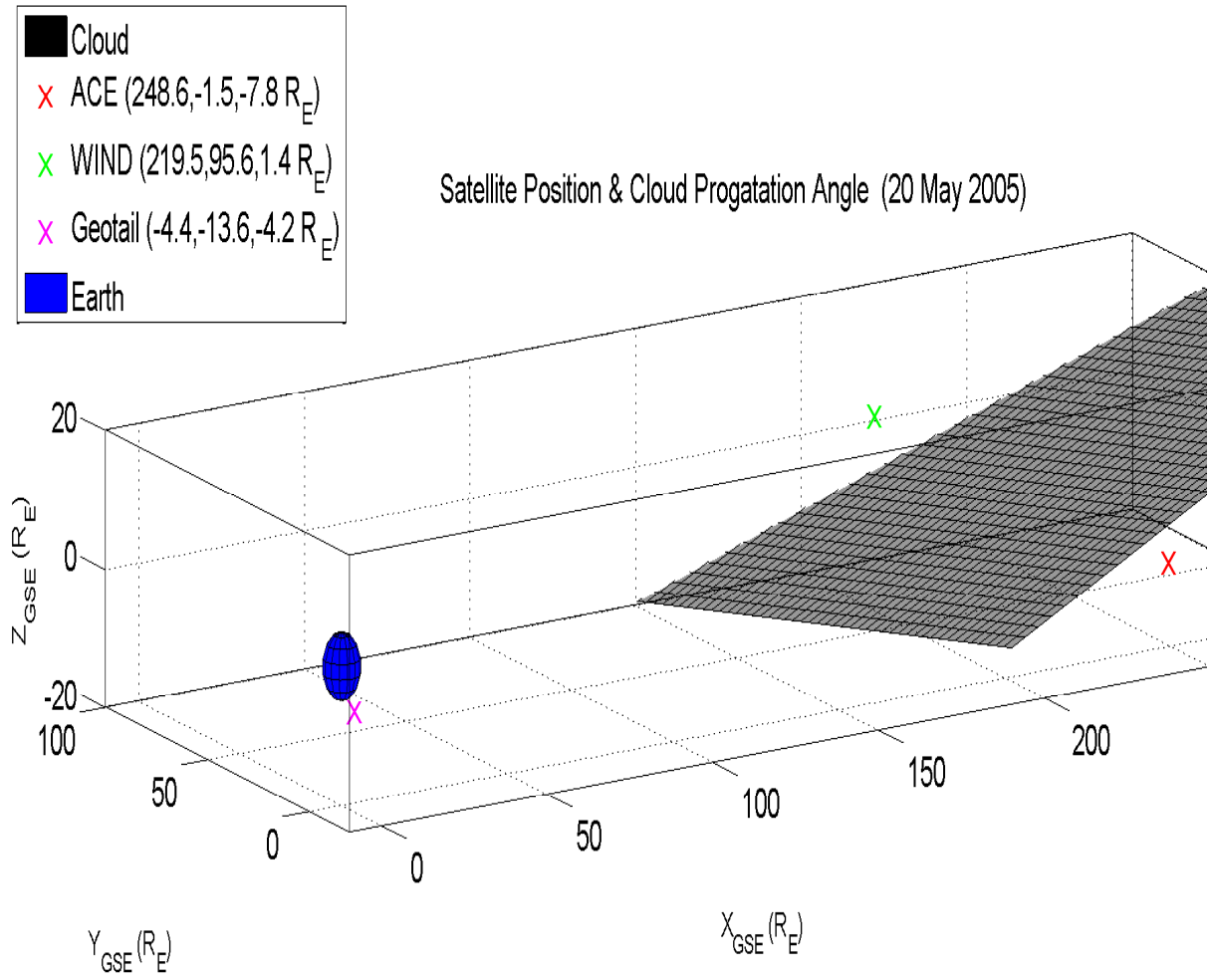

Figure 5.4: *3D view of the cloud boundary (GSE coordinates)*

5.1.1 Time Delay

When the IMF components are changing and thus the clock angle are changing, the convection pattern is in a transition state (see section 2.2). To be able to establish the proper correspondence between a convection pattern and the external conditions, it is important to know the time delay form the spacecraft, where we get our interplanetary data from (Wind), to the ionosphere. If we do not know this time it is hard to relate the ionospheric signatures to transitions of the IMF clock angle. It is common to calculate this time delay by taking the distance of GSE_x-component between the satellite and the Earth and dividing by the V_x-component of the solar wind. This is then the time the solar wind will take to reach the magnetopause and further by adding $\sim$ 10 minutes delay between the magnetopause and the ionosphere (so called ”convection delay”; e.g. Lockwood et al., 2006) the time delay is obtained. This is appropriate as long as the cloud propagating axis is perpendicular to the Sun-Earth line. This is, however, not true for the May, 20-21, 2005 magnetic cloud.
In a much-used, first approximation the orientation of the axis may be obtained by minimum variance analyses of the magnetic field data (Sonnerup and Cahill, 1967), in which the direction of the intermediate eigenvector gives the direction of the axis (Goldstein, 1983), i.e the vector related to the intermediate eigenvalue. Carrying out this procedure with high resolution

magnetic field data for the magnetic cloud on May 21-21, 2005, as seen by the Wind spacecraft, we find a boundary normal vector which is highly inclined with respect to the ecliptic plane ($\theta \sim 72°$). Plotted in GSE coordinates we find a "wave front" (front cloud boundary) as sketched in figure 5.4. The location of the spacecraft ACE, Wind and Geotail are as indicated in the upper right corner and the scale is in R_E.
A way of visualizing this is to consider the shock. There is namely a weak shock driven by the magnetic cloud. As the shock interacts with the magnetosphere it produces a sharp rise in the H-component of the terrestrial field at low latitudes, called a sudden impulse (SI) (see section 3.3.1 and Kivelson and Russell, 1995, chap. 9.2). We examined ground data from Kototabang, (KTB), and found a small SI. Which we can use as a timer. Figure 5.2 shows the shock front with the parameters density N, total velocity V and the total magnetic field B for the spacecraft's ACE, Wind and Geotail and figure 5.3 shows the SI at the ground station Kototabang . Kototabang is located at latitude $-0.20°$ and longitude $100.32°$ in geographic coordinates ($-10.63°$ MLAT and $171.93°$ MLONG). The following time of arrival of the shock front and the SCC is given in the table 5.1. We find the Wind-KTB delay to be 34 minutes. Because it is a weak shock the increase in the bulk speed is very small (see middle row in 5.2 and panel 3 in figure 5.1). The delay found from the shock can be interpreted/applied for the rest of the interval as well because the bulk speed does not change much. This makes the interpretation more straightforward. A delay time of 34 min has been added to figure 5.2 which again will give us a more accurate picture when analysing and comparing the DMSP data to interplanetary parameters.

5.2 DMSP results

Since the rotation of the cloud field is different from our previous case, the convection pattern of the ionosphere will also be different. From ~1700 UT B_y is strongly negative, and a convection pattern with opposite dawn-dusk asymmetry compared to the one observed in our case study for August 12, 2000 is expected. The different DMSP passes are described below, ordered by interval, time and clock angle.

5.2.1 Interval I, 0730 - 1045 UT, Clock Angle [changing from ~180-0°]

In the time period 0730 - 1045 UT (~ 3 hours) we have a South-East-North (SEN) rotation of the magnetic field. We cover a full clock angle range in 3 hours almost monotonically except for a large spike at around 8 UT. The rapid change clock angle is related to a positive gradient in B_z (panel 9) and a negative gradient in B_y (panel 8). The solar wind density is high (~7-10 cm^{-3}) and the speed is constant at ~500 km/s In the period between 0910-0930 a strong discontinuity in B_z can be seen. The half an hour after this discontinuity, when the major component is B_y, is investigated closer with the help of DSMP F13.

DMSP F13 0858-0928 UT,
Clock Angle [changing from 100° to 70° and then back to 100°]

Figure 5.5 shows the DMSP F13 data obtained at ~0900 UT. In the bottom panel of figure 5.1 we see that throughout this time period we have a small decrease followed by an increase in the

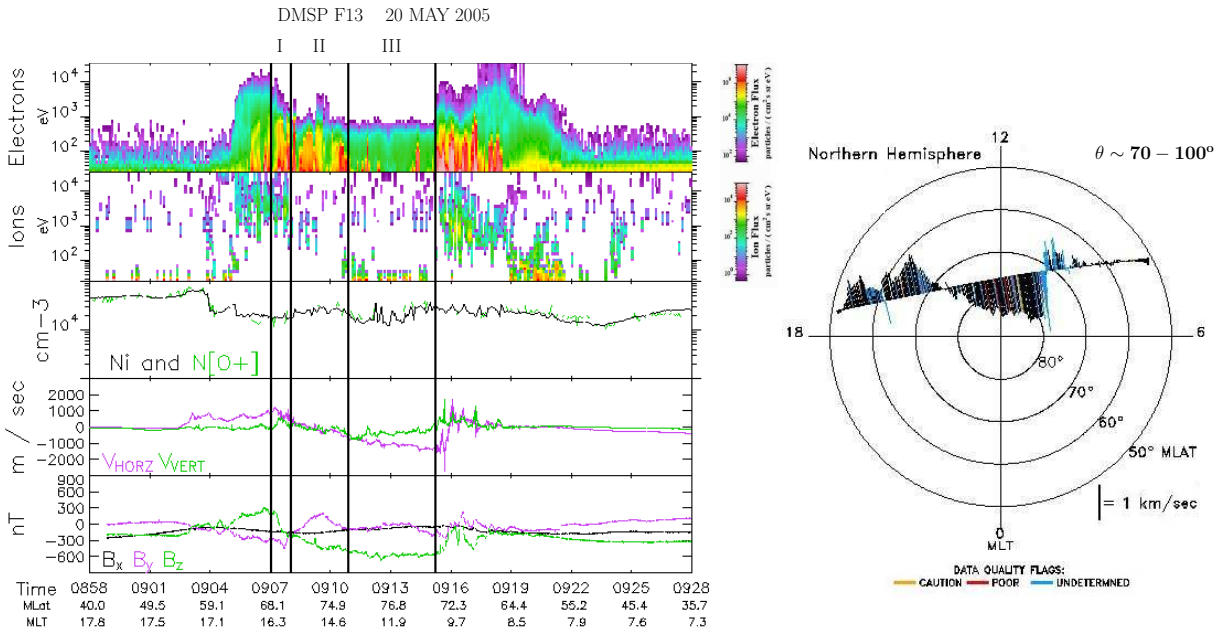

Figure 5.5: *Data obtained by DMSP F13 during the interval 0858 - 0928 UT on 20 May 2005. Same format as figure 3.2 in section 3.2.1.*

clock angle (100° to 70° and then back to 100°). A closer look at the magnetic field recorded by Wind shows that in the period with decreasing clock angle, B_z changes from - 5 nT till 0 nT (and stays around this value for the rest of this interval) while the B_y is above 5 nT. Just as the B_z finishes its increase, the B_y starts to decrease from 6 nT to 2 nT. This again causes the clock angle to change back to 100°. The spacecraft never reaches higher magnetic latitude than 79° during the ~17-7.5 MLT orbit. We used vertical guidelines (I,II & III) in the panels to the left in figure 5.5 to separate different convection and precipitation regions in the same way as in the previous case study.

From the precipitation (panel 1) we see a region of homogeneous electrons of CPS-like fluxes (~10 keV) at 1600 MLT/62-68° MLAT. From 0907 to 0908 UT (68-70° MLAT) the satellite traverses into region I where high fluxes of electrons are encountered with typical BPS-like energies (~800-1000 eV). At higher latitude at dusk (~70-74° MLT) signs of discrete high-latitude arc and occasional cusp-like precipitation (region II) are seen. As the satellite enters region III (0909-0915) it detects polar rain. Throughout this region some areas with high electron fluxes (200 eV) are encountered.

The cross-track plasma drift data (right panel) show sunward flows (~700-1000 km/s) in the region 54-71° MLAT at dusk. At 0907-0910 UT (region I and II) a flow shear from sunward flow of ~ 1000 m/s to antisunward flow is followed by a gradually stronger antisunward convection as the satellite moves over the polar cap toward dawn (region III). The antisunward flow reaches a maximum of - 1800 m/s at 1000 MLT/72° MLAT. This maximum at dawn is in close vicinity of where we have marked the end of polar rain precipitation, and is followed by a strong flow reversal from -1800 m/s antisunward to 1200 m/s sunward.

A weak positive B_z gradient in the region of CPS-like precipitation and sunward convection is interpreted as the upward R2 FAC. On the basis of a decreasing gradient in B_z (green) we conclude that an upward R1 FAC coincides with the BPS precipitation and the sunward part of the

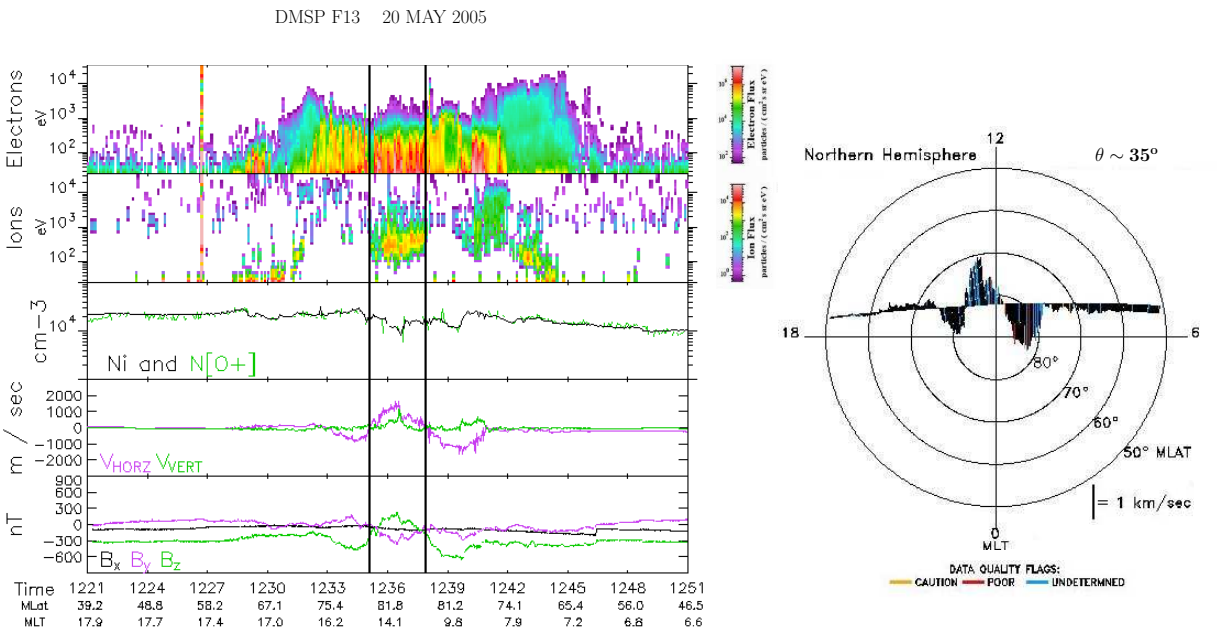

Figure 5.6: *Data obtained by DMSP F13 during the interval 1221 - 1251 UT on 20 May 2005. Same format as figure 3.2 in section 3.2.1.*

flow shear encountered in region I. We link the weaker negative trend in B_z in region II which coincides with the convection reversal and high-latitude arcs to an upward NBZ-like FAC. The ion drift data shows a dawn-dusk convection asymmetry with a corresponding negative trend in B_z towards dawn.

5.2.2 Interval II, 1200 - 1900 UT, Clock Angle [> 45°]

The total magnetic field strength of interval II was 10-15 nT with the component values as follows: B_z > 10 nT, B_y changing and B_x >0. The IMF B_y was mainly positive before the component changed polarity from positive (~7-8 nT) to negative (~ −5 nT) around 1645 UT. A discontinuity around 1530 UT in the magnetic cloud is seen in figure 5.1. Wind measured a fairly stable solar wind with speed of 500 km/s and density fluctuating between 3-20 cm^{-3}. In this interval we will show three different DMSP F13 passes over the northern hemisphere and one in the southern hemisphere which we will combine with IMAGE data. A interesting fact is that the four DMSP passes at ~1220, 1400, 1730 and 1815 UT all occur under strongly positive B_z while the B_y component changes polarity from the two first to the two latter DMSP F13 passage.

DMSP F13 1221-1251 UT, Clock Angle [35°]

Between the vertical guidelines (80° MLAT at dusk to 87° MLAT at dawn) high fluxes of electrons with energy 300 eV and ions with energy 200-800 eV show cusp-like particle precipitation. Both duskward and dawnward of this the satellite encounters electrons of BPS-like precipitation. We see that the ions have totally disappeared on both sides and the electrons energy at dusk has increased to 500-1000 eV. An inverted-V with electron energy of 3-4 keV is seen at dawn around 1239 UT.

From the cross-track plasma drift data (right panel) we see two antisunward flows at high latitudes separated by a sunward convection in the central polar cap. The sunward convection, which converge from both dusk and dawn to a maximum of 1.5 km/s at 85° MLAT at dusk, coincide with the cusp-type precipitation (inside the vertical guidelines). A reversal and a small sunward convection channel are seen equatorward of the antisunward flow at dusk (1233 UT) can be an indication of a small "viscously-driven" convection cell. In the region of the vertical guideline at dawn we observe a strong velocity shear from sunward ($\sim$ 500 m/s) to antisunward (~ -1000 m/s).
Two clear regimes of field-aligned currents (negative gradients in B_z in bottom panel) are directed upward in the BPS-like precipitation at dusk and in the BPS/inverted-V precipitation at dawn-side of the sunward convection regime.
The convection is dominated by a system of reverse cells in the central polar cap. The dawn-side cell is accompanied by upward FAC and inverted-V electron precipitation. The upward FAC at dusk coincides with the small "viscously-driven" convection cell and BPS-like precipitation.

DMSP F13 1403-1433 UT, Clock Angle [20°]

From the Wind data in figure 5.1 we see that the difference in the clock angle between the two passes at $\sim$ 1220 UT and $\sim$ 1400 UT is that B_z becomes a little more positive while the B_y becomes a somewhat weaker but remains still positive in the latter case.
In figure 5.7 we see that almost the whole sunward flow from 84° at dusk to 89° at dawn is mark undetermined (right panel). DMSP F15 (not shown) passes over the northern hemisphere in a 2000-1000 MLT orbit 18 minutes before DMSP F13 and the same sunward flow and with nearly the same intensity and in the same region as the undetermined points in figure 5.7 and this allow us to interpret this sunward flow as determined data points.
This sunward convection channel ($\sim$ 1.75 km/s) is bordered on each side by antisunward flows. Equatorward of the antisunward flows a flow reversals from antisunward to sunward convection are observed both at dusk ($\sim$ 76° MLAT) and dawn ($\sim$ 78° MLAT). This is most likely small "viscously-driven" convection cell on closed field lines. Just like in the previous pass we see a strong velocity shear from positive ($\sim$ 2000 m/s) to negative (~ -1000 m/s) speeds toward dawn-side at $\sim 1418 - 1420$ UT.
We see BPS-like precipitation in the dusk sector during the interval ~1414-1416:30 UT. In the region between the two first vertical guidelines (~1416:30-1419 UT) high electron fluxes < 600 eV and an inverted V-pattern in the ion dispersion (inverse energy dispersion profile) have cusp-like character. The ion energy maximizes at highest latitude (7 keV) with lower energy (2 keV) on both sides. This is a good indication of reverse convection signature. The lower energy cut-off first increases as the latitude increases and then decreases as the latitude decreases. A strong and distinct inverted-V with electron energy of several keV is seen throughout the flow reversal at 87-89° MLAT (region between the two last vertical guidelines).
In figure 5.7 we see that the profile of the B_z gradient (bottom panel) is similar to the profile of the convection (panel 4). From ~1416:30 UT till 1418 UT, i.e in the region of the strong flow reversal at dusk (82-85° MLAT), a positive B_z gradient occurs. Just like in the previous pass at $\sim$ 1220 UT two clear regimes of upward FAC at dusk and dawn are seen. The upward FAC at dawn is mainly within the two vertical guidelines that indicated the region of the strong and distinct inverted-V electron precipitation.
The particle data seen in figure 5.7, which are almost identical to the previous data seen at

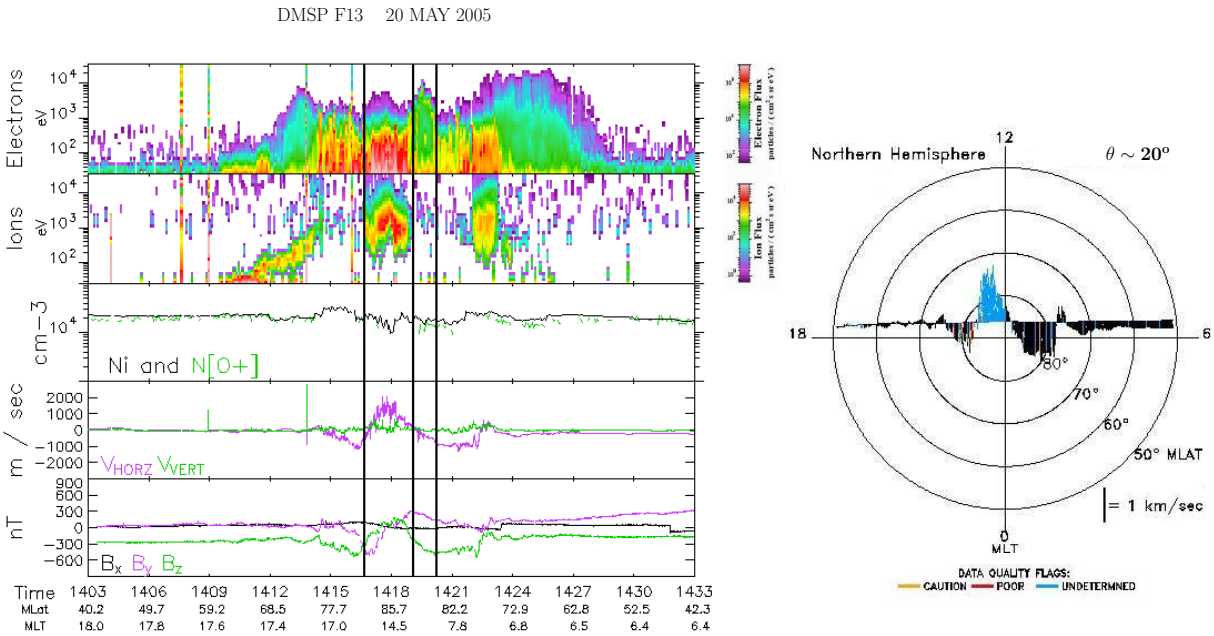

Figure 5.7: *Data obtained by DMSP F13 during the interval 1403 - 1433 UT on 20 May 2005. Same format as figure 3.2 in section 3.2.1.*

~ 1220 UT in figure 5.6, consist of 2 well-defined reverse convection cell with a upward FAC and inverted-V electron precipitation in the dawn-side cell. Once again we see that the small "viscously-driven" convection cell at dusk (equatorwards of the first vertical guideline) coincides BPS-like precipitation and a upward FAC.

DMSP F13 1727-1757 UT, Clock Angle [10-20°]

In the time period of Figure 5.8 the IMF is strongly north as in the previous pass but B_y has changed polarity from positive to negative.
At low latitudes both on dusk and dawn high fluxes of electron and ion with CPS and BPS origin are seen. A characteristic feature with the precipitation is that there is a total drop in the ion fluxes in the region (marked bracketed by the vertical guidelines). Discrete electron fluxes with cusp-like precipitation are observed throughout this region.
We see two regions of antisunward flow separated by a region of sunward flow at high latitudes. Only weak flows are present over the central polar cap, with smaller values both antisunward and sunward than in the two previous passes. This indicates that the global ionospheric convection is relatively weak. A velocity shear from sunward to antisunward flow at dusk (poleward of the left vertical line) is colocated with a downward directed FAC (bottom panel). Equatorward of the first vertical line a convection reversal from sunward (equatorwards) to antisunward (poleward) is seen. This could be a the small "viscously-driven" convection cell that coincides with BPS-like precipitation and a upward FAC.
Still there is evidence of two-reverse cells in the polar cap. This time the dusk cell is more pronounced then the dawn cell.

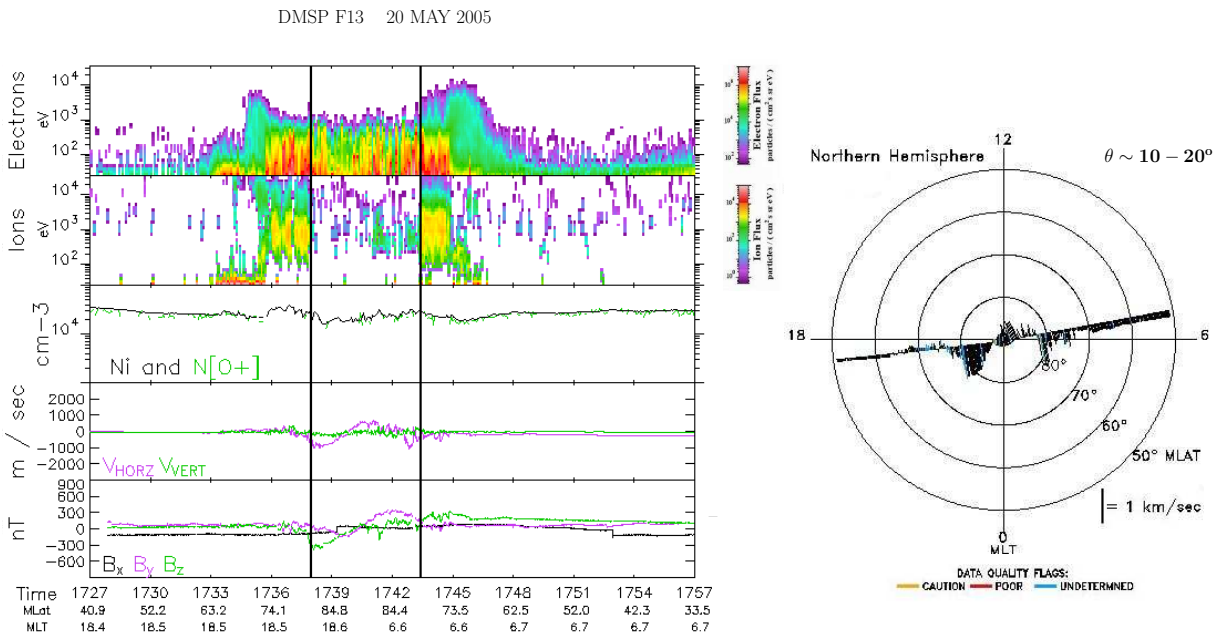

Figure 5.8: *Data obtained by DMSP F13 during the interval 1727 - 1757 UT on 20 May 2005. Same format as figure 3.2 in section 3.2.1.*

DMSP F13 1814-1844 UT, Clock Angle [35°]

During the time interval 1814-1844 UT the interplanetary conditions are stable and dominated by the IMF B_z component (∼ 14 nT). The IMF clock angle is 35° and the solar wind dynamic pressure is ∼2 nPa.
Figure 5.9 shows the particle data obtained from the southern hemisphere during the interval 1814-1844 UT. The orbit of the DMSP F13 satellite over the southern hemisphere is from dawn to dusk. The left panels in figure 5.9 show data obtained from dawn to dusk as the DMSP F13 traverses over the polar cap. This means that the data shown at lower latitude to the left are from dawn-side. We notice in figure 5.9 that the convection pattern has areas marked with undetermined and poor data points. We use DMSP F15 and F16 (not shown), which passes over the southern hemisphere only ∼15-20 min prior to DMSP F13, to help us in our judgement to decide if the data is usable or not. DMSP F15 and F16 have an orbit with equatorial crossing times near 0900 local time and 2100 local time and both satellite reveals a irregular flow pattern towards postnoon and postmidnight at higher latitudes ($< -75°$ MLAT). Thus we have rated the DMSP cross-track plasma drift data shown in figure 5.9 as good enough to be used for our purpose.
From the electron precipitation (panel 1) we see a region of distinct polar arcs with energy between 200-600 eV from $-78°$ MLAT at dawn to $-83°$ MLAT at dusk. The polar arcs coincide with irregular flow consisting of multiple small-scale flow shears (panel 4).

The IMAGE WIC image (see section 3.2.3) obtained during the DMSP F13 orbit gives an overview of the auroral oval and the development of polar arcs in the southern hemisphere in the time period 1830–1834 UT. We have overlaid the DMSP F13 track as a thick black line in figure 5.10. The major arc emanating from the nightside auroral oval and elongated towards noon is referred to as midnight arc (Kullen et al., 2002).

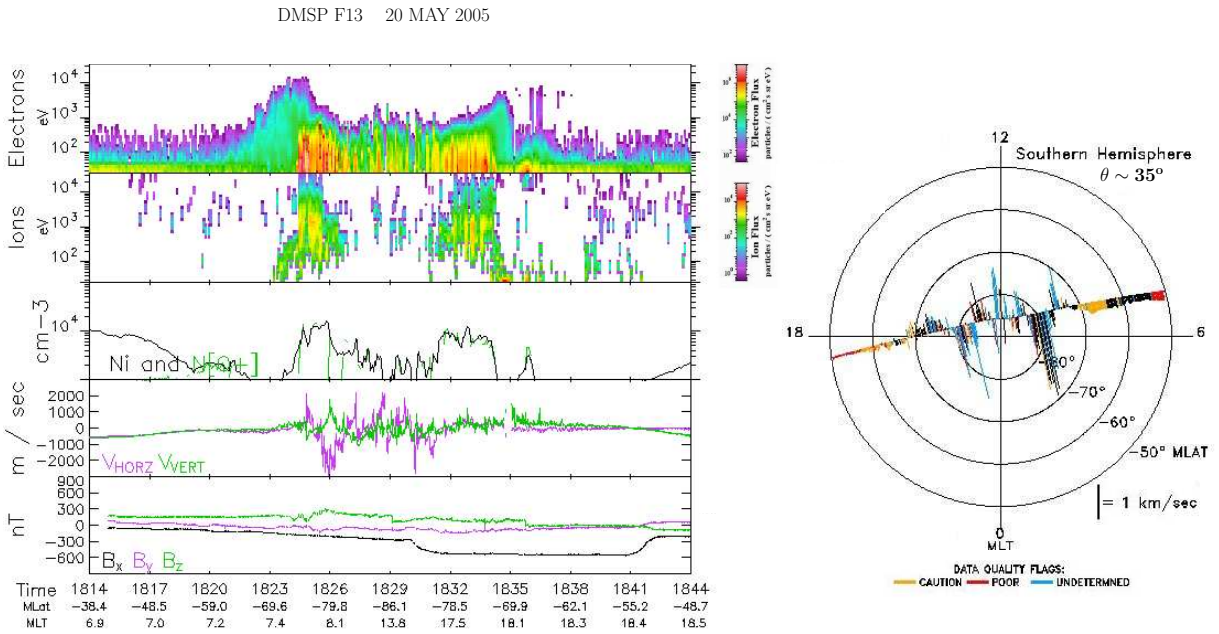

Figure 5.9: *Data obtained by DMSP F13 during the interval 1814 - 1844 UT on 20 May 2005 in the southern hemisphere. Same format as figure 3.2 in section 3.2.1.*

1830 UT **1832 UT** **1834 UT**

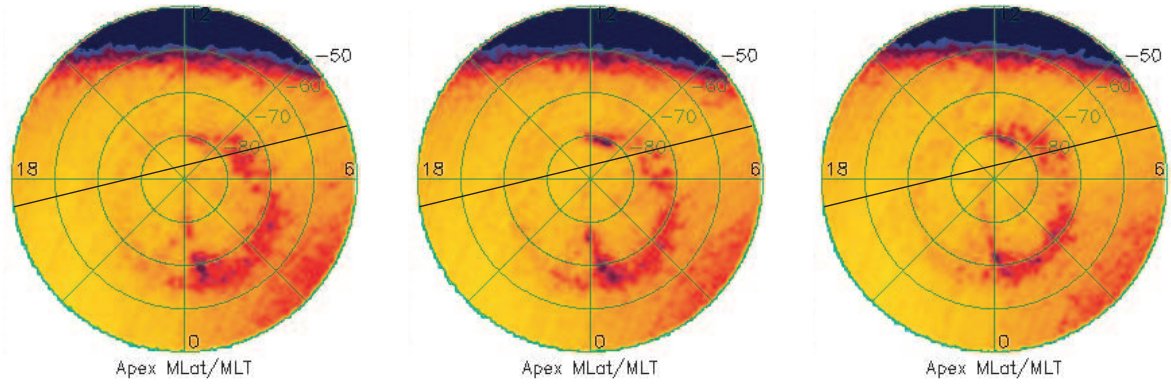

Figure 5.10: *Picture sequence from the Wide-band Imaging Camera (WIC) on the spacecraft IMAGE during the interval 1830-1834 UT from the southern hemisphere. The DMSP F13 track has been overlaid as a thick black line.*

For the whole sequence a midnight arc stretching towards noon from the poleward boundary of the nightside oval in the region between 70 and 85 MLAT is present. Note also the presence of auroral intensification region in the noon sector around 80 MLAT. This bright spot is identified as a typical signature of the northward IMF cusp (Milan et al., 2000).

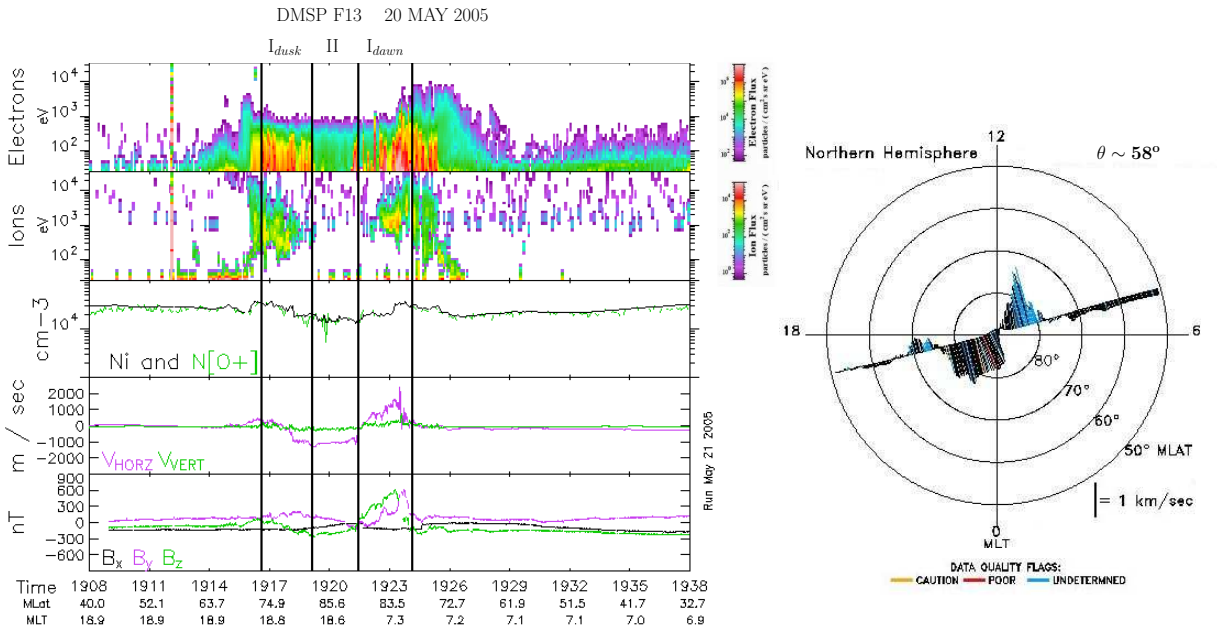

Figure 5.11: *Data obtained by DMSP F13 during the interval 1908 - 1938 UT on 20 May 2005. Same format as figure in section 3.2.1.*

5.2.3 Interval III, 1900 - 2200 UT, Clock Angle [Changing form ~45° to 90°]

During interval III the IMF goes from strongly north to westward orientation and the clock angle increases from ~45° to 90°. The density slowly decreases from 8 to 5 cm^{-3} and the plasma beta is less then 0.040 throughout interval III (see panel 1 and 11 in figure 5.1). The solar wind speed remains high (> 450 km/s) and the solar wind dynamic pressure decreases from 3 to 1.7 nPa. In interval III we study one DMSP F13 pass in the northern hemisphere and we combined this pass with SuperDARN data.

DMSP F13 1908-1938 UT, Clock Angle [58°]

Figure 5.11 shows data observed in the northern hemisphere between 1908 UT and 1938 UT. In the time interval of figure 5.11 the IMF clock angle is 58°. Both B_z and B_y has decreased since the previous pass to values around -7 and -14 nT, respectively.
In the upper panel of figure 5.11 an intensification of electrons with energy around 200-300 eV (BPS-like precipitation) is visible in the intervals marked I_{dusk} and I_{dawn}. As the satellite moves poleward into interval II it encounters polar rain. CPS-like precipitation is seen equatorwards of interval I_{dusk} and I_{dawn}.
Within the double vertical guidelines marked I_{dusk} we see flow reversal with a small sunward flow channel towards dusk/equator and a peaked antisunward flow (~ 1000 m/s) towards the central polar cap. Antisunward convection with speed of ~ 1000 m/s (interval II) is followed by a flow reversal and sunward flow (interval I_{dawn}). The sunward flow channel maximizes (~ 1.5 km/s) in the end of interval I_{dawn}.
A pair of dawnward and upward FAC in the region of the BPS at dusk may correspond to the R2 and R1 current system. The ~ 1921 – 1924 UT time interval (interval I_{dawn}) shows a strong

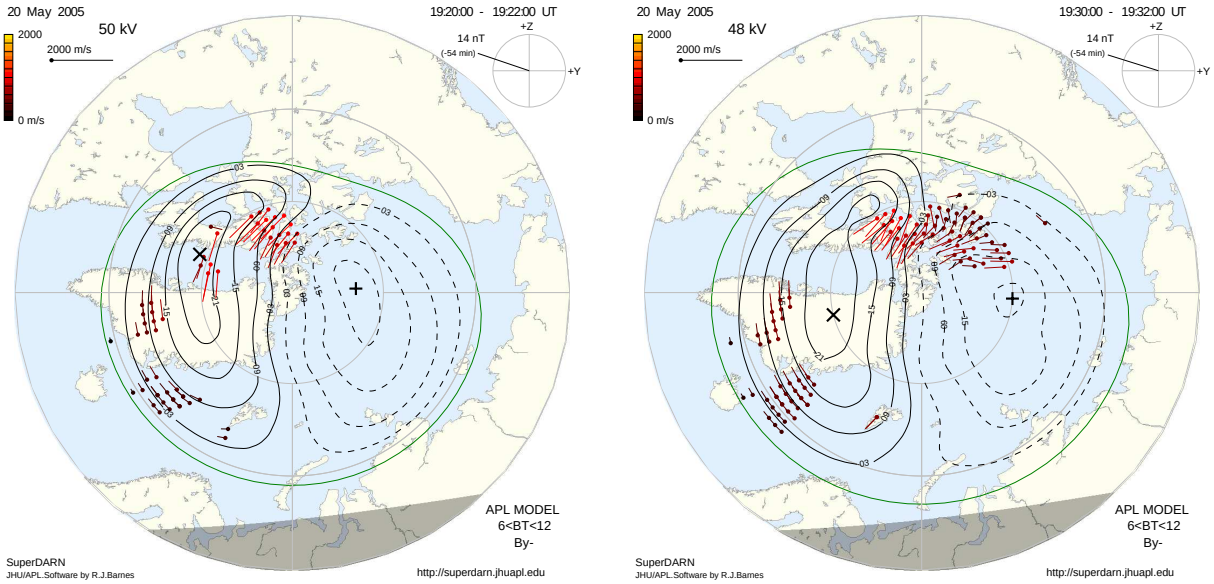

Figure 5.12: *Large scale convection maps from the SuperDARN radars at 1920 UT (left figure) and 1930 UT (right figure). Same format as previous figures.*

positive B_z gradient (downward FAC) followed by a strong negative gradient (upward FAC). We believe that the convection pattern has changed from a 2-cell reverse convection to a distorted 2-cell pattern for $B_y < 0$ with a round dawn cell and a crescent-shaped dusk cell. We note that the polar cap is contracted after a long period of northward IMF. There is a good correlation between the B_z gradient (green, bottom panel) and the ion drift component transverse to the satellite trajectory (violet, panel 4) during the whole interval.

SuperDARN Convection maps for 1920 UT and 1930 UT

Figure 5.12 shows plasma convection streamlines and ion drift vectors from the SuperDARN radar during the time interval 1920-1930 UT and correspond to the DMSP F13 pass shown in figure 5.11. In the region 1000-1400 MLT/80-85° MLAT we find an antisunward flow with speeds around 1-1.5 km/s. This flow has the same intensity as the corresponding antisunward flow found in figure 5.11. A sunward return flow at lower latitude in the 18-22 MLT sector is similar to the small sunward convection channel encountered at dusk in figure 5.11. The figure at left (1920–1922 UT) shows some strong antisunward flow at 1800 MLT/80° MLAT. The figure at right (1930–1932 UT) gives an indication of convection towards dusk/premidnight in the sector 1000-0700 MLT/80-85° MLAT. The general view of the flows in the polar cap throughout the interval 1920-1932 is similar to the convection pattern found in figure 5.11, i.e. a distorted two-cell with dawn-dusk asymmetry as expected for $B_y < 0$.

5.2.4 Interval IV, 2200 (May 20) - 0130 (May 21) UT, Clock Angle [~75-100°]

The B_y (~ -13 nT) remained strongly negative while the B_z fluctuated around zero between 2200-0130 UT. Because of the large values of B_y and the small values of B_z, i.e. a westward

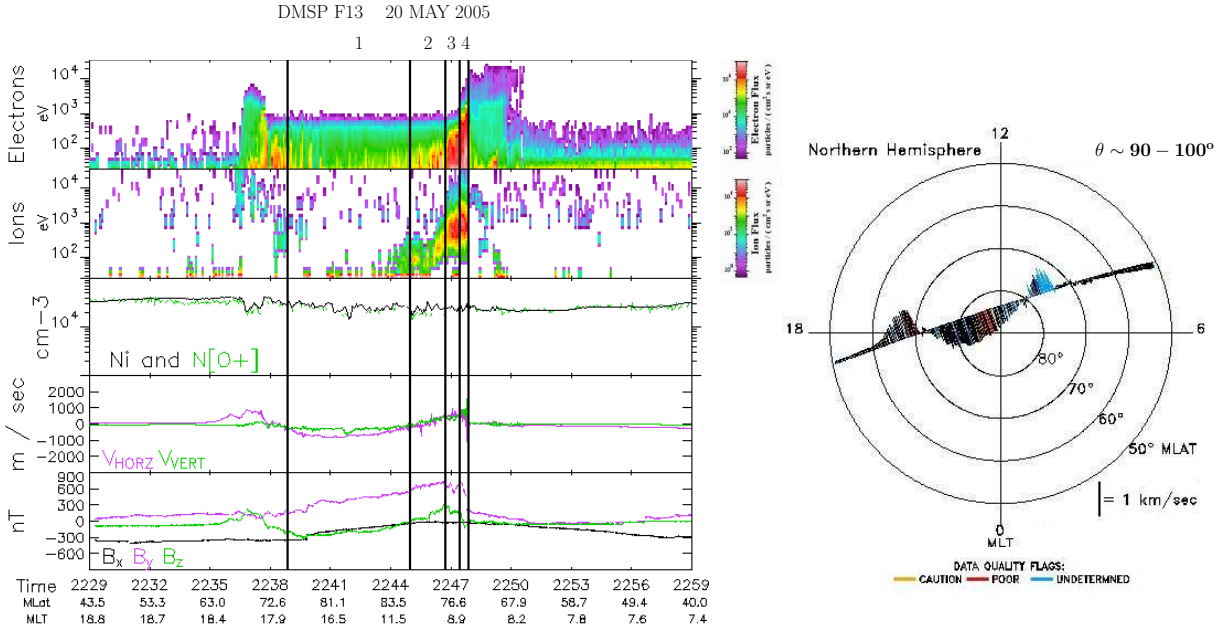

Figure 5.13: *Data obtained by DMSP F13 during the interval 2229 - 2259 UT on 21 May 2005. Same format as figure 3.2 in section 3.2.1.*

oriented field, the clock angle is stable around 90° ± 10°. We are now entering a clock angle regime similar to the two last DMSP passes in the previous case study on 12 August 2000. The difference is that the IMF B_y is strongly negative for this interval while it was strongly positive in the previous case. At ~2230 and 0000 UT DMSP F13 traverses the northern hemisphere polar cap in a 1900-0800 MLT orbit and the data obtained is presented in figures 5.13 and 5.14, respectively. The orbit is somewhat tilted compared to theoretical the dusk–dawn orbit DMSP F13 normally has.

DMSP F13 2229-2259 UT, Clock Angle [90-100°]

In the time interval of figure 5.13 the clock angle is between 90-100°.
At low latitude at dusk electron fluxes of 6-8 keV indicate a CPS-like source (2237 UT). The characteristic homogeneous polar rain which we observed in all the intervals in the previous case study (12 August 2000) is once again observed from 2239-2245 UT (from 1800 MLT/76° MLAT to 1000 MLT/80° MLAT). With help of vertical guidelines we have marked this interval as 1. Precipitation at lower latitudes at dawn (interval 2-4), suggests a large scale ion dispersion (panel 2) with energy up to 2-3 keV at 2246-2248 UT in the region 79-74° MLAT. In the same region, electron energy (panel 1) shows sign of different precipitation origin from mantle-type at 82-77° MLAT (marked 2) to LLBL-type at 77-75° MLAT (marked 3) and a small region of BPS-type at 75-74° MLAT (marked 4). We see CPS-like electron precipitation with fluxes of 4-6 keV equatorward of interval 4. Compared to the previous pass the polar cap has expanded. The convection pattern with homogeneous antisunward convection from 71° MLAT at dusk to 80° MALT at dusk with return flows at lower latitudes is seen. The antisunward convection maximizes on the dusk side (interval 1). We interpret this convection pattern as a distorted 2-cell with a big round dawn cell and a crescent-shaped dusk cell. A flow shear from antisunward to sunward is observed in interval 2.

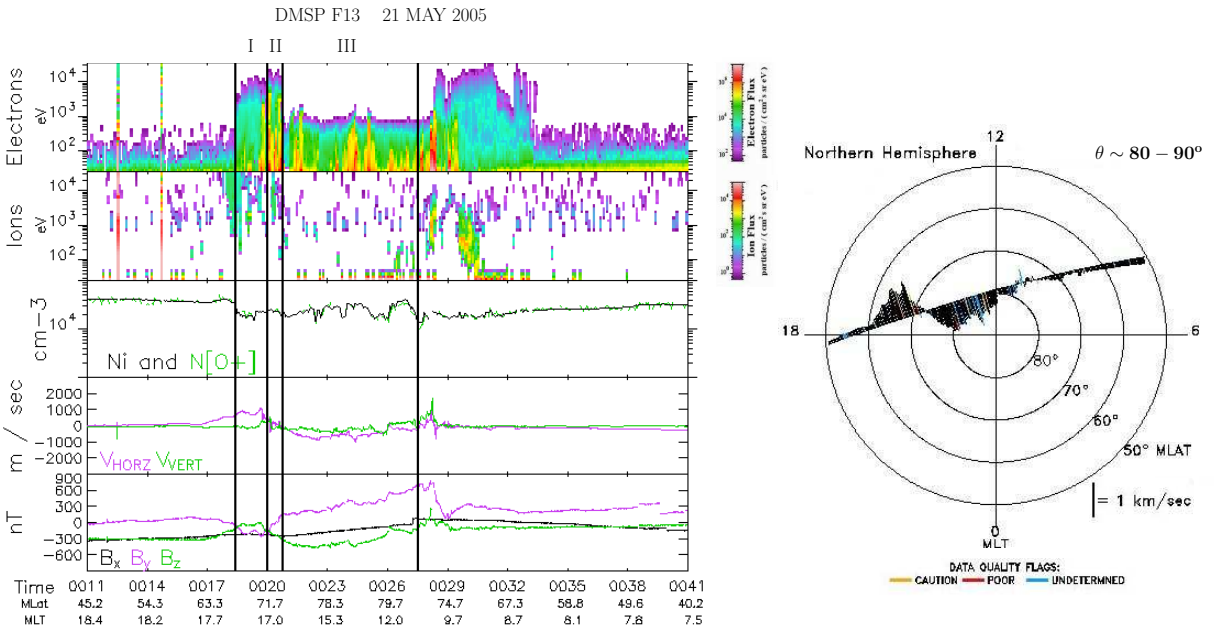

Figure 5.14: *Data obtained by DMSP F13 during the interval 0011 - 0041 UT on 20 May 2005. Same format as figure 3.2 in section 3.2.1.*

An upward FAC coincides with convection reversal and BPS precipitation at 2238 UT (equatorward and duskward of interval 1). A downward (interval 2) and upward (interval 4) FAC par are seen throughout the ion dispersion at dawn. The downward FAC coincides with a convection reversal and mantle-type precipitation. In interval 4 the upward FAC is co-located with the sunward convection and BPS-like precipitation.

DMSP F13 0011-0041 UT, Clock Angle [80-90°]

Figure 5.14 shows the data obtained form DMSP F13 between 0011-0041 UT. The solar wind parameters shown in figure 5.1 are similar to the previous DMSP F13 pass at ~2230 UT.
We note that the electrons of CPS-like origin (10-15 keV) are present during the interval 0018:30-0020 UT in figure 5.14 (interval I). As the satellite traverses poleward into the central polar cap it encounters a region of distinct fluxes of electrons of BPS-type precipitation (marked as II). During 0021-0027:30 UT (interval III) polar rain precipitation with three district polar arcs of 1 keV electron energy is observed. The first polar arc is located at 1600 MLT/74° and the two other polar arcs are centred near 1400-1300 MLT/79° MLAT.
A gradually stronger sunward flow at dusk with a maximum (1 km/s) in the end of interval 1 is followed by a convection reversal from sunward to antisunward in interval 2. The antisunward flow (interval III) is somewhat irregular with two velocity peaks at 77° and 79° in the dusk region.
Equatorward of interval 1 where the cross-track plasma drift (right panel) component has a positive gradient we see a downward FAC. This FAC could be coupled to a SAPS (subauroral polarization stream) flow channel. This R2 FAC extends into interval I. In interval II (0020-0021 UT) an upward R1 FAC coincides with a convection reversal (from sunward to antisunward) and BPS-type precipitation. Irregular convection with complex flow shear pattern and small-scale gradients in B_z (panel 5) contains polar arcs throughout the region of polar rain precipitation.

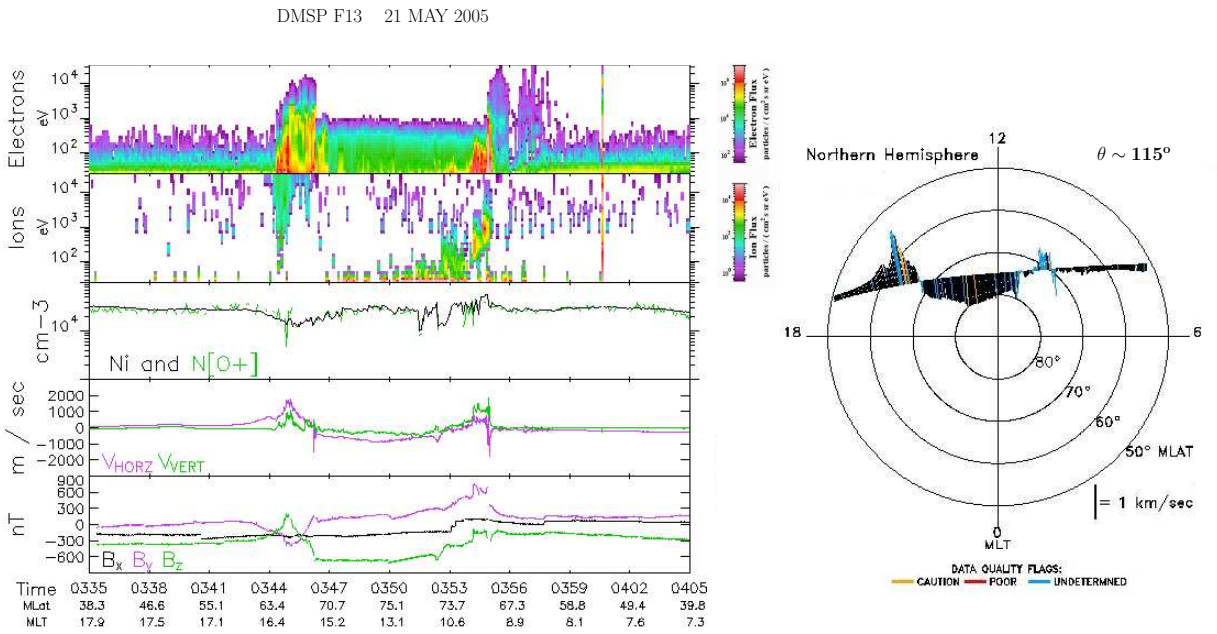

Figure 5.15: *Data obtained by DMSP F13 during the interval 0335 - 0405 UT on 21 May 2005. Same format as figure 3.2 in section 3.2.1.*

A district but small upward NBZ-like FAC is coupled to the polar arc seen at 0022 UT (1400 MLT/79° MLAT). As the satellite trajectory is tilted compared to the dusk-dawn line (~1800-0800 MLT), convection pattern at dawn gets harder to detect. A small sunward component (<150 m/s) at 1000 MLT/~76-74 MLAT indicates that the sunward convection pattern is confined to higher latitude. We conclude that the arcs in this interval are observed in a region of irregular flow shear.

5.2.5 Interval V, 0210 - 0500 UT, Clock Angle [~135°]

Interval V completes our case study and the magnetic field rotates to a south-west orientation (clock angle ~135°). Throughout interval V B_y increases to values around - 5 nT while the B_z stays around - 5-7 nT. From the solar wind parameter shown in figure 5.1) we see several indications of that we have entered the last part of the magnetic cloud. The solar wind speed and the total magnetic field have decreased to below 425 km/s and 10 nT, respectively. DMSP F13 collected data from the northern hemisphere in the middle of this interval at ~0330 UT, and figure 5.15 shows the data from this pass.

DMSP F13 0335-0405 UT, Clock Angle [130-135°]

In this time interval the IMF clock angle is stable around 130 – 135°. From figure 5.15 we see that DMSP F13 reached a peak magnetic latitude of only 75° and thus we have only limited information about the precipitation and convection pattern at this time. For our purpose this is still okay since the IMF is strong and thus the convection pattern is not only confined to high latitudes.
From 0344-0345 UT CPS-type precipitation with electrons below 10 keV is observed. High fluxes of electrons with energy ~ 1 keV of typical BPS-origin are encountered at 0345-0346

UT followed by a region of homogeneous polar rain in the interval 0346-0354 UT.
A positive gradient in the ion drift (panel 4) and in the magnetic deflection component B_z (panel 5) coincides with the CPS-type precipitation at 0344-0345 UT and we suggest that this region is coupled to the downward R2 system. Further poleward we see a strong sunward flow channel ($\sim$ 1800 m/s) and an accompanying upward R1 FAC in the region of BPS-like precipitation. Stable antisunward flow maximize on the dusk side (1 km/s at 0350 UT). As in the previous interval only a weak sunward flow is visible on lower latitude at dawn and further we see that as in our previous pass we have a rather symmetrical two-cell convection pattern with antisunward convection at high latitudes and sunward return flow on lower latitudes.

5.3 Summary and Discussion

We shall summarize and discuss the results on the basis of the observations found on May 20-21, 2005. Since we have a double field rotation in the magnetic cloud/complex eject we are able to study the ionospheric convection for many stable IMF conditions. As we have seen in this case study the changes in all three IMF components contribute to a wide range of different ionospheric conditions. The dipole tilt of the Earth at late May, like in our event, favours lobe reconnection in the northern hemisphere (see section 2.3). We have an unfavourable B_x polarity for the northern hemisphere from the start of the cloud to 1930 UT on 20th of May ($B_x > 0$). In the period of unfavourable B_x polarity we will have two opposing effects for exiting lobe cell circulation, i.e the dipole tilt will favour the northern hemisphere (MAY) while the B_x polarity favours the southern hemisphere. Another factor that may favour lobe reconnection is the strong B_y component especially from 1800 UT on 20 May onwards (Eriksson et al., 2003 and many others, see section 2.3).

The first DMSP F13 pass we look at is shown in figure 5.5 at ~0900 UT (interval I). The data is to a large extent similar to our prevous case study on August 12, 2000, i.e. a large rounded merging cell at dusk and a smaller (”crescent-shaped”) dawn cell. Inside the merging cell at dusk we observe high-latitude arcs in the region of upward NBZ-like FAC (region II in figure 5.5). The high-latitude arcs in conjunction with flow shear on the dusk side of the polar cap are taken as signature of the presence of a lobe cell. The presence of a composite pattern of merging and lobe cells for this IMF condition is in agreement with our previous case study.

In interval II the clock angle is less then 45° the whole time. What seems to be clear when we look at interval II (which is in the period of unfavourable B_x polarity) is that lobe reconnection occurs in the northern hemisphere.
The DMSP F13 satellite traverses over the northern hemisphere in a dusk-dawn MLT/MLAT orbit in the day sector. For each orbit over central northern polar cap, DSMP F13 reaches higher latitudes from noon. (compare right panel in figure 5.6, 5.7 and 5.8). This means that the most equatorward pass occurs at $\sim$ 1220 UT (figure 5.6) while the most poleward pass occurs at $\sim$ 1730 UT (figure 5.8). We also note that the to first passes occur on the sunward side of the geomagnetic pole while latter traverses on the antisunward side. In the three DMSP F13 passes over the northern hemisphere we see evidence of two lobe cell in the polar cap (reverse convection; i.e. sunward flow over the polar cap confined to very high latitudes, and return antisunwward flows at lower latitudes, compare to bottom panel in figure 2.4)) with cusp-type

precipitation in the regime of sunward convection. The two first passes occur under B_y positive condition while last pass occurred when the B_y changed polarity.
There is clear difference in the ion precipitation in the regime of sunward convection between the three DMSP passes at ~ 1220, ~ 1400 and ~ 1730 UT. For the passes that occurs on the sunward side of the geomagnetic pole, i.e. at ~ 1220 and ~ 1400 UT, we can see that the ions are more intense and have higher energy (keV) in figure 5.7 at ~ 1400 UT. For the pass that traverses over the central polar cap on the antisunward side of the geomagnetic pole (figure 5.8 at ~ 1730 UT) there are no sign of ion fluxes in the regime of sunward convection. We believe that this difference in data is related to the location of the cusp and the trajectory of the DMSP F13 satellite. The pass with the highest ion energy on the sunward side of the pole (~ 14 UT) is the one that traverses the central polar cap at the highest latitudes. The inverse energy-latitude dispersion observed slightly equatorward of the geomagnetic pole, at ~ 86° MLAT in figure 5.7 at ~ 1400 UT is likely the location of the cusp merging site. With this in mind we see that the F13 pass at ~ 1220 UT UT traverses the central polar cap to a small degree on the sunward side of the cusp and therefore only encounters low ion energy. The F13 pass at ~ 1730 traverses the central polar cap on the antisunward side of the cusp and ions where seen. This is consistent with the what we have implied, i.e. that the location of merging site and the precipitation energy is higher at highest latitudes.
A clear upward FAC with a associated inverted-V arcs is seen at ~ 1220 UT and ~ 1400 UT in the dawn cell. After the B_y polarity changes to negative values, the dusk cell becomes more pronounced than the dawn cell. The Inverted-V arcs seen in the dawn cell in the two previous passes have disappeared. The small ”viscously-driven” convection cell at dusk that coincided with BPS-like precipitation and a upward FAC is seen throughout the whole interval.

In interval III the clock angle changes from ~ 45° to 90°. From around 1900 UT onwards the dominant IMF component is the strongly negative B_y. In the prior interval we noted that the dominant convection system was the reverse 2-cell convection pattern related to strongly northward IMF. In figure 5.11 at ~ 1910 UT we observed a distorted two-cell system with dawn-dusk asymmetry as expected for $B_y < 0$. The polar cap is contracted after a long period of northward IMF. Thus, a transition from the reverse two-cell (lobe) pattern to a distorted merging cell convection pattern has taken place in the response to clock angle change from $< 45°$ to $> 60°$.

In interval IV the magnetic field is oriented westward with a clock angle around 80 – 100°. We see a distorted 2-cell with a big round merging cell at dawn and a crescent-shaped dusk cell. Compared to the previous interval the polar cap has expanded. Isolated arcs associated with localized flow shears and small scale negative B_z-gradient in the central polar cap where encountered for negative B_y and clock angle of 80-90° (see figure 5.14 at ~0010 UT. The presence of polar arcs were seen in two DMSP F13 passes in the same clock angle regime in case study 1 (see figure 4.8 at ~1820 UT and 4.10 at ~2140 UT in section 4. However, the B_y is strongly negative in interval IV while it was strongly positive in case study 1. While we observed composite pattern with distinct arcs inside the lobe cell for August 12, 2000 (case study 1), we observed a distorted two cell pattern with absence of lobe cell when B_y was negative (case study 2). The clock angle increases to ~ 135° in interval V. The polar cap has expanded and a 2-cell pattern is seen. The convection is characterised by relatively homogeneous antisunward flow and the absent of polar arcs.

With the purpose of investigating the question of interhemisphere asymmetries we look at a DMPS pass in the southern hemisphere in interval II (figure 5.9 at ~ 1815). The most prominent difference between the southern and northern hemisphere is that the convection pattern is more irregular in the south.
From the electron precipitation (panel 1) we see a region of distinct polar arcs with energy between 200-600 eV which coincides with irregular flow shears in the polar cap. With help of picture sequence from the IMAGE WIC camera, obtained in the same time period as DMSP F13 passes over the southern hemisphere, we observed a midnight arc in the period 1823-1857 UT (We only showed a sequence from 1830-1834 UT). We noted that the arc showed signatures of being stretched towards noon from the poleward boundary of the nightside oval in the region between 70 and 85° MLAT. We also notice a bright auroral in the noon sector around 80° MLAT. We believe that the one large scale midnight arc in figure 5.10 is the same as the small scale distinct polar arcs in figure 5.9. The image sequence seen from IMAGE is not accurate enough to see the small scale arcs. However, we get a more comprehensive global overview of the polar arcs.
Kullen et al. (2002) reported that most midnight arcs occur during times of high solar wind velocities (> 450 km/s) and solar wind dynamic pressure (> 1.7 nPa). Other important factors concerning midnight arcs are that B_z should be predominantly northward for at least 1 hour before the arc occur and that the majority of the midnight arcs involve a B_y and B_z sign change. When we compare this claims with our interplanetary parameters in the time period of the midnight arc we see that the B_z has been strongly positive for a long period and that B_y changed polarity (~ 1650 UT) one and a half hour before the midnight arc becomes visible around 1823 UT (not shown). The solar wind velocity and dynamic pressure were higher than 450 km/s and 2.5 nPa, respectively. All the midnight arc properties we observed seem to be in agreement with what Kullen et al. (2002) found.

Chapter 6

Case study 3: June 12-13, 2005

On June 12-13, 2005 we investigate the ionospheric flows during the interval when a magnetic cloud (MC) interacts with the Earth's magnetosphere. The leading edge of the cloud was detected by Wind at 1500 UT on June 12, 2005. Within the MC the magnetic field vector rotates from south to north. The cloud caused a strong storm (D_{ST} minimum -106 nT) and the arrival of the shock, driven by the cloud caused a sudden impulse (SI) in low-latitude ground magnetograms. The field rotation of the magnetic cloud is somewhat similar to the August 12, 2000 case study and according to polarity of our magnetic clouds it is classified as a South-East-North (SEN) flux rope. We will focus on the clock angle regime between $100 - 135°$, i.e. from $\sim$ 2400 UT, June 12, 2005 and onwards. Below we shall for convenience use the notation 0600 UT (13) to refer to 0600 UT, June 13, 2005, etc.

6.1 Interplanetary Data Set

Interplanetary field and plasma data from the solar wind experiment (SWE) (Ogilvie et al., 1995) and the magnetic field investigation (MFI) (Lepping et al., 1995) on the Wind spacecraft is presented in figure 6.1. The data resolutions are 3 sec (MFI) and 90 sec (SWE). From top to bottom, the panels show the proton density (cm^{-3}), temperature (K), the bulk speed (km/s), dynamic pressure (nPa), the total magnitude (nT) and GSM X, Y, and Z components of the magnetic field (nT), plasma β, and the IMF clock angle (polar angle in the GSM YZ plane) for the period 0700 UT (12) -1500 UT (13) (we will from now on refer to ground time, see section 6.1.1) on June 2005, 12-13. During the cloud passage the Wind satellite was located at (244.6, -32, 10.4) R_E in GSE coordinates. In figure 6.1 the magnetic cloud front boundary is encountered at 1600 UT (12) and can be seen as a sudden decrease in the proton temperature and plasma β to values lower than the expected for the solar wind (red trace in the temperature panel gives the expected temperature for normal solar wind expansion from the statistical studies of Lopez and Freeman (1986)). The rear boundary of the cloud is encountered at $\sim$ 1400 UT (13).
A prominent feature of this event is the steady positive $B_y > 5$ nT from $\sim$ 1930 UT (12) to $\sim$ 1420 UT (13), for most of the cloud interval. We also note the following features: (i) A relatively weak, negative B_x ($\sim -$ 2-3 nT). A steady positive gradient in the IMF B_z (panel 8) throughout the whole cloud, taking it from -18 nT to -2 nT at the beginning and end of the cloud, respectively. (ii) The smooth and slow rotation of the magnetic field direction through a relatively large angle and the low proton temperature ($< 3 \times 10^4$ K) and low plasma β (< 0.1)

during the whole interval is consistent with the essential features for a magnetic cloud (Burlaga et al., 1981; Klein and Burlaga, 1982; Burlaga, 1995). (iii) The solar wind temperature and plasma β increase in the rear boundary of the cloud. This evident increase in the solar wind temperature and plasma β, might be the rear boundary of the magnetic cloud but these matters need not concern us here. (iv) As the structure advances over the satellite, the strength of the total magnetic field decreases steadily from $\sim$ 20 nT in the beginning to $\sim 5-6$ nT in the rear boundary of the cloud. (v)We note an interesting behaviour in the profile of proton density (top panel). A region of high density $\sim 8-12\ cm^{-3}$ is seen in the time period from 0600 UT till 1000 UT. Relatively low density ($< 3.0\ cm^{-3}$) is encountered on both sides of this interval except in the beginning of the cloud from 1600 to 2350 UT (12), i.e. in the region where the clock angle is strongly south. As mentioned before, our focus is in the time interval $\sim$ 2400 UT (12) onwards (13) where the clock angle regime is between 100-135°.
The two first vertical guidelines at 7.51 UT and 16 UT in figure 6.1 mark the arrival of the shock and front cloud boundary, respectively. Different time intervals have been named I,II and III (panel 1) and marked with vertical guidelines. The intervals are mainly chosen after the behaviour of the density profile. In Interval I from 2350 UT (12) to 0600 UT (13) the clock angle is between $\sim 110-135°$. From figure 6.1 we see that proton density (top panel) is less then 3.0 cm^{-3} for the entire interval. The prominent feature during the interval II from 0600-1000 UT (13) is that the proton density (top panel) has increased to $\sim 8-12\ cm^{-3}$. This is an increase in the density by a factor of 3-4 compared to the previous interval. The clock angle is between $\sim 100-140°$ in this interval. In the time period 1000-1400 UT (13), marked as interval III, the field is pointing south-east and the clock angle is fluctuating between $100-130°$. The proton density is once again low ($< 3.0\ cm^{-3}$).

6.1.1 Time Delay

The start of the cloud sheath, which is characterized by strong magnetic field fluctuations, is detected by Wind as a strong increase in the total magnetic field, density and dynamic pressure at 0651 UT. As the shock interacts with the magnetosphere it produced a sharp rise in the H-component of the terrestrial field at low latitudes. This is called a storm sudden commencement (SSC) (see section 3.3.1 and Kivelson and Russell, 1995, chap. 9.2). Figure 6.2 shows the SSC at the ground station Kototabang which is located at latitude $-0.20°$ and longitude 100.32° in geographic coordinates ($-10.63°$ MLAT and 171.93° MLONG). The SSC is marked with a vertical line at 0748 UT in figure 6.2. We see that the time delay from Wind to Kototabang is $\sim$ 1 hour and we will use a delay time of 1 hour for the rest of the interval as well.

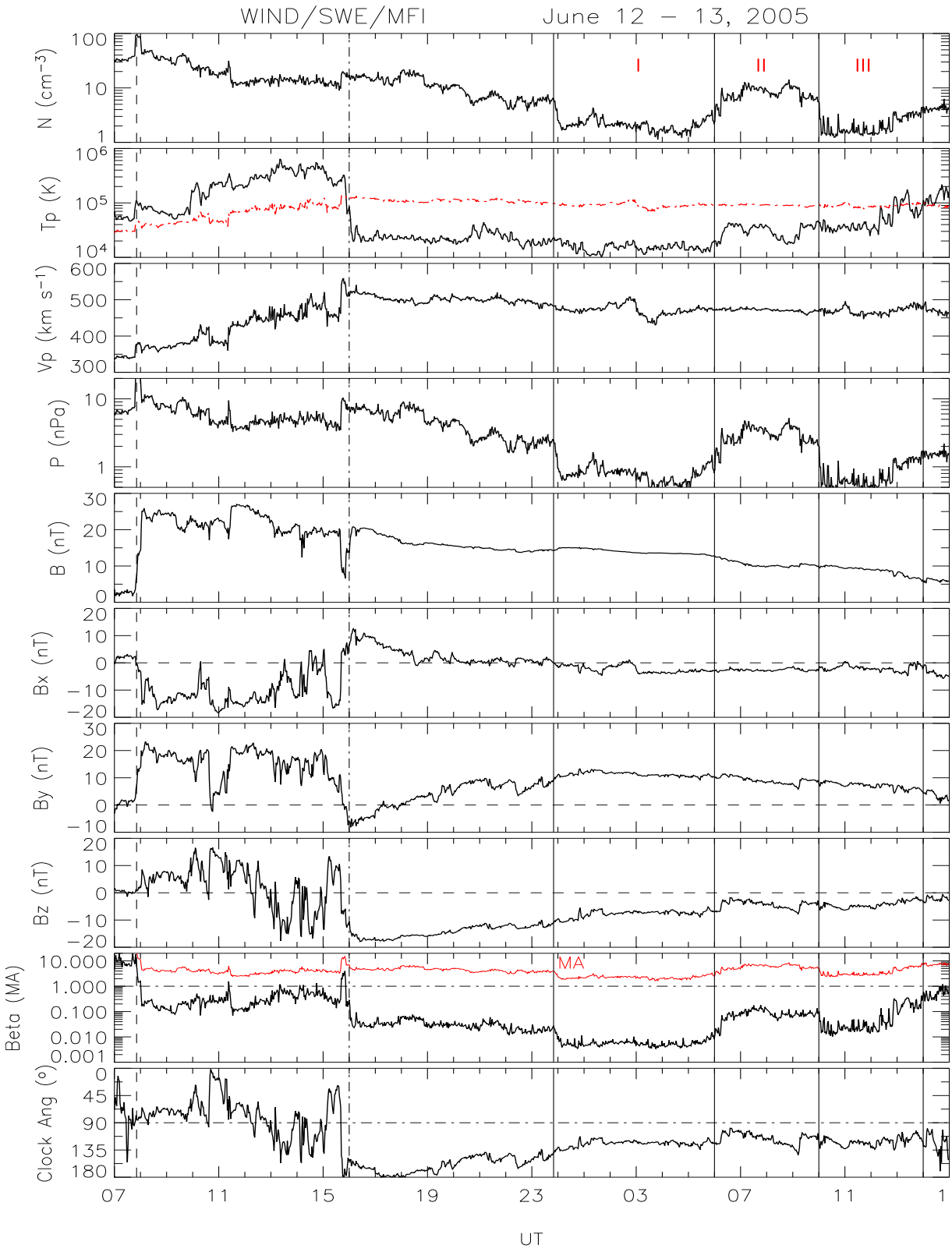

Figure 6.1: *Solar wind plasma and interplanetary magnetic field (IMF) data obtained from spacecraft Wind during the interval from 0700 on 12 June 2005 to 1500 UT on 13 June 2005. Panels from top to bottom show proton density, temperature, bulk speed, dynamic pressure, the total field, the GSM components of the magnetic field, plasma β and Alfv́en-Mach number (the latter in red) and the IMF clock angle. The red trace in the temperature panel gives the expected temperature for normal solar wind expansion from the statistical studies of Lopez and Freeman (1986). The horizontal axis shows the universal time (UT) in hours when the delay time is added.*

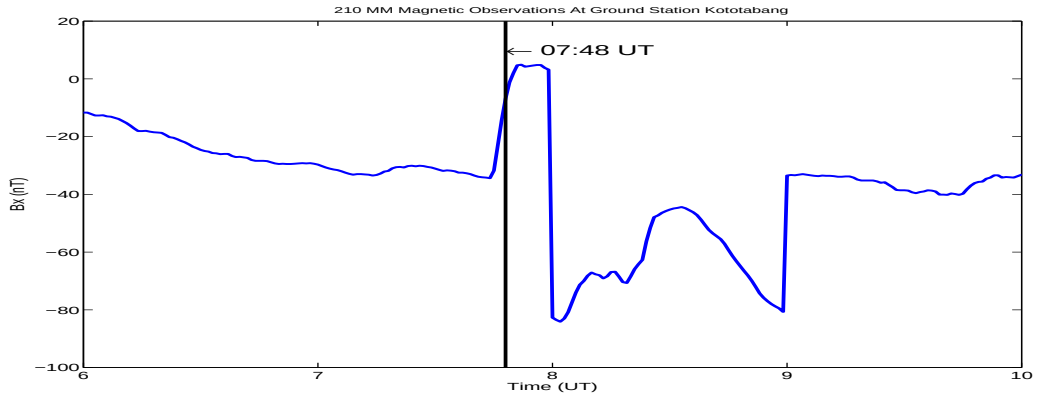

Figure 6.2: *Time of arrival of the SSC at the ground station Kototabang (KTB)*

6.2 DMSP results

The rotation of the cloud field and the clock angle is to some extent similar to our case study on August 12, 2000 and we expect that the convection pattern of the ionosphere also should be similar. The different DMSP data is described below, ordered by interval, time, clock angle and density. Basically, for Bz < 0 and clock angle between 110−135°, we expect to see asymmetries in the standard two-cell convection pattern due to the B_y.

6.2.1 Interval I, 2350 - 0600 UT (June 12-13), Clock Angle [110-135°], Density [< 3.0 cm^{-3}]

During interval I, the B_y is strongly positive (~10 nT) and the B_z slowly decreases from -10 nT to -7 nT. There are only small scale fluctuation in clock angle throughout the entire region and the clock angle is between ~ 110-135°. The total field strength decreases from ~ 20 nT to ~ 17 nT. The density and the solar wind dynamic pressure is low, < 3.0 cm^{-3} and < 1.7 nPa (see panel 1 and 4 in figure 6.1). Throughout interval I the plasma β is less then 0.010 and the solar wind speed remained moderately high (~ 475 km/s). We study two DMSP F13 passes over the northern hemisphere in interval I.

DMSP F13 2347 UT (12) - 0017 UT (13), Clock Angle [~135°], Density [~2.0 cm^{-3}]

Around 2350 UT (12) the Wind spacecraft observed a sudden decrease in the density from ~7 to ~2.0 cm^{-3}. In the following period the density and the clock angle was stable around ~2.0 cm^{-3} and ~135°, respectively. Figure 6.3 show the particle and drift data measured by the DMSP F13 in between 2347 (12) and 0017 UT (13) and we have again indicated various precipitation regions by vertical guidelines

From the precipitation (panel 1) we see that as the satellite traverses over the northern polar regions from dusk it enters a region of homogeneous electrons of CPS-like fluxes (~ 10 keV) at ~ 2352 – 2355 UT (58 – 65° MLT). As the satellite enters the region marked I (65 – 69° MLT) it encounters typical BPS-like precipitation with average energies of 1-2 keV for electrons. At higher latitude at dusk (~ 69 – 74° MLT) signs of discrete high-latitude arcs (region II) are seen.

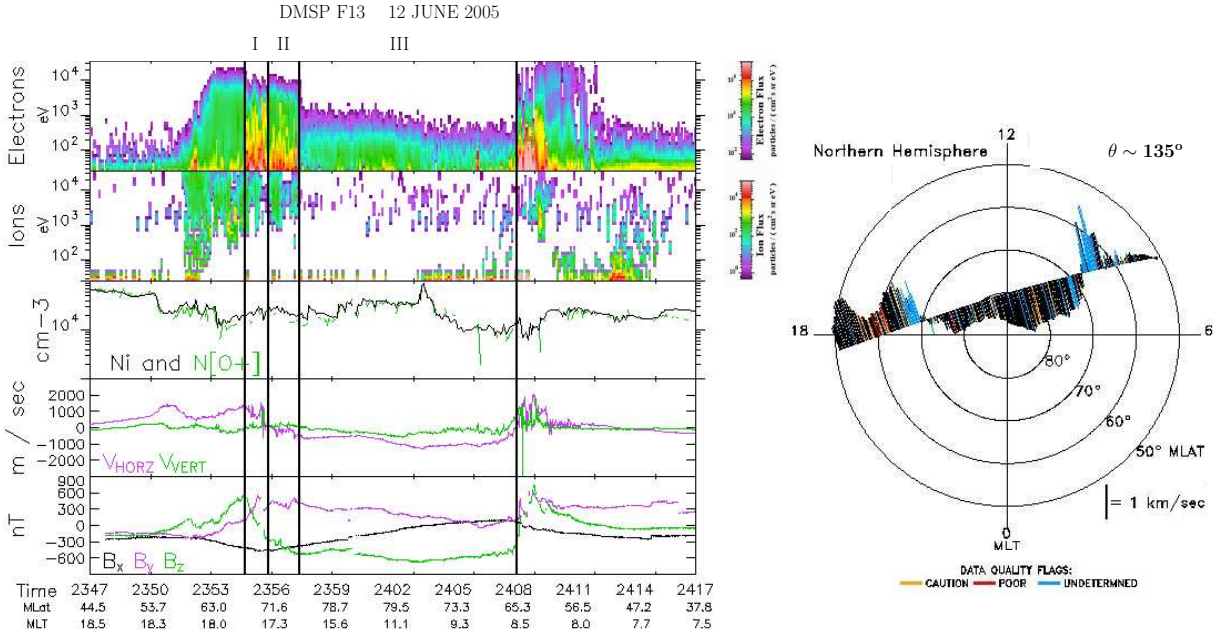

Figure 6.3: *Data obtained by DMSP F13 during the interval 2347 - 0017 UT on 12-13 June 2005. Same format as figure 3.2 in section 3.2.1.*

As the satellite enters region III it detects polar rain.
The cross-track plasma drift data (right panel) show two distinct enhanced sunward flow channel (~ 1 km/s) are seen at 55° and 69° MLAT and we notice that the the latitudinal width of the sunward flow pattern is large (45 – 69° MLAT). A strong flow shear from sunward flow to antisunward flow is seen in the beginning of interval II (69 – 70° MLAT). A local minimum of -500 m/s in antisunward flow on the duskside is followed by another minimum of - 1100 m/s in the middle of region III at 10.5 MLT/79° MLAT. In close vicinity of where we have marked the end of polar rain precipitation (region III) a strong flow reversal from antisunward (-500 m/s) to sunward (2000 m/s) is followed by a narrow channel of sunward flow at dawn (76 – 73° MLAT). A weak positive B_z gradient in the region of CPS-like precipitation and sunward convection is interpreted as the upward R2 FAC on closed field lines. In region I a decreasing gradient in B_z (green) is interpreted as an upward R1 FAC which coincides with the BPS precipitation and the sunward convection. We see a weaker negative trend in B_z in region II. The flow pattern could be described as a 2-cell pattern with a dusk-dawn asymmetry. A lobe cell may be present at dusk and we will discuss this more thoroughly in the discussion of this case study. We conclude that region II is characterized by a strong flow shear (convection reversal) and high-latitude arcs and an upward NBZ-like FAC.

DMSP F13 0130-0200 UT (13), Clock Angle [~115°], Density [~2.0 cm^{-3}]

The clock angle has decreased to ~115° while the density (~2.0 cm^{-3}) is the same as in the previous pass.
In figure 6.4, a region of high energy electron (1-10 keV) is located between 60 – 63° MLAT at dusk. These values corresponds to the energies of typical CPS-type precipitations. As the satellite enters region I (63-70° MLAT) it encounters a region of BPS precipitation. Just as in

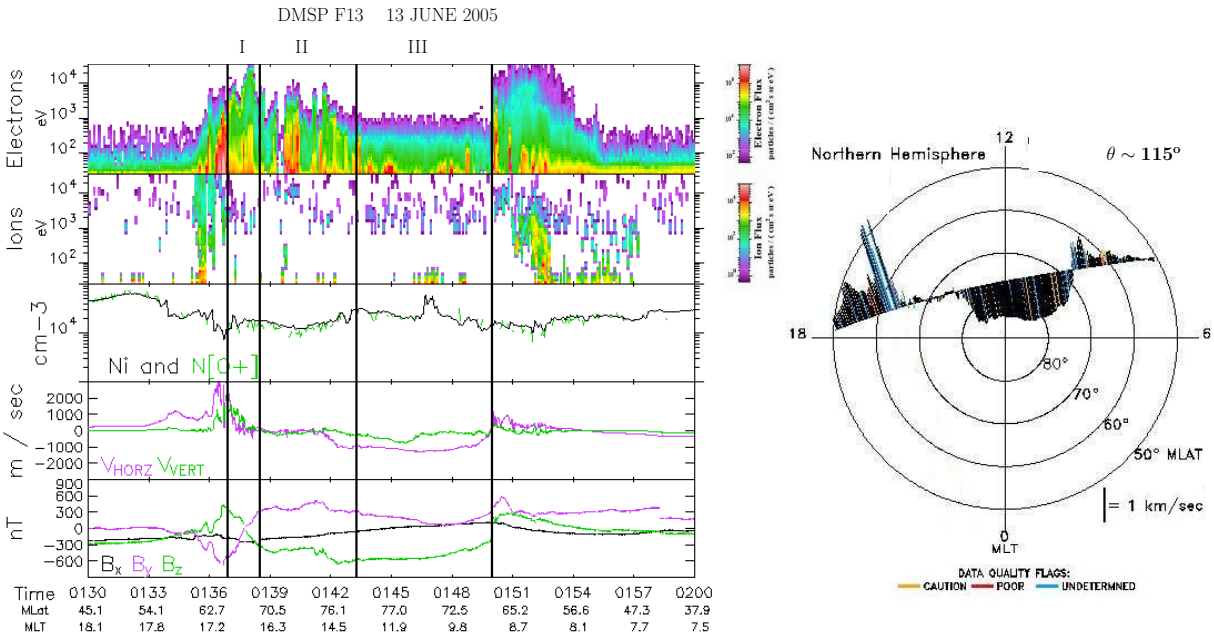

Figure 6.4: *Data obtained by DMSP F13 during the interval 0130 - 0200 UT on 13 June 2005. Same format as figure 3.2 in section 3.2.1.*

the previous pass signs of discrete high-latitude arc is seen in the end region II. As the satellite enters region III the precipitation changes to polar rain.

A narrow region of enhanced (> 3 km/s) sunward flow in the close vicinity of the equatorward edge of region I (62 – 64° MLAT) is followed by a strong flow shear (end of region I). A region of small flow irregularities around 0 m/s (65 – 73°) is followed by another flow shear from small irregular convection to antisunward flow in region II. Homogeneous antisunward flow with velocity ~ −1 km/s is seen throughout region III. With respect to the previous diagram, the part of the antisunward flow at dusk has been suppressed and is close to zero. The convection reversal is thus now ill-defined in a large part of region I.

A downward R2 FAC at low latitude coincides with CPS precipitation and strong sunward convection. An upward R1 field-aligned current is co-located with the strong flow shear and BPS precipitation in region I. A negative gradient in the B_z (panel 5) occur in the same region as the high-latitude arcs and flow shear from small irregular velocities to antisunward flow (end of region II). We conclude that the high-latitude arcs in the end of region II are observed in a region of relatively strong flow shears and upward NBZ-like FAC.

6.2.2 Interval II, 0600 - 1000 UT (June 13), Clock Angle [95-140°], Density [~8-12 cm^{-3}]

In interval II we study one DMSP F13 pass over the northern hemisphere. Following the increase in solar wind density to ~8-12 cm^{-3} and dynamic pressure to ~ 4-5 nPa, the clock angle varies between ~ 95-140°. The B_y decreases from > 10 nT to ~ 7 nT and the B_z fluctuate around -5 nT. The total field strength is ~ 10 nT. The plasma β increased to 0.1 and the solar wind speed remained high (~ 475 km/s). Compared to the previous interval the main difference in the cloud parameters is the high solar wind density and dynamic pressure .

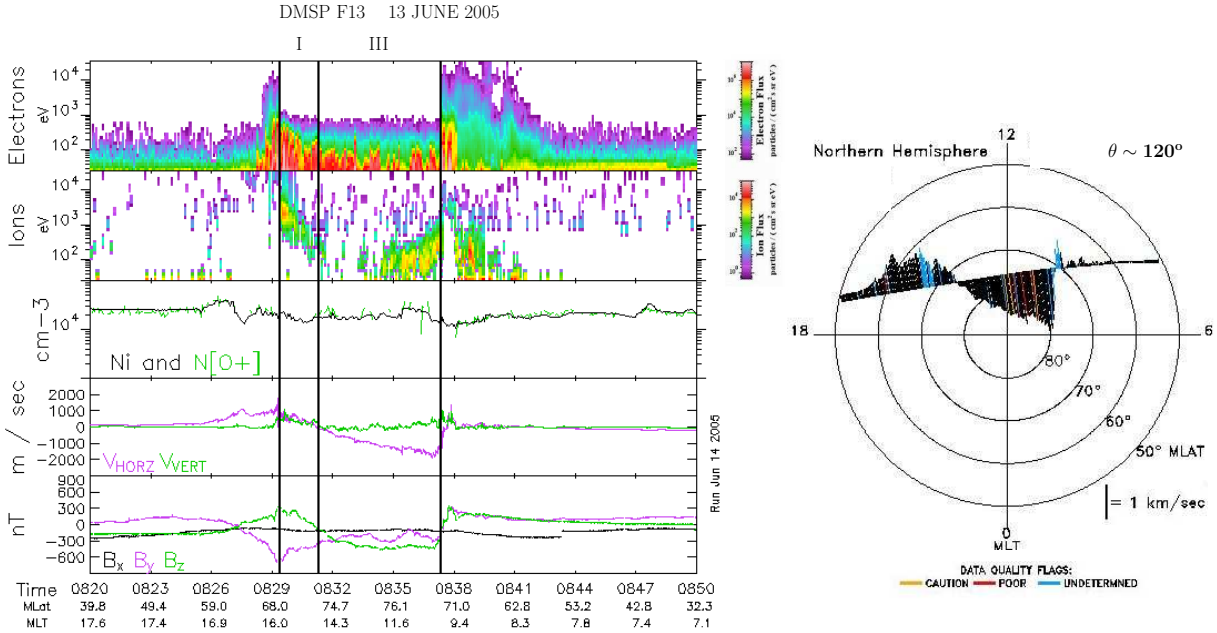

Figure 6.5: *Data obtained by DMSP F13 during the interval 0820 - 0850 UT on 13 June 2005. Same format as figure 3.2 in section 3.2.1.*

DMSP F13 0820-0850 UT (13),
Clock Angle [$\sim 120°$**], Density [**$\sim 10.0\ cm^{-3}$**]**

During the tie interval of DSMP F13in figure 6.5, the clock angle is $\sim 120°$. The solar wind density and dynamic pressure are ~ 10 cm^{-3} and ~ 4 nPa.
CPS precipitation is encountered at low MLT at dusk ($68-69°$ MLAT). In the region marked I ($69-76°$) the satellite encounters discrete BPS precipitation. The high-latitude arcs we observed in the previous region is absent, and the general electron fluxes is weak with electron energy up to a few hundred eV are seen in the central polar cap (region III). This seems to be a mixture of tenuous polar rain and weak mantle-like precipitation confined to high MLATs on the dawnside. In the cross-track plasma drift (right panel) we see a region of sunward flow ($\sim$ 1000 m/s) at dusk followed by a flow shear from sunward to antisunward convection in region I (73° MLAT). There is a strong negative gradient towards dawn in the antisunward convection pattern with a minimum of -2000 m/s at 71° MLAT (region III). There is evidence of a weak narrow sunward flow ($\sim 200-300$ m/s) just equatorward of a strong convection reversal in the close vicinity of the vertical line that marks the end of region III (71° MLAT at dawn). Considering the to distinct convection reversals we suggest that the polar cap boundary is located approximately at 73° MLAT (duskside) and 71° MLAT (dawnside).
We associate the upward and downward pair of FAC at dusk to be the R2 and R1 field-aligned currents. However there are no signs of the upward NBZ-like FAC poleward of the R1 current, which we observed in the previous interval. There is a good correlation between the B_z gradient (green, bottom panel) and the ion drift component transverse to the satellite trajectory (violet, panel 4) during the whole interval. In conclusion, we see a sunward flow on low latitude on both side separated by a strong antisunward gradient in the central polar cap. The convection pattern is likely a twin-cell with a big round merging cell at dusk and a small crescent-shaped cell at dawn.

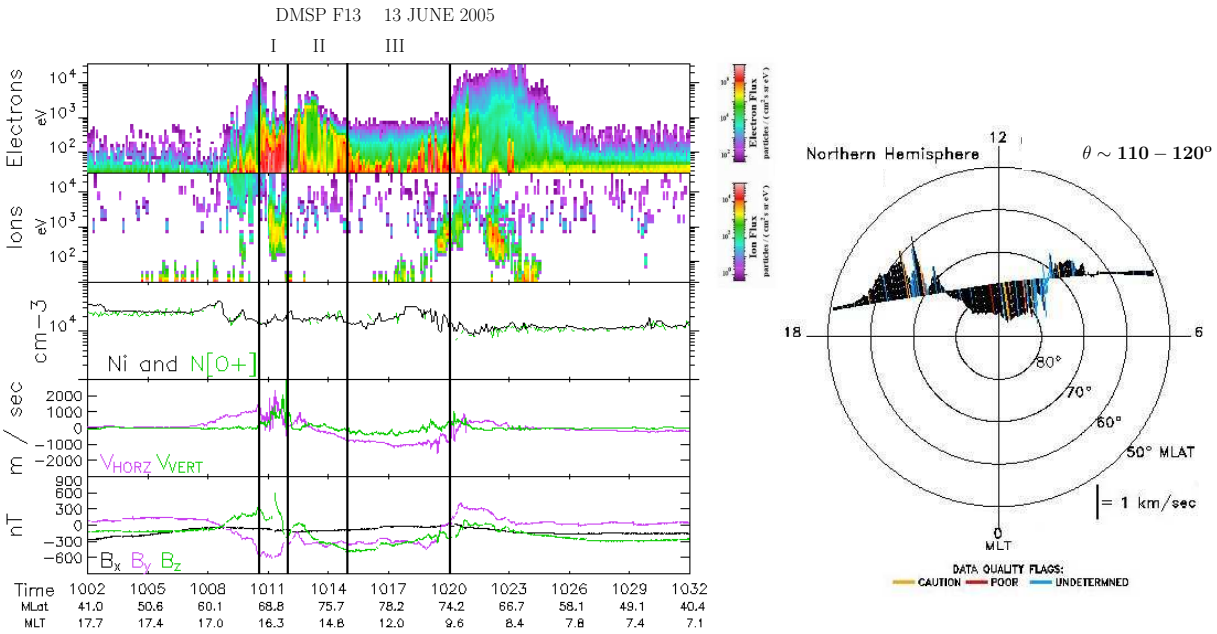

Figure 6.6: *Data obtained by DMSP F13 during the interval 1002 - 1032 UT on 13 June 2005. Same format as figure 3.2 in section 3.2.1.*

6.2.3 Interval III, 1000 - 1400 UT (June 13), Clock Angle [100-130°], Density [<3.0 cm^{-3}]

Throughout interval III the clock angle is fluctuating between $100-130°$ and the proton density is once again low (< 3.0 cm^{-3}). The IMF B_z has a small positive gradient in the whole interval and increases from - 7 nT to -2 nT in the beginning and end of the interval, respectively. Like in the previous interval the B_y continue to decreases from $\sim$ 9 nT to $\sim$ 4 nT. The solar wind speed is $\sim$ 475 km/s. We notice that both the solar wind proton density, temperature and plasma β increases at the end of this interval. If we compare the cloud parameters in this interval with the the two previous intervals, we notice that the the main difference is once again the solar wind density and dynamic pressure. We expect to see similar precipitation and convection pattern as in interval I in the two DMSP F13 observations which we summarized in this interval.

DMSP F13 1002-1032 UT (13), Clock Angle [110-120°], Density [<2.0 cm^{-3}]

Figure 6.6 show data from the DMSP F13 over the northern hemisphere in the interval 1002-1032 UT (13). The IMF clock angle is between $110-120°$; $B_y \sim 8-9$nT; B_x and B_z are slightly negative. The solar wind density and dynamic pressure are both low, with values of $\sim$2.0 cm^{-3} and $\sim$ 1 nPa .

The precipitation in figure 6.6 is very much like the precipitation found in interval I. This means that we encounter CPS precipitation at low latitude at dusk and BPS-type precipitation in region I ($67-70°$ MLAT) with electron energy between 700-1000 eV; Distinct high-latitude arcs in region II and polar rain in region III. A pattern with two channels of enhanced sunward flow ($\sim$ 2 km/s) is encountered at dusk (region I). Another but somewhat weaker channel of enhanced sunward flow $\sim$ 1 km/s followed by a convection reversal from sunward to antisunward

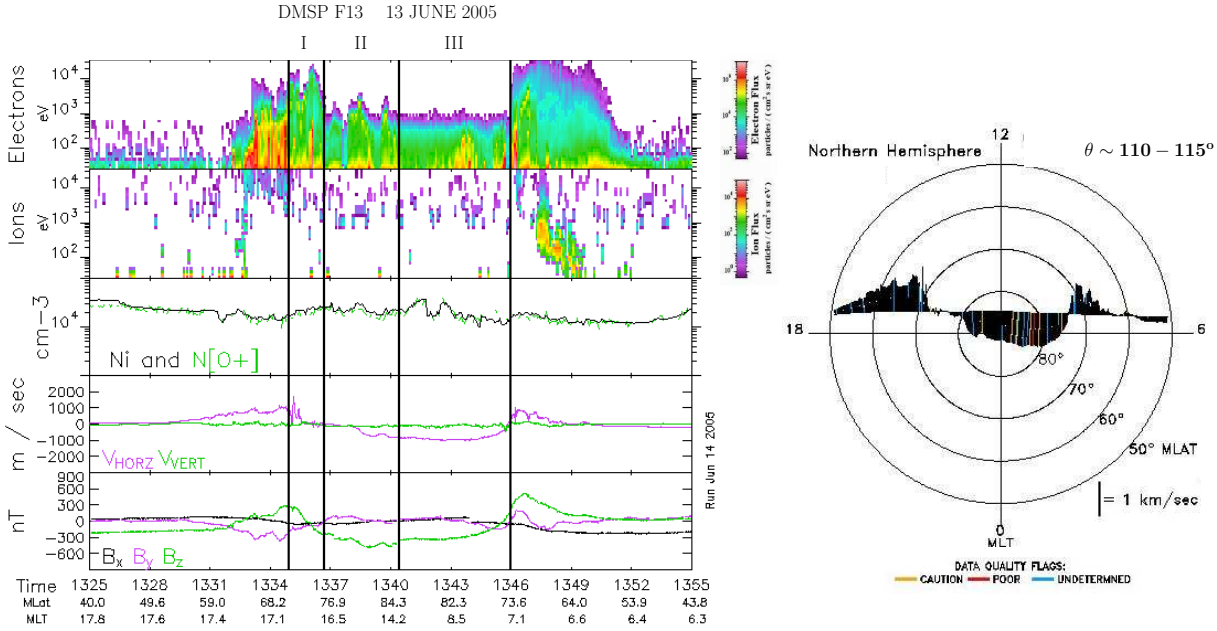

Figure 6.7: *Data obtained by DMSP F13 during the interval 1325 - 1355 UT on 13 June 2005. Same format as figure 3.2 in section 3.2.1.*

flow in region II. A local minimum is seen in close vicinity of the boundary between region II and III. The antisunward convection reaches another minimum of ~ -1000 m/s at 87° MLAT (dawnside).
We associate a positive B_z gradient eqatorward of region I to CPS-like precipitation and sunward convection. Two intense upward R1 FAC are seen in interval II. The upward R1 FAC system coincides with the BPS precipitation and the multiple channels of enhanced sunward convection. A weaker negative trend in B_z is seen in region II. The relatively strong flow shear following the enhanced sunward flow channels and high-latitude arcs coincide with this negative gradient in B_z. We believe this to be an upward NBZ-like FAC.

DMSP F13 1325-1355 UT (13), Clock Angle [110-115°], Density [2-3 cm^{-3}]

Compared to the previous pass at $\sim$ 1000 UT the magnetic field components of the cloud has become weaker. We note the following features: The IMF clock angle is between 110 – 115°; $B_y \sim$ 5nT; B_z is slightly negative (~ -1 nT) and $B_x \sim 0$ nT. The solar wind density (~2-3 cm^{-3}) and dynamic pressure ($\sim$ 1.5 nPa) has increased somewhat since the previous pass but the values are still considerable low.
The auroral oval with CPS-like precipitation is seen in the region 62 – 69° MLAT at dusk in figure 6.7. From 70 to 76° MLAT the satellite traverses into a region of discrete low flux BPS electron precipitation (marked I). Three distinct high-latitude arcs with electron energy of 2-3 keV is encountered throughout region II. In region III homogeneous polar rain with electron fluxes of ~600-700 eV is observed.
A rather steady sunward convection with positive gradient towards the central polar cap is seen at dusk. The sunward flow get enhanced ($\sim$ 1.3 km/s) in the beginning of region I (71° MLAT). Irregular small scale flow (end of region I) is followed by a flow shear in region II. A small peak

in the antisunward flow is seen just poleward of the flow shear. In the region of homogeneous polar rain, stable antisunward flow is seen.
Just like in the previous pass at ~ 1000 UT, a clear regime of downward R2 and upward R1 FAC is seen at dusk. The downward R2 current system coincide with the observed sunward convection and CPS precipitation equatorward of region I. We couple the BPS precipitation and enhanced sunward flow to the distinct upward R1 current. As the satellite traverses in the the region II it encounters three small scale upward FACs. We see that these currents coincide with the three distinct high-latitude arcs. We interpret the small scale upward FACs as NBZ-like FACs accompanied with a flow shear and high-latitude arcs.

6.3 Summary and Discussion

We have presented a set of observations during the magnetic cloud passage on June, 12-13 2005 that includes measurements from the Wind and DMSP F13 spacecrafts. These data sets provides information about the convection pattern and precipitation throughout the cloud passage. There are only small fluctuations in the clock angle in the time period of our three intervals. The clock angle is between 100° and 135° in all our DMSP F13 passes, and this allows us the to look at how other cloud parameters influence the magnetosphere. The intervals where mainly chosen according to the behaviour of the solar wind proton density. In interval I between 2350-0600 UT (June 12-13) and interval III between 1000 - 1400 UT (June 13), the solar wind proton density is less then 3.0 cm^{-3} while in interval II the density is between $8 - 12$ cm^{-3}. The dipole tilt of the Earth in June and the negative B_x polarity from ~ 0000 UT (13) onwards favour lobe reconnection in the northern hemisphere (see section 2.3). Another factor that may favour lobe reconnection is the strong B_y component (> 5 nT) from 1800 UT (12) to 1300 UT (13) (Eriksson et al., 2003 and many others, see section 2.3). The presence of a positive IMF B_y and a clock angle between 100° and 135° is similar to our case study on 12 August 2000. We notice that all DMSP F13 passes traverses over the northern hemisphere polar cap in a dusk-dawn MLT/M-LAT orbit on the dayside of the 06-18 MLT line. We will come back to this later in the disussion.

In interval I the clock angle is in the region $110 - 135°$ and the proton density is low (< 3.0 cm^{-3}) throughout the whole interval. In the two DMSP shown in figure 6.3 at ~ 0000 UT (13) and 6.4 at ~ 0140 UT (13) the polar cap was expanded due to a long period of strong negative B_z (~ −15 nT) prior to this interval. In both figures we see a similar convection pattern with a large rounded merging cell at dusk and a smaller crescent-shaped dawn cell. Inside the merging cell at dusk we observe high-latitude arcs in the region of the upward NBZ-like FAC (region II). The high-latitude arcs in conjunction with strong flow shear on the dusk side of the polar cap are taken as signature of a lobe cell. For this IMF condition the presence of a composite pattern of merging and lobe cells with dusk-dawn asymmetry is in agreement with the convection pattern found on 12 August 2000.

One DMSP F13 pass in northern hemisphere was studied in interval II. As mention earlier the proton density has increased to ~8-12 cm^{-3}. The clock angle varies between ~100-140°. Figure 6.5 at ~0830 UT (13) shows a rather different precipitation pattern than in the previous interval. The distinct high-latitude arcs seen in interval I are absent. The central polar cap has contracted since the B_z gradually becomes weaker. The convection pattern is likely a two cell

pattern with a big round merging cell at dusk and a small crescent-shaped cell at dawn.

In the time period 1000 - 1400 UT (interval III) the proton density was low ($< 3.0\ cm^{-3}$) and the clock angle fluctuated between $100 - 130°$. The two DSMP F13 passes in this interval, figure 6.6 at ~ 1010 UT (13) and 6.7 at ~ 1330 UT (13), showed similar precipitation and convection pattern as in interval I. The flow/field pattern can again be described as a composite pattern of merging and lobe cells with high-latitude arcs with upward NBZ FAC and enhanced sunward flow followed by flow shear. These we find to be prototype examples of the convection/precipitation state for clock angle regimes $100 - 135°$.

We notice that in the four DSMP passes with high-latitude arcs, i.e at ~ 0000 UT, ~ 0140 UT, ~ 1010 UT and ~ 1330 UT, the sunward convection at dusk and the antisunward convection show signs of two maxima/mimima. One in the close vicinity of the convection reversal at dusk and one at high latitude ($> 74°$ MLAT) at dawn. The presence of the local maximum towards dusk can be taken as a sign of the existence of a lobe cell inside the dusk merging cell. In the DMSP pass where the high-latitude arcs were absent (~ 0830 UT) a strong dawnward antisunward gradient with just one maximum at 71° MLAT is seen. This is consistent with an asymmetrical two-cell convection pattern without a lobe cell.

During the time of the high-latitude arcs in this case study no signature of ion precipitation is seen. As all our DMSP passes traverses over the northern hemisphere in a dusk-dawn MLT/MLAT orbit on the dayside of high-latitude arcs are detected in the region 14-17 MLT and poleward of 70° MLAT. This is consistent with the criteria Frey et al. (2004) used to identify High Latitude Dayside Aurora (HiLDA); Arcs had to be localized poleward of the dayside auroral oval ($> 70°$ MLAT) and no signs of ion precipitation was allowed. This is likely that what Frey et al. (2003) define as HiLDA is the same phenomena as the high-latitude arcs studied in this thesis.
In the article of Frey et al. (2004) the favourable conditions for HiLDA/high-latitude arcs were found to be: (1) The solar wind proton density should be $<4.0\ cm^{-3}$; (2) IMF B_y should be positive and (3) the clock angle should be between 50° and 90°; HiLDA is more likely to occur in the northern hemisphere in summer when the field-aligned current strength is strong. The proposed relationship is that a strong field-aligned potential drop is needed for the magnetosphere/ionosphere system to drive the required intensity of the upward current to the HiLDA (Frey et al., 2004).
The drop out of high-latitude arcs in interval II when the proton density increases to values $> 4.0\ cm^{-3}$ in our case is consistent with what Frey et al. (2004) found. We note, however, that in our case the presence of HiLDAs is documented for higher clock angles ($110 - 135°$).

As mention earlier Reiff and Burch (1985) (see section 2.2) predicted that a composite pattern of merging and lobe cells could occur for B_z negative conditions. This interpretation has been questioned by the recent work of Twitty et al. (2004). Twitty et al. (2004) found that cusp reconnection seem to occur almost exclusively when the IMF has a northward component, i.e less than 90° clock angle. Our DMSP passes combined with Wind data seems to confirm that we indeed have a composite pattern of merging and lobe cells for negative B_z conditions. In our case the clock angle was between $100 - 135°$.

Chapter 7

Final Summary and Discussion

In this thesis we have reported observations made by the DMSP F13 satellite of different patterns of ionospheric plasma convection and particle precipitation corresponding to the different magnetic fields and plasma conditions to which the Earth is exposed during the passage of three interplanetary magnetic clouds. For such studies magnetic clouds offer distinct advantages. Not only do interplanetary parameters reach extreme values which are otherwise hardly ever sampled, but the parameters also undergo temporal variations on time scales generally longer than typical ionospheric response times. The first accentuates any asymmetries in the convection so that these can be studied in detail; the second allows a given ionospheric pattern to be mapped back fairly confidently to the interplanetary state which gave rise to it. From the three case studies presented we may discriminate between the following plasma convection and particle precipitation states as ordered by the IMF clock angle (θ) and the B_y polarity. Our main findings may be summarized as follows:

- (1) $0^\circ < \theta < 45^\circ$ ($B_y > 0$):

  (i) Reverse 2-cell convection (two lobe cells) in the northern summer even for $B_x > 0$,

  (ii) Inverted-V arcs in the center of the dawnside lobe cell corresponding to clockwise plasma flow vorticity,

  (iii) Small viscous cells at lower latitudes.

- (2a) $70^\circ < \theta < 135^\circ$ ($B_y > 0$):

  (i) A composite pattern with merging and lobe cells.

  (ii) High-latitude arcs co-located with upward NBZ-like FAC and flow shear (region II) in dusk-side lobe cell.

- (2b) $100^\circ < \theta < 135^\circ$ ($B_y > 0$): Distorted 2-cell pattern with absence of polar arcs/lobe cells when the solar wind (cloud) density is high (~ 10 cm^{-3}).

- (3) $45^\circ < \theta < 60^\circ$ ($B_y < 0$): Distorted 2-cell pattern in contracted polar cap, absence of polar arcs.

- (4) $80^\circ < \theta < 90^\circ$ ($B_y < 0$): Asymmetric (distorted) 2-cell pattern with localized flow shears in central polar cap, and correspondingly localized arcs and negative B_z-gradient (upward NBZ FAC).

- (5) $90^\circ < \theta < 135^\circ$ ($B_y < 0$): A standard 2-cell convection pattern asymmetric about the noon meridian with homogeneous antisunward convection and absence of polar arcs.

A summary of the different convection configurations is given in figure 2.4, modified after (Cowley, 1998). In this thesis we have related these convection patterns to precipitation and FAC structures and determine the corresponding external (solar wind/IMF) conditions.

In relation to category 2b) we note that a relatively low density in the magnetic cloud seems to be a favourable condition for the polar arc presence. This tendency is in agreement with the results of Frey et al. (2004). The HiLDA's of Frey et al. (2004), obtained from IMAGE UV images, were observed for IMF clock angles in the 50-90° regime. By our more sensitive DMSP observations we are able to extend this range to 50-135°. The complexity of the problem of determining the relative importance of the various external parameters (IMF orientation, solar wind density/dynamic pressure, plasma β, Alfv́en-Mach number) for the realization of lobe cells and polar arcs is illustrated by the fact that we do see polar arcs in case study 1 (August 12, 2000) even for the relatively high solar wind (cloud) density observed in case study 1.

The presence of a lobe cell in the composite pattern is identified from the observations in spatial region II along the F13 track and is based on the following considerations: (i) the presence of polar arcs poleward of the oval (BPS) aurora in region of (ii) flow shear on the poleward side of a channel of enhanced sunward flow, and is accompanied by (iii) a negative gradient in the B_z-trace (NBZ-type FAC) separated from the R1 FAC on its poleward side. Often the channel of enhanced sunward flow in the lobe cell appears as a second flow channel well separated from the flow peak in the merging cell, which is located at lower latitudes. In the latter cases the polar arcs are particularly strong (see discussion in case study 1).

Knipp et al. (1993) showed by analysing ionospheric convection patterns over the northern polar regions during a magnetic cloud passage that reverse convection in the summer hemisphere broke down when the ratio $\left|B_y\right| / B_z$ exceeded unity (see figure 7.1). This transition is confirmed by our study (see points 1 and 3 above and case study 2). To be able to establish a more precise measurement of the transition between convection patterns, a more comprehensive study involving continuous monitoring by ground-based radars combined with spacecraft like DMSP is needed.

In case study 2 (see section 5) a large scale midnight arc stretching towards noon from the poleward boundary of the nightside oval, with properties in agreement with the conditions found by Kullen et al. (2002), was seen in figure 5.10. When comparing the picture sequence from the IMAGE WIC camera with DMSP electron precipitation in figure 5.9 we found that this large scale "single" arc is likely to be a multiplicity of arcs which IMAGE does not resolve. However, using IMAGE, we get a more comprehensive global overview of the polar arcs.

The observations may be related to the reconnection topology
1) Distorted, standard 2-cell pattern reaching down to 50°. This supports the presence of subsolar (component) merging for clock angles > 50°. This is in agreement with in situ observations at the magnetopause (Phan et al., 1994, 1996).
2) Composite pattern when the clock angle θ lies in the range 70-135° and $B_y > 0$. Simulta-

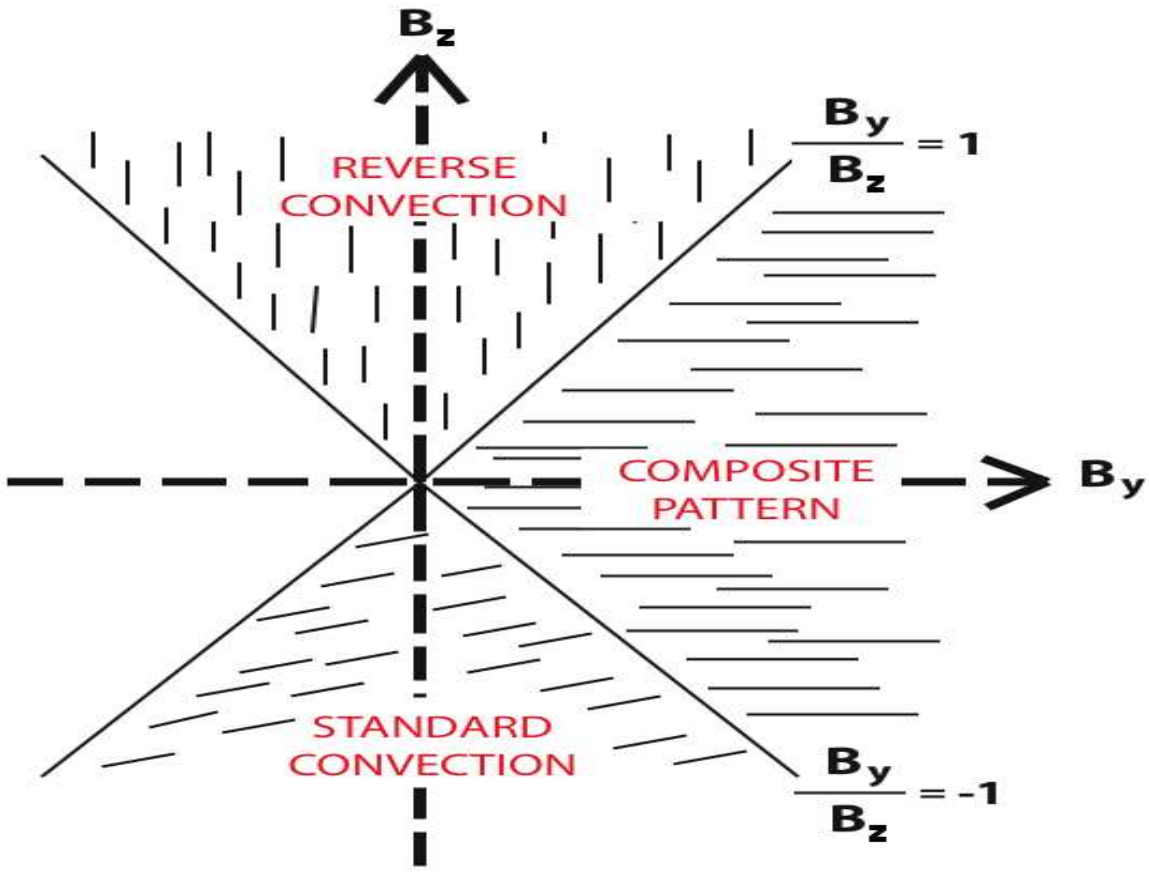

Figure 7.1: *Relationship between the ratio B_y/B_z for different convection patterns.*

neous presence of subsolar and lobe reconnection in a geometry similar to that indicated by the reconnection topology in figure 2.3. Thus lobe reconnection is present even for B_z negative conditions, in agreement with the case studies of Eriksson et al. (2002, 2003, 2005); Sandholt and Farrugia (2006).
3) The question of whether single or dual lobe reconnection (see figure 2.5) exists for low clock angles (Chisham et al., 2005) is unresolved in our cases. However, this problem may be studied further by application of observations from both hemispheres (Watanabe et al., 2006).

The approach adopted here has some limitations which should be borne in mind when we determine different patterns of plasma convection and particle precipitation with the help of DMSP F13 spacecraft.The DMSP F13 track gives a good indication of dawn-dusk asymmetries, but only a limited (2-dimensions) view of convection pattern along the dusk-dawn track is obtained. Furthermore, the variability of the satellite track must be taken into account when comparing the different cases, i.e the DMSP F13 ground track ”walks” back and forth with respect to the 0600-1800 MLT meridian during the course of a day. We discussed this problem in relation to case study 2 (where the cusp position with respect to the track is changing from pass to pass).

7.1 In conclusion:

In this thesis emphasis is placed on distinguishing between different categories of plasma convection cells and the corresponding particle precipitation and field-aligned current characteristics in the polar cap obtained by the DMSP F13 spacecraft under wide variety solar wind conditions. By use of solar wind data from the Wind spacecraft we aim at establishing the correspondence between the polar cap convection/precipitation states and external conditions driving the magnetosphere, such as (i) the IMF orientation given by the clock angle, (ii) the IMF B_x and B_y polarities, and (iii) the solar wind density and dynamic pressure. A more extensive data base than shown in this case study is needed in order to determine the relative importance of the various solar wind plasma and IMF parameters for the excitation of the different magnetospheric states.

Appendix A

DMSP cross-track plasma drift data

The DMSP cross-track plasma drift data is mark with different quality flags. Each flag has one of four values:

- 1 means the data are good and can be used with high confidence
- 2 means the data are somewhat questionable and should be used with caution
- 3 means the data are bad and should not be used at all
- 4 means the quality could not be determined for these data and so should probably not be used or (depending on the circumstances) used with caution

On the plots the quality flags is marked with a colour code where 1 being black, 2 being yellow, 3 being red and 4 being blue.

The design of the SSIES thermal plasma instruments makes it work best in a predominately O+ plasma environment. Even in low-density plasmas (e.g. 10^3 ions per cc) the instruments continue to produce usable data so long as the plasma is essentially all O+. However, once the percentage of light ions (H+ and He+) goes above 15%, even under relatively high densities (e.g. 10^4 - 10^5 ions per cc) the data quality becomes poor and the results are difficult to interpret. In the topside F-layer the solar cycle and the season of the year changes the composition of the plasma. In general we can say that around solar maximum (2001) the scale height of O+ is big enough so that the composition of the plasma at 840 km (DMSP orbit hight) is greater than 90% at almost all points in the satellites orbit and in those conditions the data are almost all good. Around solar minimum (2006) the O+ scale height has dropped so that the satellite is frequently in regions that are dominated by light ions where the instruments do not function properly and those data cannot be used. Because the scale height drops further in darkness we end up with a situation where winter hemisphere data are worse than summer hemisphere data. Thus around the solar minimum near the solstices, the data from the summer hemisphere is good while the winter hemisphere data need to be treated with more care. Around solar minimum and the equinoxes both hemispheres data are marginal and should be treated with caution.

When the drift meter data is marked as caution (2), poor (3) and some times undetermined (4) we have to use our own judgement to decide if the data can be used or not. On the right

side of figure 3.2 cross-track plasma drift data for F13 on 13 June 2005 is shown. Looking at the figure we see some data marked as caution (2), poor (3) and undetermined (4) in the flow pattern at the highest latitudes. Since the flagged data occurs as a few isolated flows with determined data on both sides, it is clear that the questionable flows fit exactly with the surrounding flows, that are rated as good (1). So we can safely ignore the caution flags for this kind of data. Sometimes the questionable flows occur not as isolated flows but as area and then we need to be a bit more cautious about using the DMSP cross-track plasma drift data. In this thesis we will only use DMSP cross-track plasma drift data which we have rated as good.

Appendix B

DMSP Instruments

The SSJ4 detector flown on F13 measures the flux of precipitating electrons and ions in the range of 30 eV to 30 keV. The measurements are made by 4 detectors, one high energy detector and one low energy detector for each of the particle types.
The Special Sensor-Ions, Electrons, and Scintillation (SSIES) measure the thermal plasma at the location of the spacecraft. The SSIES sensors are tailored to the anticipated environment at 840 km altitude and at all latitudes, all local times, all seasons and all phases of the sunspot cycle. Typically this environment is composed of three ion species; hydrogen (H+), helium (He+) and oxygen (O+).
The SSM is a triaxial fluxgate magnetometer system used to measure the magnetic field. This field has three sources: (1) the magnetic field from the solid Earth, (2) the magnetic field from electrical currents flowing in the ionosphere and magnetosphere, and (3) the magnetic field from the spacecraft. Measurement of source 2 is the principal objective of the SSM, measurement of source 1 is a secondary objective, and measurement of source 3 is a nuisance which is eliminated from the data as much as possible during data processing. These are the essential instruments that we are using in this thesis.

Bibliography

Axford, W. I. and C. O. Hines (1961). A unifying theory of high-latitude geophysical phenomena and geomagnetic storms. *Canadian Journal of Physics 39*, 1433–1463.

Burch, J. L., P. H. Reiff, J. D. Menietti, J. D. Winningham, R. A. Heelis, W. B. Hanson, S. D. Shawhan, E. G. Shelley, M. Sugiura, and D. R. Weimer (1985, February). IMF By-dependent plasma flow and Birkeland currents in the dayside magnetosphere. I - Dynamics Explorer observations. *Journal of Geophysical Research 90*, 1577–1593.

Burlaga, L., E. Sittler, F. Mariani, and R. Schwenn (1981, August). Magnetic loop behind an interplanetary shock - Voyager, Helios, and IMP 8 observations. *Journal of Geophysical Research 86*, 6673–6684.

Burlaga, L. F. (1988, July). Magnetic clouds and force-free fields with constant alpha. *Journal of Geophysical Research 93*, 7217–7224.

Burlaga, L. F. (1995). *Interplanetary magnetohydrodynamics*. New York: Oxford University Press,.

Burlaga, L. F., R. M. Skoug, C. W. Smith, D. F. Webb, T. H. Zurbuchen, and A. Reinard (2001, October). Fast ejecta during the ascending phase of solar cycle 23: ACE observations, 1998-1999. *Journal of Geophysical Research 106*, 20957–20978.

Chisham, G., M. P. Freeman, M. M. Lam, G. A. Abel, T. Sotirelis, R. A. Greenwald, and M. Lester (2005, December). A statistical comparison of SuperDARN spectral width boundaries and DMSP particle precipitation boundaries in the afternoon sector ionosphere. *Annales Geophysicae 23*, 3645–3654.

Cowley, S. W. H. (1973, November). A qualitative study of the reconnection between the Earth's magnetic field and an interplanetary field of arbitrary orientation. *Radio Science 8*, 903–+.

Cowley, S. W. H. (1981, February). Magnetospheric and ionospheric flow and the interplanetary magnetic field. In H. Kohl (Ed.), *The Physical Basis of the Ionosphere in the Solar-Terrestrial System, no. 295 in Conference Proceedings, AGARD (Advisory Group for Aerospace Research & Development), NATO, Neuilly sur Seine, France,*.

Cowley, S. W. H. (1984, September). Solar wind control of magnetospheric convection. In B. Battrick and E. Rolfe (Eds.), *Achievements of the International Magnetospheric Study (IMS)*, pp. 483–494.

Cowley, S. W. H. (1998). Excitation of Flow in the Earth's Magnetosphere-Ionosphere System: Observations by Incoherent-Scatter Radar. In J. Moen, A. Egeland, and M. Lockwood (Eds.), *Polar Cap Boundary Phenomena*, pp. 127–140.

Cowley, S. W. H. and M. Lockwood (1992, February). Excitation and decay of solar wind-driven flows in the magnetosphere-ionosphere system. *Annales Geophysicae 10*, 103–115.

Crooker, N. U. (1992, December). Reverse convection. *Journal of Geophysical Research 97*(A12), 19363–19372.

Crooker, N. U., T. E. Eastman, and G. S. Stiles (1979, March). Observations of plasma depletion in the magnetosheath at the dayside magnetopause. *Journal of Geophysical Research 84*, 869–874.

Crooker, N. U., J. G. Lyon, and J. A. Fedder (1998, May). MHD model merging with IMF B_y: Lobe cells, sunward polar cap convection, and overdraped lobes. *Journal of Geophysical Research 103*, 9143–9152.

Crooker, N. U. and F. J. Rich (1993, August). Lobe cell convection as a summer phenomenon. *Journal of Geophysical Research 98*, 13403–+.

de Keyser, J., M. W. Dunlop, C. J. Owen, B. U. Ö. Sonnerup, S. E. Haaland, A. Vaivads, G. Paschmann, R. Lundin, and L. Rezeau (2005, June). Magnetopause and Boundary Layer. *Space Science Reviews 118*, 231–320.

DMSP SSIES Data Distribution at UT-Dallas Website (12 April 2007).

DMSP/AFRL Space Weather Data Survey Website (12 April 2007).

Dungey, J. W. (1961, January). Interplanetary Magnetic Field and the Auroral Zones. *Physical Review Letters 6*, 47–48.

Dungey, J. W. (1963). The Earth's Environment. In C. DeWitt, J. Hieblot, and A. Leneau (Eds.), *The structure of the exosphere or adventures in velocity space in Geophysics*, pp. 503–550. New York: Gordon Breach.

Eastman, T. E., E. W. Hones, Jr., S. J. Bame, and J. R. Asbridge (1976, November). The magnetospheric boundary layer - Site of plasma, momentum and energy transfer from the magnetosheath into the magnetosphere. *Geophysical Research Letters 3*, 685–688.

Elphinstone, R. D., K. Jankowska, J. S. Murphree, and L. L. Cogger (1990, May). The configuration of the auroral distribution for interplanetary magnetic field Bz northward. I - IMF Bx and By dependencies as observed by the Viking satellite. *Journal of Geophysical Research 95*, 5791–5804.

Eriksson, S., J. B. H. Baker, S. M. Petrinec, H. Wang, F. J. Rich, M. Kuznetsova, M. W. Dunlop, H. Rème, R. A. Greenwald, H. U. Frey, H. Lühr, R. E. Ergun, A. Balogh, and C. W. Carlson (2005, November). On the generation of enhanced sunward convection and transpolar aurora in the high-latitude ionosphere by magnetic merging. *Journal of Geophysical Research 110*, 11218–+.

Eriksson, S., J. W. Bonnell, L. G. Blomberg, R. E. Ergun, G. T. Marklund, and C. W. Carlson (2002, August). Lobe cell convection and field-aligned currents poleward of the region 1 current system. *Journal of Geophysical Research 107*(A8), 16–1.

Eriksson, S., W. J. Peria, J. W. Bonnell, Y.-J. Su, R. E. Ergun, Y.-K. Tung, G. K. Parks, and C. W. Carlson (2003, May). Lobe cell convection and polar cap precipitation. *Journal of Geophysical Research 108*(A5), 11–1.

Fairfield, D. H. (1971). Average and unusual locations of hte Earth's magnetopause and bow shock. *Journal of Geophysical Research 76*, 6700–+.

Fairfield, D. H. and J. D. Scudder (1985, May). Polar rain - Solar coronal electrons in the earth's magnetosphere. *Journal of Geophysical Research 90*, 4055–4068.

Farrugia, C. J., H. Kucharek, H. Matsui, and et al. (2005, September). Cross-Correlation of Interplanetary Parameters for Large X (450 Re) Separation: Dependence on Interplanetary Structure. In *ESA SP-592: Solar Wind 11/SOHO 16, Connecting Sun and Heliosphere*, Volume 16.

Farrugia, C. J., H. Matsui, H. Kucharek, R. B. Torbert, C. W. Smith, V. K. Jordanova, K. W. Ogilvie, R. P. Lepping, D. B. Berdichevsky, T. Terasawa, J. Kasper, T. Mukai, Y. Saito, and R. Skoug (2005, September). Interplanetary coronal mass ejection and ambient interplanetary magnetic field correlations during the Sun-Earth connection events of October-November 2003. *Journal of Geophysical Research 110*, 9–+.

Frey, H. U., T. J. Immel, G. Lu, J. Bonnell, S. A. Fuselier, S. B. Mende, B. Hubert, N. Østgaard, and G. Le (2003, February). Properties of localized, high latitude, dayside aurora. *Journal of Geophysical Research 108*, 9–1.

Frey, H. U., N. Østgaard, T. J. Immel, H. Korth, and S. B. Mende (2004, April). Seasonal dependence of localized, high-latitude dayside aurora (HiLDA). *Journal of Geophysical Research 109*, 4303–+.

Goldstein, H. (1983, November). On the field configuration in magnetic clouds. In M. Neugebauer (Ed.), *Solar Wind Conference*, pp. 731–733.

Gonzalez, W. D. and F. S. Mozer (1974, October). A quantitative model for the potential resulting from reconnection with an arbitrary interplanetary magnetic field. *Journal of Geophysical Research 79*, 4186–4194.

Gosling, J. T., M. F. Thomsen, S. J. Bame, R. C. Elphic, and C. T. Russell (1990, June). Plasma flow reversals at the dayside magnetopause and the origin of asymmetric polar cap convection. *Journal of Geophysical Research 95*, 8073–8084.

Gosling, J. T., M. F. Thomsen, G. Le, and C. T. Russell (1996, November). Observations of magnetic reconnection at the lobe magnetopause. *Journal of Geophysical Research 101*, 24765–24774.

Greenwald, R. A., K. B. Baker, J. R. Dudeney, M. Pinnock, T. B. Jones, E. C. Thomas, J.-P. Villain, J.-C. Cerisier, C. Senior, C. Hanuise, R. D. Hunsucker, G. Sofko, J. Koehler, E. Nielsen, R. Pellinen, A. D. M. Walker, N. Sato, and H. Yamagishi (1995, February). Darn/Superdarn: A Global View of the Dynamics of High-Lattitude Convection. *Space Science Reviews 71*, 761–796.

Heppner, J. P. and N. C. Maynard (1987, May). Empirical high-latitude electric field models. *Journal of Geophysical Research 92*, 4467–4489.

Hill, T. W. (1975, December). Magnetic merging in a collisionless plasma. *Journal of Geophysical Research 80*, 4689–4699.

Huttunen, K. E. J., R. Schwenn, V. Bothmer, and H. E. J. Koskinen (2005, February). Properties and geoeffectiveness of magnetic clouds in the rising, maximum and early declining phases of solar cycle 23. *Annales Geophysicae 23*, 625–641.

IMAGE Far-Ultraviolet (FUV) imager Website (03 MAY 2007).

Kessel, R. L., S.-H. Chen, J. L. Green, S. F. Fung, S. A. Boardsen, L. C. Tan, T. E. Eastman, J. D. Craven, and L. A. Frank (1996). Evidence of high-latitude reconnecting during northward IMF: Hawkeye observations. *Geophysical Research Letters 23*, 583–586.

Khan, H. and S. W. H. Cowley (1999, October). Observations of the response time of high-latitude ionospheric convection to variations in the interplanetary magnetic field using EISCAT and IMP-8 data. *Annales Geophysicae 17*, 1306–1335.

Kivelson, M. G. and C. T. Russell (1995, April). *Introduction to Space Physics*. Edited by Margaret G. Kivelson and Christopher T. Russell, pp. 586. ISBN 0521451043., Cambridge University Press.

Klein, L. W. and L. F. Burlaga (1982, February). Interplanetary magnetic clouds at 1 AU. *Journal of Geophysical Research 87*, 613–624.

Knipp, D. J., B. A. Emery, A. D. Richmond, N. U. Crooker, M. R. Hairston, J. A. Cumnock, W. F. Denig, F. J. Rich, O. de La Beaujardiere, and J. M. Ruohoniemi (1993, November). Ionospheric convection response to slow, strong variations in a Northward interplanetary magnetic field: A case study for January 14, 1988. *Journal of Geophysical Research 98*, 19273–+.

Kullen, A., M. Brittnacher, J. A. Cumnock, and L. G. Blomberg (2002, November). Solar wind dependence of the occurrence and motion of polar auroral arcs: A statistical study. *Journal of Geophysical Research 107*, 13–1.

Kullen, A. and P. Janhunen (2004, March). Relation of polar auroral arcs to magnetotail twisting and IMF rotation: a systematic MHD simulation study. *Annales Geophysicae 22*, 951–970.

Lepping, R. P., M. H. Acuna, L. F. Burlaga, W. M. Farrell, J. A. Slavin, K. H. Schatten, F. Mariani, N. F. Ness, F. M. Neubauer, Y. C. Whang, J. B. Byrnes, R. S. Kennon, P. V. Panetta, J. Scheifele, and E. M. Worley (1995, February). The Wind Magnetic Field Investigation. *Space Science Reviews 71*, 207–229.

Lepping, R. P. and D. Berdichevsky (2000). Interplanetary magnetic clouds: Sources, properties, modeling, and geomagnetic relationship. *Recent Research Developments in Geophysical Research, 3, Research Signpost, Trivandrum-8, India*, 77–96.

Lepping, R. P., C.-C. Wu, and D. B. Berdichevsky (2005, October). Automatic identification of magnetic clouds and cloud-like regions at 1 AU: occurrence rate and other properties. *Annales Geophysicae 23*, 2687–2704.

Lin, R. P., K. A. Anderson, S. Ashford, C. Carlson, D. Curtis, R. Ergun, D. Larson, J. McFadden, M. McCarthy, G. K. Parks, H. Reme, J. M. Bosqued, J. Coutelier, F. Cotin, C. D'Uston, K.-P. Wenzel, T. R. Sanderson, J. Henrion, J. C. Ronnet, and G. Paschmann (1995, February). A Three-Dimensional Plasma and Energetic Particle Investigation for the Wind Spacecraft. *Space Science Reviews 71*, 125–153.

Liou, K., P. T. Newell, C.-I. Meng, T. Sotirelis, M. Brittnacher, and G. Parks (1999, November). Source region of 1500 MLT auroral bright spots: Simultaneous Polar UV-images and DMSP particle data. *Journal of Geophysical Research 104*, 24587–24602.

Lockwood, M., B. S. Lanchester, S. K. Morley, K. Throp, S. E. Milan, M. Lester, and H. U. Frey (2006, February). Modeling the observed proton aurora and ionospheric convection responses to changes in the IMF clock angle: 2. Persistence of ionospheric convection. *Journal of Geophysical Research 111*, 2306–+.

Loewe, C. A. and G. W. Prölss (1997, July). Classification and mean behavior of magnetic storms. *Journal of Geophysical Research 102*, 14209–14214.

Lopez, R. E. and J. W. Freeman (1986, February). Solar wind proton temperature-velocity relationship. *Journal of Geophysical Research 91*, 1701–1705.

Luhmann, J. G., R. J. Walker, C. T. Russell, N. U. Crooker, J. R. Spreiter, and S. S. Stahara (1984, March). Patterns of potential magnetic field merging sites on the dayside magnetopause. *Journal of Geophysical Research 89*, 1739–1742.

Magnetic Field Investigation (MFI) on the WIND Spacecraft Website (12 April 2007).

Marubashi, K. (1997). Interplanetary magnetic flux ropes and solar filaments. In N. Crooker, J. A. Joselyn, and J. Feynman (Eds.), *Coronal Mass Ejections, Geophys. Monogr. Ser., vol. 99*, pp. 147–156. AGU, Washington,D. C.

Mende, S. B., H. Heetderks, H. U. Frey, M. Lampton, S. P. Geller, R. Abiad, O. H. W. Siegmund, A. S. Tremsin, J. Spann, H. Dougani, S. A. Fuselier, A. L. Magoncelli, M. B. Bumala, S. Murphree, and T. Trondsen (2000, January). Far ultraviolet imaging from the IMAGE spacecraft. 2. Wideband FUV imaging. *Space Science Reviews 91*, 271–285.

Milan, S. E., M. Lester, S. W. H. Cowley, and M. Brittnacher (2000, April). Dayside convection and auroral morphology during an interval of northward interplanetary magnetic field. *Annales Geophysicae 18*, 436–444.

Moore, T. E., M.-C. Fok, and M. O. Chandler (2002, October). The dayside reconnection X line. *Journal of Geophysical Research 107*(A10), 26–1.

Murphree, J. S., J. B. Austin, D. J. Hearn, L. L. Cogger, R. D. Elphinstone, and J. Woch (1994, February). Satellite observations of polar arcs. *Journal of Atmospheric and Terrestrial Physics 56*, 265–284.

Newell, P. T. and C.-I. Meng (1992, March). Mapping the dayside ionosphere to the magnetosphere according to particle precipitation characteristics. *Geophysical Research Letters 19*, 609–612.

Newell, P. T. and T. Onsager (2003). *Earth's low-latitude boundary layer*. Geophysical Monograph 133, American Geophysical Union, Washington, DC.

Newell, P. T., J. M. Ruohoniemi, and C.-I. Meng (2004, October). Maps of precipitation by source region, binned by IMF, with inertial convection streamlines. *Journal of Geophysical Research 109*(A18), 10206–+.

Nishida, A. (1978). *Geomagnetic diagnosis of the magnetosphere*. Physics and Chemistry in Space, New York: Springer, 1978.

Ogilvie, K. W., D. J. Chornay, R. J. Fritzenreiter, F. Hunsaker, J. Keller, J. Lobell, G. Miller, J. D. Scudder, E. C. Sittler, Jr., R. B. Torbert, D. Bodet, G. Needell, A. J. Lazarus, J. T. Steinberg, J. H. Tappan, A. Mavretic, and E. Gergin (1995, February). SWE, A Comprehensive Plasma Instrument for the Wind Spacecraft. *Space Science Reviews 71*, 55–77.

Onsager, T. G. and S. A. Fuselier (1994). The location of magnetic reconnection for northward and southward interplanetary magnetic field. In J. L. Burch and W. J. H. (Eds.), *Solar System Plasmas in Space and Time, Geophys. Monogr. Ser., vol. 84*, pp. 183. AGU, Washington,D. C.

Park, K. S., T. Ogino, and R. J. Walker (2006, May). On the importance of antiparallel reconnection when the dipole tilt and IMF B_y are nonzero. *Journal of Geophysical Research 111*(A10), 5202–5214.

Parker, E. N. (1957, December). Sweet's Mechanism for Merging Magnetic Fields in Conducting Fluids. *Journal of Geophysical Research 62*, 509–520.

Parker, E. N. (1958, November). Dynamics of the Interplanetary Gas and Magnetic Fields. *Astrophysical Journal 128*, 664–+.

Paschmann, G. (1984). Plasma and particle observations at the magnetopause: Implications for reconnection. In E. W. Hones (Ed.), *Magnetic Reconnection in Space and Laboratory Plasmas, Geophysical Monograph Series 30, American Geophysical Union, Washington, DC.*

Paschmann, G. (1991). *Geomagnetism*, Volume 4, Chapter 3 "The Earth's Magnetopause", pp. 295–331. Academic Press Limited.

Paschmann, G., W. Baumjohann, N. Sckopke, I. Papamastorakis, and C. W. Carlson (1986, October). The magnetopause for large magnetic shear - AMPTE/IRM observations. *Journal of Geophysical Research 91*, 11099–11115.

Paschmann, G., B. U. Ö. Sonnerup, I. Papamastorakis, N. Sckopke, and G. Haerendel (1979, November). Plasma acceleration at the Earth's magnetopause: evidence for reconnection. *Nature 282*, 243–246.

Petschek, H. E. (1964). Magnetic Field Annihilation. In W. N. Hess (Ed.), *The Physics of Solar Flares*, pp. 425–+.

Phan, T.-D., G. Paschmann, W. Baumjohann, N. Sckopke, and H. Luehr (1994, January). The magnetosheath region adjacent to the dayside magnetopause: AMPTE/IRM observations. *Journal of Geophysical Research 99*, 121–141.

Phan, T.-D., G. Paschmann, and B. U. Ö. Sonnerup (1996, April). Low-latitude dayside magnetopause and boundary layer for high magnetic shear 2. Occurrence of magnetic reconnection. *Journal of Geophysical Research 101*, 7817–7828.

Pryse, S. E., A. M. Smith, and L. Kersley (2000, July). Dayside ionospheric response to changes in IMF polarity: optical and plasma-flow observations. *Annales Geophysicae 18*, 782–788.

Reiff, P. H. and J. L. Burch (1985, February). IMF B_y-dependent plasma flow and Birkeland currents in the dayside magnetosphere. II - A global model for northward and southward IMF. *Journal of Geophysical Research 90*, 1595–1609.

Reiff, P. H., J. L. Burch, and R. A. Heelis (1978, May). Dayside auroral arcs and convection. *Geophysical Research Letters 5*, 391–394.

Rich, F. J. (1994). Users Guide for the Topside Ionospheric Plasma Monitor (SSIES, SSIES-2 and SSIES-3) on Spacecraft of the Defense Meteorological Satellite Program, Volume 1, PLTR942187. Technical report, Air Force Phillips Laboratory, Hanscom AFB, MA.

Rijnbeek, R. P., S. W. H. Cowley, D. J. Southwood, and C. T. Russell (1984). Recent Investigations of Flux Transfer Events Observed at the Dayside Magnetopause. In E. W. Hones, Jr. (Ed.), *Magnetic Reconnection in Space and Laboratory Plasmas, Geophysical Monograph 30*, pp. 139–144. AGU, Washington, D.C.

Russell, C. T. (1972). The Configuration of the Magnetosphere. In E. R. Dyer (Ed.), *Critical Problems of Magnetospheric Physics*, pp. 1–+.

Russell, C. T. (2003, October). The structure of the magnetopause. *Planetary and Space Science 51*, 731–744.

Sandholt, P. E., H. C. Carlson, and A. Egeland (2002, June). *Dayside and Polar Cap Aurora*. Dayside and Polar Cap Aurora, by Per Even Sandholt, Department of Physics, University of Oslo, Norway; Herbert C. Carlson, Air Force Office of Scientific Research, Arlington, Virginia, U.S.A.; Alv Egeland, Department of Physics, University of Oslo, Norway Astrophysics and Space Science Library, Vol. 270.

Sandholt, P. E., M. Dyrland, and C. J. Farrugia (2006, December). Dayside aurorae and polar arcs under south-east IMF orientation. *Annales Geophysicae 24*, 3421–3432.

Sandholt, P. E. and C. J. Farrugia (2006, October). Spatiotemporal structure of the reconnecting magnetosphere under By-dominated interplanetary magnetic cloud conditions. *Journal of Geophysical Research 111*, 10209–+.

Sandholt, P. E., C. J. Farrugia, S. W. H. Cowley, W. F. Denig, M. Lester, J. Moen, and B. Lybekk (1999, September). Capture of magnetosheath plasma by the magnetosphere during northward IMF. *Geophysical Research Letters 26*, 2833–2836.

Sandholt, P. E., C. J. Farrugia, S. W. H. Cowley, M. Lester, W. F. Denig, J.-C. Cerisier, S. E. Milan, J. Moen, E. Trondsen, and B. Lybekk (2000, June). Dynamic cusp aurora and associated pulsed reverse convection during northward interplanetary magnetic field. *Journal of Geophysical Research 105*, 12869–12894.

Sandholt, P. E., C. J. Farrugia, S. W. H. Cowley, M. Lester, J. Moen, B. Lybekk, and E. Trondsen (1999, December). Excitation and decay of magnetospheric lobe cell convection and its associated aurora. *Geophysical Research Letters 26*, 3597–3600.

Sckopke, N., G. Paschmann, G. Haerendel, B. U. Ö . Sonnerup, S. J. Bame, T. G. Forbes, E. W. Hones, Jr., and C. T. Russell (1981, April). Structure of the low-latitude boundary layer. *Journal of Geophysical Research 86*, 2099–2110.

Song, P. and C. T. Russell (1992, February). Model of the formation of the low-latitude boundary layer for strongly northward interplanetary magnetic field. *Journal of Geophysical Research 97*, 1411–1420.

Sonnerup, B. U. Ö . (1974). Magnetopause reconnection rate. *Journal of Geophysical Research 79*(A10), 1546–1549.

Sonnerup, B. U. Ö . (1985, June). Solar wind interaction with planetary magnetic fields. In *Future Missions in Solar, Heliospheric and Space Plasma Physics*, pp. 53–64.

Sonnerup, B. U. O. and L. J. Cahill, Jr. (1967, January). Magnetopause Structure and Attitude from Explorer 12 Observations. *Journal of Geophysical Research 72*, 171–+.

Sonnerup, B. U. Ö ., G. Paschmann, I. Papamastorakis, N. Sckopke, G. Haerendel, S. J. Bame, J. R. Asbridge, J. T. Gosling, and C. T. Russell (1981, November). Evidence for magnetic field reconnection at the earth's magnetopause. *Journal of Geophysical Research 86*, 10049–10067.

Super Dual Auroral Radar Network (SuperDARN) Website (28 April 2007).

Sweet, P. A. (1958). The Neutral Point Theory of Solar Flares. In B. Lehnert (Ed.), *IAU Symp. 6: Electromagnetic Phenomena in Cosmical Physics*, pp. 123–+.

The Imager for Magnetopause-to-Aurora Global Exploration (IMAGE) Website (03 MAY 2007).

Todd, H., S. W. H. Cowley, M. Lockwood, D. M. Willis, and H. Lühr (1988, December). Response time of the high-latitude dayside ionosphere to sudden changes in the north-south component of the IMF. *Planetary and Space Science 36*, 1415–1428.

Twitty, C., T. D. Phan, G. Paschmann, B. Lavraud, H. Rème, and M. Dunlop (2004, October). Cluster survey of cusp reconnection and its IMF dependence. *Geophysical Research Letters 31*, 19808–+.

Valladares, C. E., H. C. Carlson, Jr., and K. Fukui (1994, April). Interplanetary magnetic field dependency of stable Sun-aligned polar cap arcs. *Journal of Geophysical Research 99*, 6247–6272.

Vasyliunas, V. M. (1979, August). Interaction between the magnetospheric boundary layers and the ionosphere. In J. Lemaire (Ed.), *Magnetospheric Boundary Layers*, pp. 387–393.

Watanabe, M., G. J. Sofko, D. A. André, J. M. Ruohoniemi, M. R. Hairston, and K. Kabin (2006, June). Ionospheric signatures of internal reconnection for northward interplanetary magnetic field: Observation of "reciprocal cells" and magnetosheath ion precipitation. *Journal of Geophysical Research (Space Physics) 111*, 6201–+.

Weimer, D. R. (1995, October). Models of high-latitude electric potentials derived with a least error fit of spherical harmonic coefficients. *Journal of Geophysical Research 100*, 19595–19608.

WIND-Solar Wind Experiment (SWE) - MIT Space Plasma Group Website (12 April 2007).

Winningham, J. D., W. J. Heikkila, F. Yasuhara, and S.-I. Akasofu (1975, August). The latitudinal morphology of 10-eV to 10-keV electron fluxes during magnetically quiet and disturbed times in the 2100-0300 MLT sector. *Journal of Geophysical Research 80*, 3148–3171.

Yumoto, K. and the 210 degree MM magnetic observation group (1996). The STEP 210 degree magnetic meridian network project. *Journal of Geomagnetism and Geoelectricity 48*, 1297–1309.

Zhu, L., R. W. Schunk, and J. J. Sojka (1997, July). Polar cap arcs: a review. *Journal of Atmospheric and Terrestrial Physics 59*, 1087–1126.